NASA Contractor Report

PART II

High Frequency Losses in Induction Motors

Contract No. NAG3-940
Final Report

University of Wisconsin
Department of Electrical and Computer Engineering
1415 Johnson Drive
Madison, WI 53706

Donald W. Novotny
Principal Investigator

and

Syed A. Nasar
Visiting Scientist

Prepared for
NASA Lewis Research Center
Cleveland, OH 44135

Gale R. Sundberg
NASA Project Manager

June, 1991

Table of Contents

List of Tables and Figures

HIGH FREQUENCY LOSSES IN INDUCTION MOTORS

Section 1

Summary

Donald W. Novotny

Syed A. Nasar

July 1989

Section 1
Summary
High Frequency Losses in Induction Motors

1.1. Introduction

The concept of operating a converter fed induction machine at significantly - higher fundamental frequency than the conventional 50-60 hz range raises fundamental questions concerning machine losses. The losses of concern are the "high frequency losses" which are of two types:

a) those resulting from space harmonics in the machine causing what are usually called stray losses, and

b) those caused by time harmonics in the converter excitation applied to the machine resulting in time harmonic losses.

The stray losses must be carefully considered since they result from space harmonic effects which occur at multiples of the fundamental frequency. Thus, as the fundamental frequency is increased these losses increase and, in general, they increase much more rapidly than the power output which varies linearly with fundamental frequency. The time harmonic losses clearly are an important additional loss and a fundamental issue here is how does increasing the time harmonic frequency affect these losses.

The body of the report is divided into two major parts which consider these two loss types in detail. Expressions for the important loss components are presented and discussed to allow evaluation of their relative importance in high frequency induction machines. The major findings and conclusions are presented in general terms in this introductory section of the report.

1.2. Stray losses

The stray losses are high frequency losses in the machine caused by space harmonics in the air gap flux wave. The primary causes of these space harmonics are the stator and rotor slot permeance variations and the mmf step harmonics. These losses are related to the fundamental motor frequency and can be expected to increase in importance as the motor fundamental frequency is increased.

Although thirteen separate loss components are identified in the report, three of these components appear to be of particular importance in high frequency machines. In each of these the loss tends to be relatively large and to increase rapidly with motor fundamental frequency. Hence careful consideration must be given to motor design details which will help keep these loss components under control. The three components are discussed individually and design modifications which can assist in reducing these losses are described below. Methods for estimating most of the thirteen stray loss components and additional discussion of their causes and possible means of reduction are contained in Section 2 of this report.

1.2.1. No Load Surface Loss - The stator slot openings cause ripples in the main air gap flux wave which are stationary in space. As the rotor core moves past these ripples, eddy current (and hysteresis) losses are produced in the rotor iron. Because the frequency of the flux variation is relatively high (equal to stator slots per pole pair times fundamental frequency) the loss tends to be dominated by eddy current losses and is somewhat confined to the surface of the rotor core. A similar effect can be caused by the rotor slots resulting in stator surface losses but this component is often very small since the rotor slots are usually closed or semi-closed.

The methods of predicting surface losses are semi-empirical. The indications are that these losses increase less rapidly than the square of the fundamental frequency because of the existence of a hysteretic component and because the reaction field of the eddy currents tends to suppress the flux ripples. The increase is, however, usually more than linear with respect to frequency and the surface losses can be expected to be significantly more important in high frequency machines.

Methods for reducing the surface losses include reducing the stator slot opening, using more stator slots, enlarging the air gap and using low loss, thin laminations in the rotor core. Stator slot magnetic wedges have also been shown to be very effective.

1.2.2 Load Surface Losses - The air gap harmonic leakage fluxes resulting from the load current in combination with the mmf step harmonics and slot permeance variations also cause surface core losses. These losses are similar to the no load surface losses except that they occur in both the rotor and stator core surfaces and they are load dependent. The methods of predicting these losses are very similar to the no load surface loss methods but incorporate the ratio of load current to no load current. The frequency variation is therefore predicted to be the same as the no load surface losses. Methods for reducing these losses are similar to those for the no load losses except that magnetic slot wedges are less effective since the larger slot current tends to saturate the wedges and reduce their effectiveness.

1.2.3 Tooth Flux Pulsation Cage Circulating Current Losses - A portion of the ripple flux which causes the surface losses described above does penetrate the teeth and links with the rotor cage and the stator windings. While the resulting induced currents in the stator winding are small and cause negligible loss, those in the rotor are significant and cause an important component of the stray loss. Each rotor tooth is surrounded by a high conductivity damper circuit which opposes the ripple flux. There is a significant damping action which tends to reduce the ripple flux penetration into the teeth but which results in appreciable induced I^2R losses in the rotor cage. Because of the relatively high frequency, skin effect in the rotor bars is important.

These losses can be modelled in terms of harmonic equivalent circuits which interact with the fundamental frequency equivalent circuit. The various harmonic fields (slot

permeance harmonics, mmf harmonics) interact in different ways making the model rather complex. The basic theory is presented in Section 2 of the report along with theoretical curves which indicate that the losses are strongly dependent on the stator/rotor slot ratio. Skewing the rotor slots can reduce or eliminate the portion of these losses caused by the slot harmonics. However, the resulting increased tooth flux causes a significant increase in the tooth pulsation flux losses and interbar currents resulting from imperfect cage to core insulation also become a significant loss component. Because of the difficulty of predicting interbar current losses, it is difficult to predict the losses associated with skewing. It appears, however, that skew can generally be expected to increase losses.

Methods for reducing the cage losses caused by flux pulsation include those listed earlier plus an appropriate choice of stator/rotor slot ratio. In general, strictly from a loss perspective, using fewer rotor than stator slots offers a considerable benefit and skew should be avoided.

1.3. High Frequency Time Harmonic Losses

An important issue in the type of system under consideration, and in modern power electronic motor controls in general, is the question of the effect increasing the time harmonic frequency has on time harmonic motor losses. There are many good reasons relating to control characteristics and motor acoustic noise which argue for high carrier frequency in the inverter. Opposing these arguments is the possibility of high motor losses caused by the high time harmonic frequency of the carrier. The primary goal of the analysis in the report is to evaluate the influence of frequency on these losses. In particular, the analysis is focused on converters which place a substantial portion of the harmonic energy at relatively high frequencies; in the range of 20 Khz or higher. The major findings of the analysis in Section 3 are as follows.

1.3.1 Conductor Losses - At harmonic frequencies skin and proximity effects become very significant factors in determining conductor losses. For rectangular slots, the variation of the conductor resistance and inductance with frequency follows the general pattern illustrated in Fig 1.1.

The initial change in R and L as frequency increases is rapid, being approximately dependent on f^2 . This region occurs where the skin depth and conductor depth are of the same order of magnitude. As the frequency continues to increase, the rate of change decreases and the variation ultimately becomes proportional to $f^{1/2}$ as the skin depth becomes small compared to conductor depth. These results apply only to the portion of the conductors in the slots.

The conductor losses are given by

$$P_{rv} \approx I_v^2(R_s + R_r) \approx \left(\frac{V_v}{2\pi f_v L_\sigma}\right)^2 (R_s + R_r) \tag{1.1}$$

where

I_v = harmonic current

V_v = harmonic voltage

L_σ = total leakage inductance

R_s = stator resistance

R_r = rotor resistance

f_v = time harmonic frequency

It is clear that for a fixed value of I_v skin effect will increase the conductor losses. However, for a fixed value of V_v the inverse square frequency dependence of the current tends to compensate for the resistive increases resulting from skin effect. While it is true that the leakage inductance L_σ is reduced by skin effect, this reduction is much less than

might be expected since only the slot portion of the inductance is affected. Measurements on actual machines indicate that L_σ is reduced to 0.5 to 0.3 of the normal value at f_v = 20 Khz [Ref.10, Part 3]. A useful approximation is to take

$$L_\sigma \approx K_L f_v^{-0.16} \tag{1.2}$$

as the frequency dependence of L_σ [Ref.10, Part 3].

Since the single conductor cage winding typically exhibits skin effect changes even at the fundamental frequency, for harmonic frequencies the variation is well into the frequency range where R_r follows an $f_v^{0.5}$ frequency dependence (the end ring also exhibits an increasing resistance because of the way the bar currents enter the ring). The rotor conductor losses thus vary approximately as

$$P_{rrv} \approx \left(\frac{V_v}{2\pi f_v K_L f_v^{-0.16}}\right)^2 K_r f_v^{0.5} \sim \frac{V_h^2}{f_v^{1.2}} \tag{1.3}$$

and thus drop somewhat faster than inverse to the harmonic frequency. This strong dependence clearly indicates that the rotor conductor losses drop significantly as the harmonic frequency increases.

The stator winding behavior is, however, quite different. Typically the wire size is such that very little skin effect occurs at fundamental frequency. As the harmonic frequency increases, the initial increase in resistance can be in the f_v^2 region with the result that (using the approximation in Eq. 1.2) the stator losses initially behave as

$$P_{rsv} \sim V_v^2 f_v^{0.3} \tag{1.4}$$

and therefore can exhibit a moderate increase as f_v increases. This creates a very different conductor loss distribution between rotor and stator and can lead to increased stator winding temperature. The loss distribution within the stator slot is also non-uniform with the uppermost conductors having the highest loss. As the harmonic frequency continues to increase, the rate of rise of the stator resistance decreases and eventually approaches that of the rotor as expressed in Eq. (1.3). The analysis in Part 4 of the report provides a means of modelling these changes and estimating the stator loss variation. It is, however, true that for sufficiently high harmonic frequencies the total stator conductor loss decreases with approximately an $f_v^{-\alpha}$ dependence where α is approximately 1.2, the same as the rotor loss in Eq. (1.3). There is, therefore, a significant reduction in total conductor I^2R loss as the frequency of the time harmonic voltage excitation increases for frequencies where the skin depth is small compared to the conductor depth.

1.3.2 Core Losses - The core losses associated with high frequency time harmonics are influenced by a number of factors which combine to make predictions very difficult. These factors include the following four principal effects:

1) because the motor slip is very nearly unity for the higher time harmonics, the only significant flux in the machine is leakage flux.
2) for frequencies where the skin depth in the core material is small compared to the lamination thickness, the flux only penetrates the core to approximately a skin depth.
3) the redistribution of the conductor currents caused by skin effect alters the leakage paths.
4) the eddy currents in the core material can set up a significant reaction field which opposes the inducing field.

The leakage flux distribution associated with the high slip operating condition common to all high frequency time harmonics is illustrated in Fig. 1.2. As indicated by the equivalent circuit shown in the figure, the air gap flux and the rotor leakage flux are very nearly equal under this condition with the result that there is virtually no rotor core flux (Fig. 1.2c). The core losses therefore tend to be concentrated in the stator teeth and portions of the stator core near the stator slot bottoms. There is also some loss in the rotor teeth caused by the rotor leakage flux. Note that the usual concept of rotor leakage flux encircling the rotor conductor (Fig. 1.2b) is inappropriate for core loss considerations since the loss is proportional to B^2. The usual concept, which is based on superposition, is quite acceptable for calculation of leakage but must be abandoned when core losses are of interest.

The basic variation of the core losses with frequency can be explored using the usual core loss model described by

$$P_c = P_h + P_e = \left[k_h B^n f + k_e B^2 f^2\right] V_{ol} \tag{1.5}$$

where

P_c = total core loss

P_h = hysteresis loss

P_e = eddy current loss

B = flux density

f = frequency

V_{ol} = volume of core

K_h, k_e = material dependent constants

n = hysteresis exponent, typically $n \approx 1$ to 1.5

Although this model only applies to the simple case where:

i) there is negligible reaction field - i.e. B is the pre-existing field and does not change as a result of eddy currents,

ii) the flux is uniform - i.e. no skin effect,

it serves as a useful representation if the primary effects of the reaction field are included separately.

In the time harmonic situation the total leakage flux is directly determined by the time harmonic applied voltage V_v

$$\phi_v = k_v \frac{V_v}{f_v} \tag{1.6}$$

and, conceptually, the time harmonic flux density is then given by

$$B_v = \frac{\phi_v}{A_l} = k_v \frac{V_v}{f_v A_l} \tag{1.7}$$

where A_l is the effective area of the leakage flux path. While A_l is clearly different for different portions of the leakage path, it will generally be sufficient for an overall analysis to consider an average area for the entire path. A more detailed analysis is contained in Part 3 of the report.

1.3.3 Reaction field effects - As noted above, the eddy current reaction field has two basic effects; reducing the internal B field and redistributing the field (skin effect). For the leakage fields under consideration, the reduction of the field will not take place since the total leakage flux is a fixed value determined by Eq. (1.6). Thus, any tendency to reduce

the flux will simply result in additional motor current to maintain the flux at the required level. One effect of the eddy current reaction field is, therefore, to reduce the leakage inductance. This reduction is in addition to the reduction caused by conductor skin effect.

The second effect of redistributing the leakage flux will tend to confine the leakage fields to local regions near the slot and air gap surfaces. To a first approximation, the field will only penetrate the lamination to one skin depth δ_{fe}

$$\delta_{fe} = \sqrt{\frac{\rho_{fe}}{\pi \mu_{fe} f_v}} \tag{1.8}$$

where

ρ_{fe} = resistivity of iron

μ_{fe} = permeability of iron

and the B field can be assumed to be uniform over this distance and zero beyond. This concept can be used to estimate the effective area A_l as a function of frequency.

1.3.4 Frequency dependance of core losses - To examine the frequency dependence of the time harmonic core loss, three limiting cases are considered.

Case 1 - No conductor skin effect, $\delta_{fe} >> d$, d = lamination thickness. This case corresponds to low time harmonic frequencies with, for example, a wound rotor motor. The core losses would be given by Eq. (1.5) with B evaluated from Eq. (1.7) with A_l = constant (i.e. no change in flux paths). The result is

$$P_c = \left(K_{h1} V_v^n f^{1-n} + K_{c1} V_v^2\right) A_l \, l \tag{1.9}$$

where K_{h1} and K_{c1} are constants and l is the motor stack length.

For a constant time harmonic excitation voltage V_v, the loss depends on n, the hysteresis loss exponent. Since n is usually greater than one, the loss will decline with frequency. Usually the hysteresis loss is small compared to the eddy current loss at higher frequencies and, hence, to a first approximation the total core losses would be nearly independent of the time harmonic frequency.

Case 2 - Including conductor skin effect, $\delta_{fe} >> d$. The major influence of conductor skin effect on core loss is in the rotor of cage machines. As the rotor current is forced to the top of the rotor bar by conductor skin effect, the rotor leakage flux is also forced upward toward the rotor surface (tooth tops). This has the effect of reducing the area through which the rotor leakage flux must pass, thus tending to increase B. It also reduces the volume of core material which is carrying flux, but these two effects do not completely cancel. A third effect is the change in ratio between the stator and rotor leakage inductances and hence in the flux ratio. As the rotor leakage inductance decreases, more of the total leakage flux is forced to exist in the stator leakage paths, thus increasing the stator leakage flux.

While the actual change in losses is very much motor design dependent, it seems clear that forcing more of the total leakage flux into stator paths will increase the losses because of the B^2 dependence of the eddy current losses. It is also true that this effect is already significant in most machines under 60 hz, line start conditions. At the extreme, the rotor leakage flux will be confined almost entirely to the rotor tooth tops very much like the so called zig-zag leakage flux. For most machines, it is likely that even low frequency time harmonics (i.e. 5th and 7th of fundamental) will result in all rotor flux confined to such a surface layer with additional increases of frequency having rather small impacts on the distribution of flux (as a result of rotor bar skin effect). With the assumption of fixed flux

paths, the eddy current losses are independent of frequency since the frequency increase is exactly compensated by the decrease in flux density. The hysteresis losses will decrease and eventually become negligible.

In general, then, one would expect a decrease in core loss at fairly low time harmonic frequencies and a leveling out at high frequencies. Depending on the relative importance of hysteresis losses and the flux redistribution discussed above, the net reduction in total loss at the lower time harmonic frequencies will vary from machine to machine.

Case 3 - Including conductor skin effect, $\delta_{fe} < d$. When the time harmonic frequency is large enough so the skin depth in the iron δ_{fe} is small compared to the lamination thickness, the leakage flux is confined to a skin depth layer at the iron surface. The situation is now somewhat as depicted in Fig. 1.3. The region of highest core loss is at the bottom of the stator slots where the total leakage flux must be accommodated. The flux level along the stator slot walls drops off as the stator tooth top is approached and the flux in the air gap and rotor surface is the rotor leakage flux.

The loss for this condition can be approximated by neglecting the hysteresis loss and assuming the area available for the leakage flux is limited to one skin depth. The flux density will then be given by Eq. (1.7) with $A_l = l\ \delta_{fe}$

$$B_v = k_v \frac{V_v}{f_v l\, \delta_{fe}} = \frac{k_v V_v}{l\sqrt{\frac{\rho_{fe} f_v}{\pi \mu_{fe}}}} = K f_v^{1/2} \tag{1.10}$$

and the core loss becomes (since $V_{ol} \sim \delta_{fe}$)

$$P_{cv} \approx k_e B_b^2 f_v^2 V_{ol}$$
$$\approx K_1 V_v^2 f_v^{1/2} \tag{1.11}$$

Thus, for a fixed value of time harmonic excitation voltage, the eddy current losses tend to increase as $f_v^{1/2}$, a slow but steady growth. This slow growth can be expected to persist until some other effect (capacitive currents) becomes significant.

It is also interesting to express the loss in terms of the physical parameters of the core, the resistivity and permeability. In terms of the k_e and δ_{fe} the loss is

$$P_{cv} = K_2 \frac{k_e V_v^2}{\delta_{fe}} \tag{1.12}$$

and since

$$k_e = \frac{K_e}{\rho_{fe}} \tag{1.13}$$

$$P_{cv} = K_3 \frac{V_r^2 f_v^{1/2} \mu_{fe}^{1/2}}{\rho_{fe}^{3/2}} \tag{1.14}$$

1.3.5 Total time harmonic losses - The discussion and analysis indicates that for a fixed time harmonic excitation voltage the conductor losses tend to decrease rapidly (as $f_r^{-1.2}$) and the core losses increase slowly (as $f_v^{1/2}$) as the frequency increases. This implies there is some time harmonic frequency where the total losses are a minimum as illustrated in Fig. 1.4. The location of this minimum is design dependent, the low frequency ratio of core and copper losses being an important parameter.

1.3.6 Skin depth - The approximate frequencies where the high frequency approximations given in Eqs. (1.3) and (1.11) are first applicable depend on the ratio of conductor skin

depth to conductor depth and lamination skin depth to lamination thickness. Table 1.1 gives the skin depth for a range of frequencies to assist in estimating the onset of "high frequency behavior".

Table 2.1

Skin Depth in Copper, Aluminum and Core Steel

$$\delta = \sqrt{\frac{\rho}{\pi \mu f}}$$

	$\rho_{cu} = 0.205 \times 10^{-7}\ \Omega m$ $\mu_{cu} = \mu_o$		$\rho_{al} = 0.425 \times 10^{-7}\ \Omega m$ $\mu_{al} = \mu_o$		$\rho_{fe} = 5.00 \times 10^{-7}\ \Omega m$ $\mu_{fe} = 800 \times \mu_o$	
f	δ_{cu}		δ_{al}		δ_{fe}	
hz	mm	mils	mm	mils	mm	mils
60	9.31	367	13.4	527	1.63	64.3
500	3.22	127	4.64	183	0.56	22.0
1000	2.28	89.8	3.28	129	0.40	15.9
5000	1.02	40.2	1.47	57.9	0.18	7.0
10,000	0.72	28.3	1.04	41.0	0.12	4.8
20,000	0.51	20.1	0.73	28.7	0.089	3.5
40,000	0.36	14.2	0.52	20.5	0.062	2.5

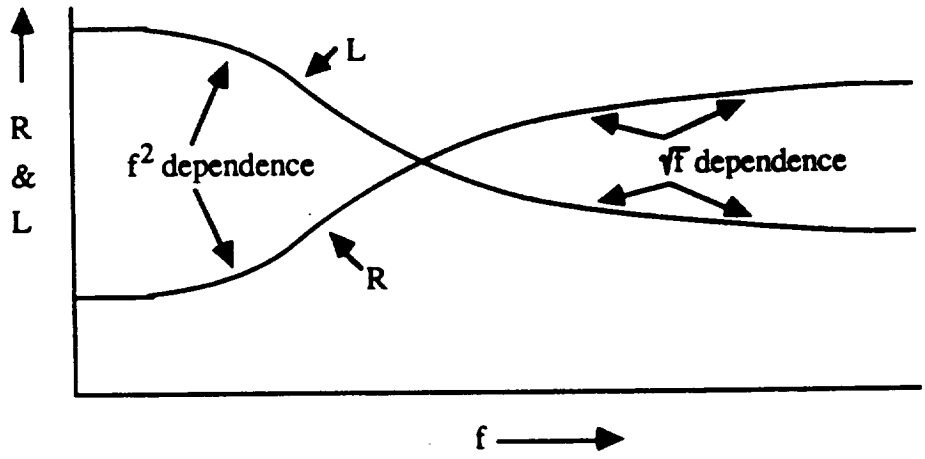

Fig. 1.1 Skin Effect R and L Variation for Conductors in Rectangular Slots

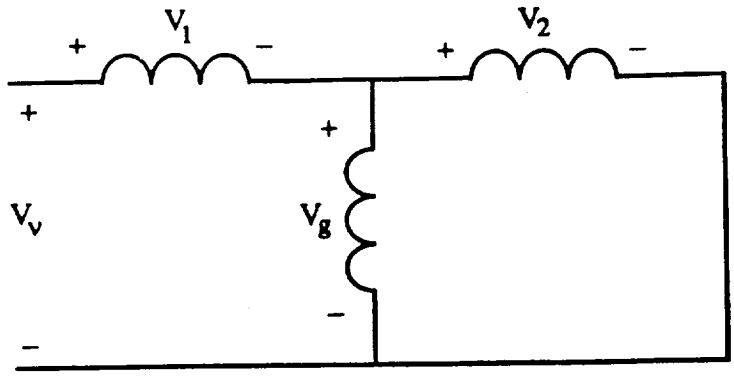

V_v – applied voltage V_1 – stator leakage voltage

V_g – air gap voltage V_2 – rotor leakage voltage

(a)

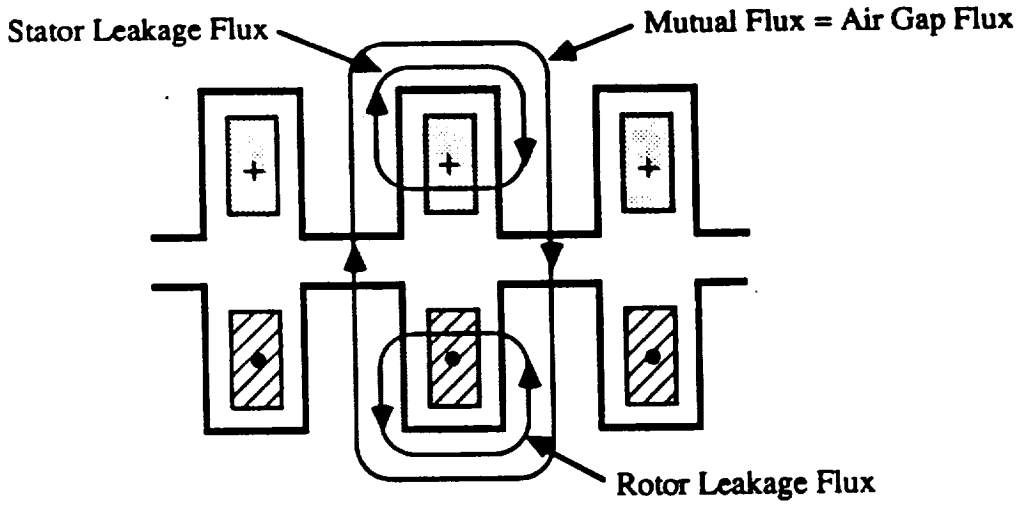

(b)

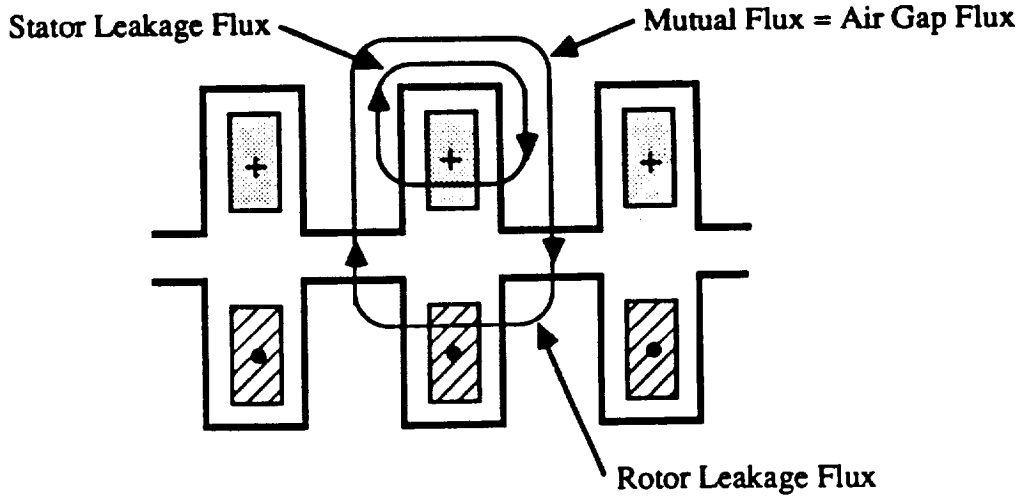

(c)

Fig.1.2 Equivalent Circuit and Flux Paths for Time Harmonics (slip ≈ 1.0)

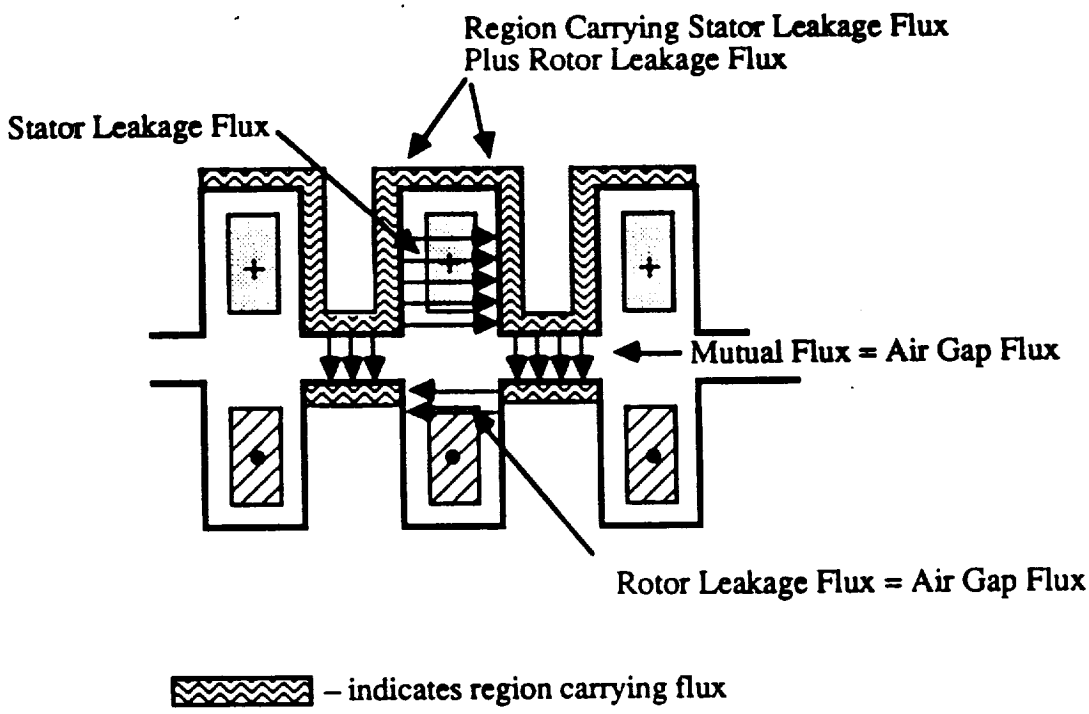

Fig.1.3 Flux Paths for High Frequency Time Harmonic Showing Effect of Skin Effect in Laminations

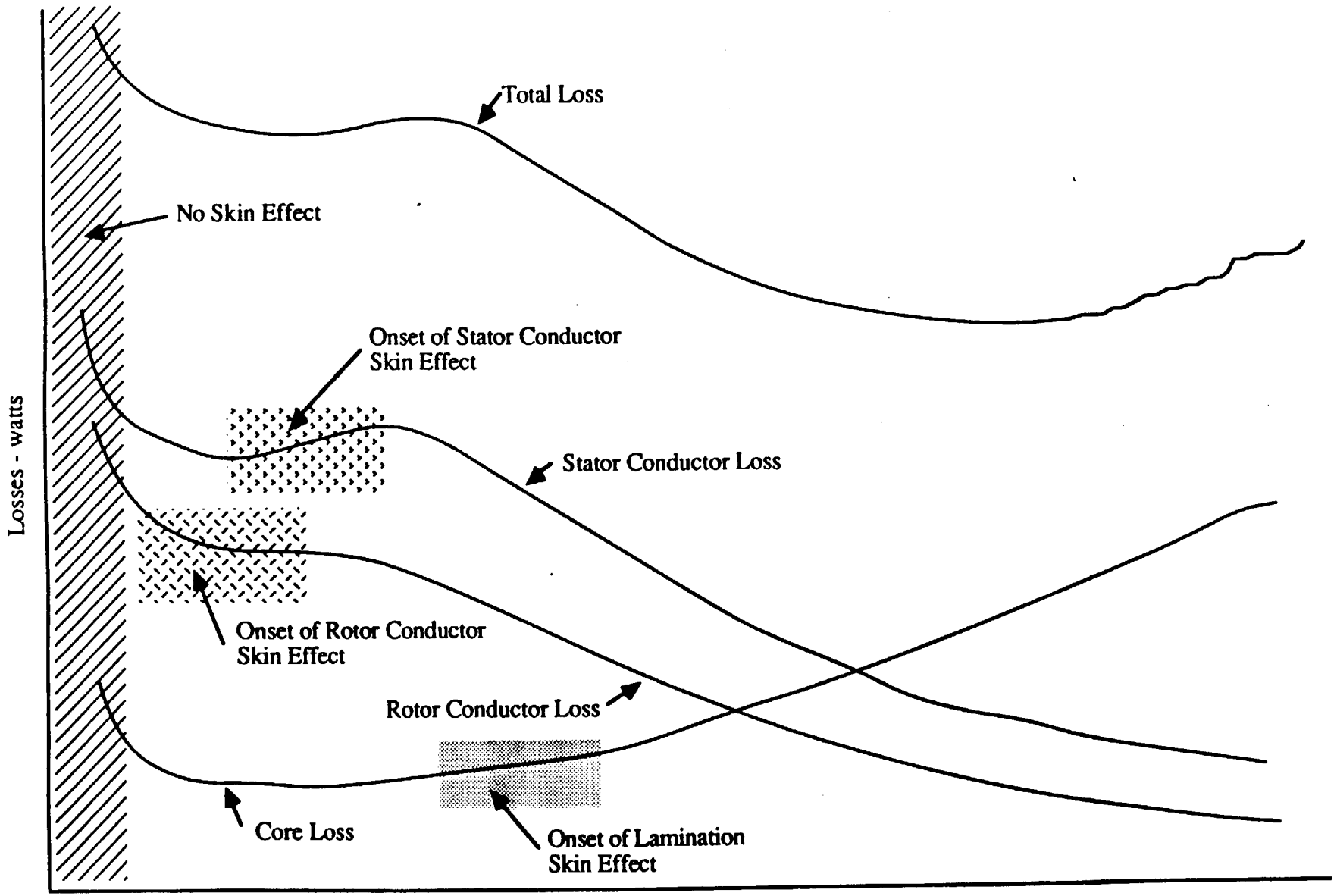

Fig.1.4 Variation of Time Harmonic Induction Motor Losses with Frequency for Constant Time Harmonic Voltage

HIGH FREQUENCY LOSSES IN INDUCTION MOTORS

Section 2

STRAY LOSSES IN INDUCTION MOTORS

-A Review of the State-of-the-Art-

Syed A. Nasar

Zhenxing Fu

Donald W. Novotny

July 1989

Section 2

Stray Losses in Induction Motors

2.1. Summary

This section of the report presents a review of the state-of-the-art concerning high frequency stray losses in induction motors. These losses are distinct harmonic losses arising from the stator and rotor geometries such as slot and tooth permeances, and discontinuous current distributions and are not necessarily generated because of time harmonics in the input waveforms.

A narrative of the origins of the above-mentioned losses is given and an explanation of most of the formulas used in loss calculations is presented. A numerical example is given to illustrate the application of the formulas. These results of numerical computations are compared with some of the results given by experienced designers, as empirical values. Finally, a comprehensive bibliography is included.

Because much of the literature was published before SI units were prevalent, original results are retained in English (FPS) units. Most graphs and charts are given in these units. Finally, the literature on the subject is rich and room for further original work is rather limited.

2.2. Introduction

The principal effects of harmonic losses (also called high frequency stray no-load and stray-load losses) in an induction motor are: heating of various machine components; reduction in output torque; noise; cusps in torque/speed curves; reduction in motor efficiency; and an ultimate derating of the machine. Even a small increase in harmonic losses over the predicted design value can have a severe impact on motor utilization resulting in economic disadvantages to both manufacturer and consumer. Literature on the subject began appearing around the turn of the century. Whereas numerous papers (and a few books) have been published on harmonic losses in induction motors, only selected papers, having a direct bearing on this report, are included in the bibliography.

2.3. Classification of high-frequency harmonic (or stray) losses

In an induction motor, stray losses are the additional high frequency losses due to the stator and rotor slotting, distributed (stepped) stator and rotor mmfs, and slot and overhang leakages. According to the nature of these losses, they may be classified as follows:

(i) Surface core loss in the stator.

(ii) Surface core loss in the rotor.

(iii) Pulsation core loss in stator teeth.

(iv) Pulsation core loss in rotor teeth.

(v) Copper (I^2R) loss in the cage winding.

(vi) Core and copper losses due to skewing.

(vii) Core and copper losses due to slot and overhang leakages in the stator core and windings.

Although surface and tooth pulsation losses are mentioned individually, it has long been recognized [53] that the pulsation losses consist of the core surface losses occurring just below the surface of the tooth tips due to the passage of the slots of the other member and are practically the same as pole-face losses. The tooth pulsation losses are caused by the high frequency pulsations of flux extending the entire length of the teeth and a little way into the core due to the reluctance changes in the airgap as the slots of one member pass the teeth of the other. Thus, the distinction between surface and tooth-pulsation losses is rather arbitrary.

According to the origins of the high-frequency losses, they may be grouped as:

(A) Stray no-load losses

(B) Stray load losses

where Group (A) losses are related to the irregularities of the main exciting flux primarily due to the permeance variations. Group (B) losses are caused partly by the effects of the current distribution in the machine producing a stepped mmf in the airgap and partly by the leakage fluxes. In order to understand this grouping, we refer to the principal harmonics in the airgap fields and their general consequences. These are:

(i) Field form harmonics due to pole shaping and magnetic saturation leading primarily to stray no-load losses.

(ii) Slot permeance harmonics due to slot openings resulting in stray no-load losses.

(iii) Slot mmf harmonics due to mmfs across slot openings producing stray-load loss (primarily because of zig-zag leakage flux).

(iv) Phase-belt harmonics due to the distribution of mmfs in phase belts, leading to stray-load losses.

It is to be noted that slot mmf harmonics and phase-belt harmonics together constitute the airgap leakage harmonics.

On the basis of the above-mentioned harmonics, Table 2.1 gives a detailed classifica-tion of the various stray losses belonging to Groups A and B. To understand the physical phenomena governing some of the components listed in Table 2.1 we further discuss the surface losses and tooth-pulsation losses.

2.3.1. Surface core losses

Surface core losses are eddy-current losses caused by surface flux pulsations, and occur just below the surface of tooth top. Surface flux pulsation is quite similar to the pole-face flux variation in a salient-pole machine, and is due to the movement of the tooth over the pole face. The flux does not penetrate the entire length of the tooth, but disappears at a certain distance from the tooth tips (see Fig. 2.1).

The magnitude of the surface flux pulsation depends on the fringing of flux in the airgap, and thus on the geometry of the flux path. Consequently, surface flux pulsations in the rotor increase with an increase in the width of the rotor tooth tip [41], but decrease with an increase in the airgap. At the same time a relatively narrower stator slot causes lesser surface flux pulsation in the rotor. With closed rotor slots, the stator surface flux pulsations are practically negligible.

2.3.2 Tooth pulsation core losses

Tooth pulsation core losses are eddy-current losses caused by tooth flux pulsations which extend through the entire length of the tooth. If an individual stator or rotor tooth is considered, as teeth of opposite member pass by, the permeance of the path terminating at

Table 2.1. Summary of basic harmonic losses.

Class		Component	Cause (what?)	Phenomenon (how?)	Type	Location	Reference to text
A Stray no-load losses	A1	Surface core losses	Permeance variation (harmonic flux)	Main flux causes surface flux pulsation due to passing teeth	Eddy-current core losses	Stator and rotor core surfaces	eq. (1)
	A2	Tooth pulsation losses	Permeance variation due to relative tooth position	Pulsation of main flux in teeth due to relative motion between stator and rotor teeth	Eddy-current core losses	Stator and rotor teeth	eq. (2)
	A3	Tooth pulsation cage circulating current losses	Permeance variation due to relative tooth position	Tooth pulsation fluxes induce harmonic currents in rotor cage bars and hence I^2R	I^2R (copper) losses	Rotor cage bars and rings	eq. (12)
B Stray load losses	B1	Surface core losses	Gap-leakage (harmonic) flux	Gap-leakage flux causes surface flux pulsations	Eddy-current core losses	Stator and rotor core surfaces	eqs. (15) and (16)
	B2	Tooth pulsation losses	Gap-leakage (harmonic) flux	Pulsations of gap leakage fluxes in teeth due to relative motion between stator and rotor teeth	Eddy-current core losses	Stator and rotor teeth	eq. (2)
	B3	Tooth pulsation cage circulating current losses	Gap-leakage (harmonic) flux	Tooth pulsation fluxes due to gap leakage induce harmonic currents in rotor bars	I^2R (copper) losses	Rotor cage bars and rings	eq. (19)
	B4	Stator-harmonic cage circulating current losses	Gap leakage (harmonic) flux	Lower order harmonics (5th, 7th, etc.) of gap leakage flux induce currents in the rotor cage	I^2R (copper) losses	Rotor cage bars and rings	eqs. (20) and (21)

Table 2.1. (continued)

Class		Component	Cause (what?)	Phenomenon (how?)	Type	Location	Reference to text
B Stray load losses	B5	Stator-slot eddy-current losses	Slot-leakage flux	Slot-leakage flux induce currents and cause additional main-frequency eddy-current losses in stator windings	I^2R (copper) losses	Stator windings	negligible
	B6	Stator over-hang eddy-current losses	Stator winding overhang leakage flux	Stator winding overhang leakage fluxes partly link with stator core and structural parts and produce main-frequency core losses	Eddy-current core losses	Stator core and structural parts	eq. (22)
	B7	Rotor slot eddy-current losses	Slot-leakage flux	Rotor slot leakage fluxes induce currents and cause additional main-frequency eddy-current losses in copper at high slips	I^2R (copper) losses	Rotor cage bars and rings	neglected
	B8	Rotor over-hang eddy-current losses	Rotor over-hang leakage flux	Rotor winding overhang leakage fluxes partly link with rotor structural parts and produce eddy-current losses a high slips	Eddy-current core losses	Rotor core and structural parts	neglected
	B9	Skew-leakage iron losses	Skew-leakage flux	Skewed rotor slots cause a phase displacement of the mmf waves of the stator and the rotor at the two ends resulting in skew-leakage flux	Eddy-current core losses	Stator and rotor surfaces	eq. (23)
	B10	Rotor-slot mmf stator-tooth pulsation losses	Rotor-slot mmf harmonics	Rotor-slot mmf harmonics cause flux pulsation in stator teeth leading to eddy-current core losses. However, these losses are negligible in normal machines	Eddy-current core losses	Stator teeth	negligible

the tooth in question oscillates with every passing tooth (Fig.2.2). The position for maximum permeance and maximum flux is shown in Fig.2.2(a), and Fig. 2.2(b) shows the position for minimum permeance and minimum flux.

Obviously, the flux in the tooth core pulsates with an amplitude that depends on the slot fringing. Because the fringing of flux increases with tooth saturation, tooth pulsation flux and tooth pulsation losses decrease with saturation.

2.4 Principal harmonic fields in the airgap

Because the above-mentioned losses arise from harmonic fields, it is advantageous to segregate the fields into the following:

(i) The fundamental field which is of the form $A\cos(Px-\omega t)$.

(ii) Stator slot-permeance harmonic fields of the form $B\{\cos[S-P)x+\omega t] + \cos[(S+P)x-\omega t]\}$.

(iii) Phase-belt harmonics which are of the form $C\cos[(2q-1)Px+\omega t]$ and $D\cos[(2q+1)Px-\omega t]$.

(iv) Stator slot mmf harmonic fields of the form $E\cos[(S-P)x+\omega t]$ and $F\cos[(S+P)x-\omega t]$.

(v) Rotor slot harmonics which are of the form $G\cos[(R-P)x+(\omega-RN)t]$ and $H\cos[(R+P)x-(\omega+RN)t]$.

(vi) Rotor mmf harmonic fields having the form $J\cos[(R-P)x+(\omega-RN)t]$ and $K\cos[(R+P)x+(\omega+RN)t]$.

(vii) Other higher-order fields and harmonic fields due to saturation.

In (i)-(vii) we have: P = number of pole pairs; S = number of stator slots; R = number of rotor slots; N = rotor mechanical speed, q = number of phase-belts.

2.5. Formulas for loss calculations

We now consider in some detail the various losses presented in Table 2.1. We also discuss the formulas and procedures for calculating these losses.

2.5.1. Stray no-load losses

These losses belong to Group A, Table 2.1, and consist of the following components.

A1 Surface core losses [5]

Slot frequency pulsation in the flux density around the airgap of an induction motor is caused by slot currents. As mentioned earlier, these pulsations cause surface losses. For analysis, the airgap flux density distribution is expressed as a series of rotating harmonic fields. The harmonic fields have pole numbers equal to (2S'±1) and (2R'±1) times the fundamental poles, where S' and R' are, respectively, the number of slots per pole on the stator and rotor.

It is clear from the above discussion that the surface core losses occur in the stator as well as in the rotor. However, as we shall see later, surface losses in the stator are generally negligible.

Empirically, the rotor surface loss due to the stator slot openings is given by:

$$W_{s0} = 2D_1 L \left(\frac{B_g}{100}\right)^2 K_{pf} C_{s2} \lambda_1 \, W \qquad (2.1)$$

where D_1 = airgap diameter, in;

L = core length, in;

B_g = average flux density over the effective gap area, kilolines/in^2;

K_{pf} = pole-face loss coefficient for stator slot openings, from Fig. 2.3;

C_{s2} = rotor iron loss coefficient, from Fig.2.4, at 100,000 lines/in^2, in W/in^3 for stator slot frequency; and

λ_1 = $\pi D_1/S$(poles) = stator slot pitch, in.

μ_r = 800 (assumed constant).

It is to be noted that, since most of the losses corresponding to Fig.2.4 are eddy-current losses (which are proportional to the square of frequency and square of lamination thickness), Fig. 2.4 may be scaled for different frequencies and lamination thickness. Obviously, for materials other than 2.5% silicon steel a different set of curves must be obtained accounting for the change in resistivity. [See Appendix A for an alternative analytical approach]

Turning now to Eq. 2.1, we observe that whereas the formula is empirical, it is dimensionally correct and is based on a broad experience of earlier investigators. The pole-face coefficient K_{pf} was obtained by first analyzing the flux distribution curve, shown in Fig. 2.5, into a Fourier series and then multiplying each harmonic by a weighting factor equal to the square root of its order and finally taking the square root of the sum of the squares of all the components to obtain the effective value of the fundamental. It is arbitrarily assumed that the depth of the flux penetration is one-eighth of the harmonic pole pitch and that the radial flux density decreases linearly with depth.

The stator surface loss due to the rotor slot openings is given by an expression similar to Eq. 2.1 where C_{s2} is replaced by C_{s1} and λ_1 by λ_2. However, for rotors with closed and semi-closed slots, K_{pf} (Fig.2.3) tends to zero resulting in a negligible stator surface loss. Also, C_s in Eq.2.1 decreases with w/g.

A2. Tooth pulsation losses [16,17,48]

Tooth pulsation losses occur in the rotor and the stator of the induction motor.

Following the approach given in reference [17], Richter's result [48] may be used to calculate the rotor teeth pulsation losses from:

$$W_{tk} = B_{tk}^2 \left[\sigma_h \left(\frac{f_{2k}}{100} \right) + \sigma_e \left(\frac{f_{2k}}{100} \right)^2 \right] \text{W/kg} \tag{2.2}$$

where σ_h and σ_e are experimentally determined material constants [48, 51] f2k is the kth harmonic frequency induced in the rotor, and B_{tk} is the kth harmonic rotor tooth flux density, T. The formula above is also partially empirical.

From Eq. 2.2 above, the total loss is given by

$$W_{t0k} = B_{tk}^2 \left[\sigma_h \left(\frac{f_{2k}}{100} \right) + \sigma_e \left(\frac{f_{2k}}{100} \right)^2 \right] v_{t2} \text{ W} \tag{2.2a}$$

where v_{t2} = weight of rotor teeth;

$$B_{tk} = K_{tk} B_k \frac{\lambda_2}{w_2} \frac{\sin \beta_k}{\beta_k} \tag{2.2b}$$

λ_2 = rotor tooth pitch;

w_2 = rotor tooth width;

$$\beta_k = \frac{kP\lambda_2}{D_2}$$

k = order of harmonic

P = number of pole pairs

D_2 = rotor diameter

$$k_{tk} = 1 - \frac{X_{mk} + X_{2dk}}{X_{mk} + X_{2dk} + X_{mk}\left(\frac{1}{k_{sk}^2} - 1\right) + X_{slot}} \qquad (2.2c)$$

X_{mk} = magnetizing reactance of kth harmonic, Ω.

X_{2dk} = differential harmonic leakage reactance for kth harmonic, Ω.

k_{sk} = skew factor of kth harmonic

X_{slot} = slot leakage reactance, Ω.

Furthermore,

$$X_{2dk} = k_{sdl}k_{dlk}\tau_{2dk}X_{mk} = \text{differential harmonic leakage reactance for kth harmonic, } \Omega \qquad (2.2d)$$

where

$$k_{dlk} = \tanh\left(\frac{h}{2\delta}\right) / \left(\frac{h}{2\delta}\right) = \text{damping factor for differential leakage} \qquad (2.2e)$$

h = lamination thickness

$\delta = \sqrt{\rho/\omega_k\mu}$ = skin depth

k = order of the harmonic

$$\tau_{2\delta k} = \left[\frac{\pi Pk/R}{\sin(\pi Pk/R)}\right]^2 - 1 \qquad (2.2f)$$

with R = total number of rotor slots. Also, in the above calculations $\mu = \Delta B/\Delta H$ should be used.

Stator tooth pulsation losses are also given by an expression similar to Eq. 2.2 where f_{2k} is replaced by f_{1k} and σ_h and σ_e correspond to the stator material. Again, it is usually negligible with closed or semi-closed rotor slots.

A.3. Tooth pulsation cage circulating current-losses [4]

These losses are also called rotor I^2R loss due to permeance harmonics [3]. The flux pulsation is measured by the flux pulsation ratio β shown in Fig. 2.5. This K_{pf} is calculated by a slightly different procedure as indicated in the text. The two values of K_{pf} are the same for $1 < w/g < 6$. For values of $w/g > 6$, the K_{pf} given by (3) gives slightly higher values compared to those given by Fig.2. 3. It has been shown [5] that the constant K_{pf} (Recall K_{pf} from Eq. 1) is given by:

$$K_{pf} = \left(\frac{\beta}{2-\beta}\right)^2 \qquad (3.3)$$

where β is the double amplitude of flux pulsation shown in Fig. 2.5.

Curves from reference [3] give magnitudes of ripples, caused by slot openings, in the no-load airgap flux. Figure 2.5 shows the flux pulsation, which is expressed as the ratio (β) of the dip to the maximum flux density in the airgap. For this dip, there are two slot permeance harmonic fields, having$(S \pm P)$ pairs of poles, where P is the number of pole pairs of the fundamental, and S is the number of stator slots. According to reference [4], the backward and forward fields referred to the rotor are given by, respectively,

$$B_b = \frac{1}{2} HP_0K \sin\left\{(S+P)x + \left[\frac{S+P}{P}(1-s)-1\right]\omega t\right\} \tag{2.4}$$

and

$$B_f = \frac{1}{2} HP_0K \sin\left\{(S-P)x + \left[\frac{S-P}{P}(1-s)+1\right]\omega t\right\} \tag{2.5}$$

where

$$K = \frac{\beta}{2-\beta} \tag{2.6}$$

P_O = average permeance

s = slip

S = number of stator slots

P = number of fundamental pole pairs; and

H = amplitude of fundamental mmf.

The magnetizing reactances corresponding to the above permeance harmonics are:

$$X_{P(S-P)} = \frac{PK}{2(S-P)} X_M \tag{2.7}$$

$$X_{P(S+P)} = \frac{PK}{2(S+P)} X_M \tag{2.8}$$

These reactances are shown in the equivalent circuit of Fig. 2.6. It has been shown in reference [4] that the permeance harmonic fields do not have any appreciable effect on the magnetizing current. But, these fields induce S/P-times line frequency voltages in the rotor (at full speed $s \simeq 0$) resulting in an appreciable I^2R loss. To calculate this loss the parameters of the equivalent circuit (Fig. 2.6) must be known. These parameters are approximately given by [4]:

$$X_{M(S-P)} = \frac{P^2 X_M}{(S-P)^2} \tag{2.9}$$

$$X_{2(S-P)} = \frac{P^2 X_M}{(S-P-R)^2} \tag{2.10}$$

and

$$X_{2(S+P)} = \frac{P^2 X_M}{(S+P-R)^2} \tag{2.11}$$

Knowing these parameters, from Fig. 2.6, the induced rotor currents of the (S±P) permeance harmonics are calculated. Calling these currents $I_{2P(S+P)}$ and $I_{2P(S-P)}$, the I^2R loss due to permeance harmonic induced current is given by:

$$W_P = K_f R_{2B} \left[I^2_{2P(S-P)} + I^2_{2P(S+P)} \right]$$

$$= K_f R_{2B} C_P I^2_M \quad W \tag{2.12}$$

where K_f = the ratio of the ac to dc resistance of the rotor bars at a frequency S/P-times the line frequency; R_{2B} = dc resistance of the bars referred to the stator times the number of phases; and I_M = per phase magnetizing current. The constant C_p is the sum of the squares of the ratios of S-P and S+P permeance harmonic rotor currents to the magnetizing current.

Values of C_p for different number of stator slots per pole (S/2P), rotor slots per pole (R/2P), and various slot-width/gap (w/g) ratios are plotted in Figs 2.7 through 2.10. These loss constants are obtained from reference [4], and are valid for unskewed straight slots. Notice that the losses rise rapidly as R/S increases above one. If rotor slots are skewed one stator slot pitch, so that the voltages of the (S ± P) fields over one rotor bar length are almost zero, the induced currents will be greatly reduced provided there is adequate insulation between the bars. Otherwise rotor I^2R losses will increase considerably [16].

In Eq. 2.12, the loss W_P increases as the ratio R/S becomes greater than one. If R is very large compared to S, C_p approaches the limit 2. The curves in Figs. 2.7 through 2.10 show that markedly lower induced current losses occur when R < S.

2.5.2 Stray load losses

These losses belong to Group B of Table 2.1. We consider these losses in the order given in the table.

B.1. Surface losses [5]

The steps in the mmf wave due to the load current produce harmonic fields. The ratio of the mmf harmonic amplitude to the fundamental mmf is:

$$\frac{\text{mmf ripple}}{\text{fundamental wave}} = \frac{1}{(2S \pm 1)} \tag{2.13}$$

The ratio of the mmf harmonic to the permeance harmonic of the same order is given by:

$$\frac{\text{mmf harmonic}}{\text{permeance harmonic}} = \frac{2(2-\beta)}{\beta(2S\pm1)}\left(\frac{I}{I_0}\right) \tag{2.14}$$

where

I = stator load current, A; and

I_0 = stator no-load current, A.

In terms of these currents, Eq. 2.1 may also be written for the rotor surface loss on load as:

$$W_{SL2} = 2D_1L\left(\frac{I}{SI_0}\right)^2\left(\frac{B_g}{100}\right)^2 C_{s2}\lambda_1 \quad W \tag{2.15}$$

where it is assumed that $S >> 1$. The total rotor surface loss is, therefore, obtained by adding Eq. 2.1 and Eq. 2.15.

According to reference [5], to find the actual load surface losses, the phase angle between the permeance and mmf ripples of the same orders must be known. The two mmf ripples are in phase at the point of maximum current, and are zero at the zero point of the current wave, so that at no load their maximum combined values occur 90° away from the maxima of the combined permeance harmonics. It has been found that if the (2S-1) permeance and mmf harmonics come into phase at a given point, the (2S+1) harmonics will then be opposed in phase. Hence, the combined losses will be either of the form $(A+B)^2 + (A-B)^2$ or of the form $2A^2 + 2B^2$ where A and B denote the two kinds of

harmonics. In either case, the loss is the same as that obtained by calculating them independently and adding the results, as if they were always 90° out of phase.

Notice that in Eq. 2.1 and Eq. 2.15 we have assumed the loss to vary with B_g^2. However, saturation (if present) decreases the relative amplitude of high-frequency pulsations. Thus, Eq. 2.1 and Eq. 2.15 will predict high values under magnetic saturation.

By analogy with Eq. 2.15, the stator surface loss under load is given by

$$W_{SL1} = 2D_1L\left(\frac{I}{RI_0}\right)^2\left(\frac{B_g}{100}\right)^2 C_{s1}\lambda_2 \quad W \tag{2.16}$$

where

C_{S1} = stator iron-loss coefficient, from Fig. 2.4, at 100,000 lines/in^2 in W/in^3 for rotor slot frequency, and

λ_2 = rotor tooth pitch, in.

Hence, the total surface loss on load is obtained by adding Eq. 2.15 and Eq.2.16.

B2. Tooth pulsation losses [17, 48]

Stator and rotor tooth pulsation losses are similar to those discussed in Section 2.5.1 under Group A2. These losses are included in Eq. 2.2.

B3. Tooth pulsation cage circulating current losses [4]

The magnetizing reactances corresponding to the harmonic fields due to the steps in the stator mmf wave are represented by $X_{M(S\pm P)}$ in Fig. 2.6, and are given by

$$X_{M(S-P)} = \frac{P^2 X_M}{(S-P)^2} \tag{2.17}$$

$$X_{M(S+P)} = \frac{P^2 X_M}{(S+P)^2} \tag{2.18}$$

Proceeding as in Section 2.5.1, Group A3 the respective currents and losses are determined [4]. The total losses due to stator mmf harmonics are then given by:

$$W_M = K_f R_{2B}\left[I^2_{2M(S-P)} + I^2_{2M(S+P)}\right]$$

$$= K_f R_{2B} C_M I_1^2 \quad W \tag{2.19}$$

where K_f and R_{2B} have the same values as in Eq. 2.12, and C_M is the sum of the squares of the ratios of the slot mmf secondary currents to the line current. This constant is also plotted in Figs. 2.7 through 2.10. These losses are especially significant at high motor slip, and cause dips in the torque/speed characteristic at their synchronous speeds of [±1/R±S)]-times synchronous speed of the fundamental wave.

B4. Stator harmonic cage circulating-current losses [5]

Gap leakage fluxes cause rotor I^2R losses, which may be divided as follows:

Rotor I^2R loss due to zigzag leakage flux -

$$W_z = C m I_1^2 (k_s R_{2b}) \quad W \tag{2.20}$$

where C = loss factor taken from Fig. 2.7 through 2.10.

m = number of phases;

I_1 = stator current/phase, A;

k_s = skin-effect ratio for rotor bars at stator slot frequency, which is $2sf_1$, at synchronous speed; and

R_{2b} = per phase rotor bar resistance referred to the stator, Ω.

Rotor I^2R loss due to belt leakage flux

$$W_B = mI_1^2 k_m R_{2b}\left[\frac{1}{k_1^2}\left(k_{2m-1}^2 + k_{2m+1}^2\right)\right] \text{ W} \qquad (2.21)$$

where k_m = skin-effect ratio for rotor bars at the phase-belt frequency, which is $2mf_1$, at synchronous speed

k_1 = pitch times distribution factor of the stator winding for the fundamental field

$k_{2m\pm1}$ = pitch times distribution factor of the stator winding for the $(2m\pm1)$ field.

[Note - m, I_1, and R_{2b} are the same as in Eq. (2.20) above].

The lower order harmonics (e.g. 5th, 7th, 11th, etc.) due to phase-belt leakage flux induce currents in the rotor. For these fields, the impedance of a cage rotor is small compared to the magnetizing reactance when the motor is operating at full speed.

B5. Stator-slot eddy-current losses [5, 54]

The formula for this I^2R loss is available in reference [54]. However, these losses are very small and are generally neglected. These losses appear primarily as increased resistance of stator conductors due to skin effect. This extra copper loss varies as the fourth

power of the strand depth and as the square of the frequency. Thus the loss is negligible in small random-wound machines, and is held down in large machines by stranding and transposition.

B6. Stator-Overhang eddy-current losses [5]

These losses occur in the motor end structure due to end leakage flux.

For the winding geometry shown in Fig. 2.11, this loss is given by:

$$W_E = 0.3m\, I_1^2 \left[\frac{0.4\, f_1 m N_1^2 D_1}{P^2 10^7} \log\left(1 + \frac{A^2}{4Y_1 Y_2}\right) \right] W \tag{2.22}$$

where A, D_1, Y_1 and Y_2 are in inches and are shown in Fig. 2.11; m is the number of phases; P is the number of pole pairs; I_1 is the stator current; and N_1 is the number of turns on the stator, per phase.

The formula given in Eq. 2.22 is partly empirical. It states that the end losses are equal to an empirical multiplier, 0.3, times the reactive kVA due to the flux entering the laminations axially. The losses are due to the eddy currents, in the end structure, by axially-directed leakage fluxes. The losses are larger for large overhangs and when the end bells, ventilating shields, etc., are close to the end turns.

B7 and B8. Rotor slot and overhang losses

These are abnormal losses and occur only at high slips.

B9. Skew-leakage iron losses

The loss due to skew leakage flux is given by

$$W_k = \frac{\pi^2}{12}\left(\frac{\sigma \bar{I}'}{S I_{01}}\right)^2 \text{ (stator iron loss + no-load rotor surface loss) W} \tag{2.23}$$

where $\bar{I}'$ = phasor difference between load current $\bar{I}_1$ and the magnetizing current $\bar{I}_{01}$

$\sigma \cong 1$ = ratio of skew to stator slot pitch

and S= stator slots/pole.

The above formula accounts for the stator iron loss and the rotor surface loss due to skewing of the rotor. It is assumed here that the loss per unit length of the rotor core length remains unchanged for a given flux density regardless of the flux distribution along the core length.

B10. Stator teeth harmonic core losses [5]

Rotor slot mmf harmonics cause flux pulsation in the stator teeth, but do not cause any appreciable high-frequency stator currents because the stator winding is nearly open-circuited to these fields. Since the rotor slot openings are usually small, the resulting flux pulsations in the stator teeth are only those caused by the rotor slot mmf harmonics. It is concluded [5] that for normal machines, high-frequency pulsation losses in the stator teeth produced by the rotor slot mmf harmonics under load is about 3% of the part of the no-load core losses occurring in the stator teeth. Thus, these are negligible.

2.6. Note on harmonic torques

Stray torques (also called parasitic torques, asynchronous torques of harmonics, or subsynchronous torques) are also caused by leakage fluxes as they cross the airgap. Harmonics give rise to variations, both positive and negative, in the torque/speed curves of induction motor, and they are a contributor to causes of noise in the machine. As the harmonic torques result from the interaction of stator and rotor harmonic fields, the slot and overhang leakage fluxes, which link with only one part (stator or rotor) of the machine, do not produce harmonic torques. However, the gap leakage fluxes, which link partly with

the other winding, do produce harmonic torques. Reluctance torques due to permeance variations also cause subsynchronous torques.

2.7. Reduction of high-frequency losses

As mentioned earlier, use of slot wedges and increasing the airgap tend to reduce the high-frequency losses in induction motors. These methods are now considered in some detail [31, 34, 35].

2.7.1. Use of slot wedges

Open-slot designs are widely used in ac machines with double-layer windings. This type of a winding results in a cost reduction in manufacture compared with single-layer windings in semi-closed slots, and has the advantage that its coil pitch and winding distribution may be freely chosen. The open-slot feature, however, has a number of disadvantages arising from large permeance variations due to relatively wide slot openings. These disadvantages include high-frequency losses on no-load, higher magnetizing current due to increased airgap, and a consequent reduction in the machine efficiency and power factor.

Some of the disadvantages of the open-slot design may be offset by fitting suitable magnetic slot wedges at the slot mouths, thereby reducing the airgap permeance. Reference [13] lists some of the requirements for a magnetic slot wedge as follows:

(i) Permeability of the wedge should be high in the radial direction to provide a low reluctance path for the main flux. If laminations are used, these may be either in the plane of the machine coreplate laminations, or in the radial plane normal to the machine coreplate. The wedges should not saturate at normal flux densities.

(ii) Permeability in the circumferential direction should be low to limit the increase of cross-slot leakage flux.

(iii) The wedges should smooth out the main flux and reduce flux bundling as near the stator bore as possible. The airgap surface of wedges should be close to the stator bore surface.

(iv) Losses in the wedges should be low at normal flux densities.

(v) Mechanical strength and durability under service conditions should be adequate.

(vi) The extra cost of the wedges should be sufficiently low to have an economic advantage by their use.

It has been experimentally verified [13] that the total high-frequency no-load loss of an induction motor may be reduced by about 60% by magnetic slot wedges. However, they have negligible influence on stray load losses, since these losses are not greatly affected by stator slot openings. It is generally believed that magnetic slot wedges aid in reducing:

(i) electromagnetic noise due to the decrease of equivalent width of stator slot;

(ii) excitation current due to the reduction in the effective airgap, and

(iii) starting current due to the increase of stator leakage reactance (which also reduces the starting torque and power factor). But reference [35] does not consider these problems significant in large machines, as, in practice, slot wedges are likely to be saturated during starting, and a decrease of power factor is offset by a decrease in the starting current).

Whereas much of the work related to the effectiveness of slot wedges has been experimental, an analysis of the flux distribution in a slot by the finite-element method is presented in Fig. 2.12, which is taken from reference [35]. It may be seen from Fig. 2.12 that the flux distribution is very much equalized by the use of a magnetic slot wedge. As a consequence, the Carter coefficient, k_c, and airgap flux density pulsation factor β vary with

the presence (or absence) of magnetic slot wedges. The constants k_c and β are defined by Eq. 2.24 and Eq.2.25 below:

$$k_c = \frac{B_{max}}{B} \tag{2.24}$$

$$\beta = \frac{B_0}{B_{max}} \tag{2.25}$$

where B_0, B_{max} and B are shown in Fig. 2.13. Both k_c and β represent the ripple in the airgap flux. Thus, the high-frequency losses are very much dependent on k_c and β; that is, larger β and k_c result in larger flux-density pulsations and larger high-frequency losses. Figures 2.14 and 2.15 show the variations in β and k_c, respectively, in the presence of magnetic slot wedges.

In Figures 2.13 and 2.14,

b = slot opening

τ = slot pitch

g = airgap length (radial)

μ_s = relative permeability of wedges

Reference [35] also gives the no-load characteristics of a 10 pole 525 kW induction motor having magnetic slot wedges. These characteristics are shown in Fig. 2.16. The effectiveness of magnetic slot wedges is clear from Figs. 2.14 through 2.16.

Using slot wedges to reduce high frequency no-load losses has also been studied for small induction motors. Reference [34] reports on the use of soft ferrite slot wedges, instead of magnetic slot wedges, in a 3-phase, 4-pole, 750 W induction motor. It has been reported that the efficiency of the ferrite-wedged motor improved by 4%, at rated output and by 11% at a quarter of the rated output with a decrease of 3% in the starting torque.

2.7.2. Effect of large airgap

The use of larger airgaps tends to reduce the stray load losses by smoothing out the ripples in leakage fluxes. The variation of the total load losses with the airgap (radial) length is shown in Fig. 2.17 [17], which may be approximated by

$$\frac{W_{ll_g}}{W_{ll_0}} = \frac{1}{2}\left[\frac{g_0}{g} + \left(\frac{g_0}{g}\right)^2\right] = \text{loss-reduction factor} \qquad (2.26)$$

where W_{llg} and W_{ll0} are the stray load losses at airgaps g and g_0 respectively.

Equation (2.26) shows that the load losses decrease as the airgap increases. But the decrease is not as rapid as the ratio $(g_0/g)^2$ suggested by Richter [48]. In order to verify (2.26) experimentally, the airgap of a 4-pole 7 1/2-hp induction motor was increased from 0.33 mm to 0.51 mm [17]. It was found that the reduction in the load losses at 0.51 mm airgap, as compared with its value at 0.33 mm airgap, was 56% as measured, and 61% as calculated form (3.30). However, lengthening the airgap is not an ideal solution as larger airgap leads to lower power transfer across the airgap.

2.7.3. Use of low loss core materials

This is an obvious solution to reduce both the high-frequency losses. However, the utilization of low core materials is limited by the cost and availability of the material.

2.7.4. Selection of Slot Ratio

As indicated in Figs 2.7 through 2.10, the harmonic rotor current losses caused by the permeance mmf harmonics are greatly reduced by choosing a rotor to stator slot ratio close to but preferably less than one. It would appear that, strictly on the basis of stray loss

considerations, a design with fewer rotor slots than stator slots has a significant advantage. Whereas many machines manufactured in the U.S. use more rotor than stator slots, the opposite is generally true for motors manufactured in Europe and elsewhere. For high speed machines, the advantage of a rotor/stator slot ratio less than one may be especially significant.

2.7.5. Use of sleeve-rotor motors with airgap windings

From the preceding discussions it is clear that much of the high-frequency losses arise from teeth and slots on the stator and on the rotor, and also from rotor bar mmfs. Obviously, all of these "evils" are not present in a sleeve-rotor (or solid-rotor) induction motor having slotless (or airgap) windings. However, at the present these motors are of relatively small ratings. Considerable amount of work has to be done to assess the usefulness of such motors for high-frequency applications.

2.8. Sample calculations of losses

We now consider a numerical example to illustrate the application of the loss calculation formulas of Section 2.3.

In the following the fundamental frequency stator and rotor core losses and the high frequency stator and rotor iron losses and rotor I^2R losses are included, emphasis being on the high frequency losses. In particular, we consider the following:

(i) Fundamental frequency stator core loss $W_t + W_y$.

(ii) Rotor surface loss on no-load, W_{s0}

(iii) Core loss in rotor teeth, W_{t0k}

(iv) Stray load losses consisting of:

(a) Eddy current loss in stator copper, W_{sc}, due to slot leakage flux

(b) Losses in the motor end structure, W_E, due to end leakage flux

(c) Stator and rotor surface losses, W_{sL}, due to zigzag leakage flux

(d) High frequency tooth pulsation and rotor I^2R loss, W_z, due to circulating currents induced by zigzag leakage flux

(e) Six-times frequency (for a 3-phase motor) rotor I^2R losses, W_B, due to circulating currents induced by stator belt leakage flux

(f) Extra iron losses in skewed slots, W_K, due to skew leakage flux

(g) Rotor I^2R loss, W_P, due to permeance harmonic zigzag leakage flux.

2.8.1. Design data

The data pertain to a 15 HP, 3-phase, 60-Hz, 1200 rpm, 220-V motor designed by Kuhlmann [37]. It is given that:

stator winding turns/phase, $N_1 = 81$

full load stator current/phase, $I_1 = 39.3$ A

number of phases, $m = 3$

no-load stator current/phase, $I_{01} = 12.4$ A

fundamental frequency pitch factor, $k_{p1} = 0.985$

fundamental frequency distribution factor, $k_{d1} = 0.96$

number of pole pairs, $P = 3$

hysteresis loss constant, $\sigma_h = 2.05$ w/lb

eddy-current loss constant $\sigma_e = 1.0$ W/lb

fundamental flux density in stator tooth, $B_{t1} = 97{,}000$ lines/in^2 (= 1.503 T)

weight of stator teeth, $w_{t1} = 1.53$ lb

stator input frequency, $f_1 = 60$ Hz

stator bore, $D_1 = 9.5$ in

rotor core length, $L_c = 4.5$ in

stator tooth pitch, $\lambda_1 = 0.553$ in

number of stator teeth, S = 54

airgap flux density, $B_g = 42{,}300$ lines/in^2

number of rotor teeth, R = 65

rotor tooth pitch, $\lambda_2 = 0.459$ in

rotor slot opening, $w_{s2} = 0.06$ in

stator yoke flux density $B_{1y} = 96{,}500$ lines/in^2 = 1.496 T

stator slot opening, $w_{s1} = 0.3$ in

stator tooth width = 0.26 in

stator yoke weight v_y= 33.2 lb

rotor tooth width, $w_{t2} = 0.399$ in

rotor teeth weight, $v_{t2} = 13.54$ lb.

overhang data (Fig. 2.11) -

$Y_1 = 1.585$ in

$Y_2 = 1.355$ in

A = 1.05 in

full-load slip = 0.037

rotor bar height, h = 0.531 in = 0.0135 m

rotor bar resistance referred to stator, $R_{2b} = 0.12\Omega$.

3.8.2. Loss calculations

We first calculate the fundamental frequency core loss by a formula similar to Eq. (2.2), and then proceed to determine the losses given in Table 2.1.

Stator core loss due to fundamental frequency flux

Core loss in stator teeth [Eq. (2.2a)]

$$W_t = 1.5035^2 \left[2.05\left(\frac{60}{100}\right) + 1\left(\frac{60}{100}\right)^2\right] 15.3$$

$$= 54.74 \text{ W} \quad (50.5 \text{ W estimated by Kuhlmann})$$

Core loss in stator yoke

$$W_y = 1.496^2 \left[2.05\left(\frac{60}{100}\right) + 1\left(\frac{60}{100}\right)^2\right] 33.2$$

$$= 118.14 \text{ W} \quad (108 \text{ W estimated by Kuhlmann})$$

A1. Rotor surface loss on no-load [Eq. (2.1)]

Pole-face loss coefficient [Fig. 2.3]

$K_{pf} = 0.45$ for w/g = 13.6

rotor iron loss coefficient [Fig. 2.4]

$C_{s2} = 38$ in Eq. (2.1)

and

$$W_{s0} = 2 \times 9.5 \times 4.5 \left(\frac{42.3}{100}\right)^2 \times 0.45 \times 38 \times 0.553 = 144.67 \text{ W}$$

No-load stator surface loss is neglected.

A2. Rotor tooth core loss - [Eq. (2.2)]

Order of harmonic $k = \frac{S_1}{P} = 18$

$$\beta_k = \frac{kP\lambda_2}{D_2} = \frac{18 \times 3 \times 0.459}{9.5} = 2.61$$

From Fig. 2.5, $\beta = 0.6$

Amplitude of kth order harmonic flux density,

$$B_k = \frac{\pi}{2}\left(\frac{\beta}{2-\beta}\right) B_g = \frac{\pi}{2}\left(\frac{0.6}{2-0.6}\right) 42.3 = 28{,}480 \text{ lines/in}^2 = 0.448 \text{ T}$$

Let rotor core damping factor $k_{tk} = 0.5$ [Eq. 2.2c], then from (2.2b):

$$B_{tk} = 0.5 \times 0.448 \times \frac{0.459}{0.399} \times \frac{\sin 2.61}{2.61} = 0.0494 \text{ T}$$

$$W_{t0k} = 0.0494^2 \left[2.05\left(\frac{1080}{100}\right) + 1\left(\frac{1080}{100}\right)^2\right] \times 13.54 = 4.59 \text{ W}$$

[Eq. (2.2), and note that $f_{2k} = kf_1 = 18 \times 60 = 1080$].

Stator tooth pulsation loss neglected.

A3. Tooth pulsation circulating current loss

From the given data we have

$$k_f = 6.12,\ R_{2B} = 3 \times 0.12,\ C_P = 0.06,$$

$$I_M = 12.3\ \text{A}.$$

Consequently, Eq. (2.12) yields

$$W_P = 6.12 \times 3 \times 0.12 \times 0.06 \times 12.3^2 = 20.0\ \text{W}$$

B1. Surface losses on load [Eq. (2.15) and (2.16)]

Rotor surface loss (with S = 54/6 = 9)

$$W_{SL2} = 2 \times 9.5 \times 4.5 \left(\frac{39.3}{9 \times 12.4}\right)^2 \left(\frac{42.3}{100}\right)^2 \times 38 \times 0.553 = 39.87\ \text{W}$$

For the stator, from Fig. 3.4, $C_{s1} = 50$ and with R = 65/6 = 10.83 slots/pole (on the rotor) we have:

$$W_{SL1} = 2 \times 9.5 \times 4.5 \left(\frac{39.3}{10.83 \times 12.4}\right)^2 \left(\frac{42.3}{100}\right)^2 50 \times 0.459 = 30.07\ \text{W}$$

B.2. Tooth pulsation losses

Neglected.

B.3. Tooth pulsation cage circulating-current losses

[See Eq. (2.19)]

Proceeding as in A3 we have

$$K_f = 6.12,\ R_{2B} = 3 \times 0.12,\ C_M = 0.015\ ,$$

$$I_1 = 39.3\ \text{A}\ .$$

Thus, from Eq. (2.19) we have

$$W_M = 6.12 \times 0.12 \times 0.015 \times 39.3^2 = 51.0\ \text{W}$$

B4. Stator harmonic cage circulating-current losses

Loss due to belt leakage [Eq. (2.21)]. Phase-belt frequency referred to the rotor,

$$f_m = 2mf(1\text{-}s) = 2 \times 3 \times 60(1\text{–}0.037) = 346.68\ \text{Hz}$$

$$\eta_m = \sqrt{\frac{\pi \times 346.68 \times 4\pi \times 10^{-7}}{0.02 \times 10^{-6}}} \times 0.01\,35 = 3.53$$

then

$$k_m = \eta_m \frac{\sinh 2\eta_m + \sin 2\eta_m}{\cosh 2\eta_\mu - \cos 2\eta_m} = 3.53$$

electrical angle between two adjacent stator slots, $\alpha_1 = 20°$

slots/pole/phase, q = 3

fundamental distribution factor

$$k_{q1} = \frac{\sin(q\alpha_1/2)}{q\sin(\alpha_1/2)} = 0.96$$

(2m+1)th harmonic distribution factor

$$k_{q(2m+1)} = \frac{\sin[q(2m+1)\alpha_1/2]}{q\sin[(2m+1)\alpha_1/2]} = -0.177$$

(2m-1)th harmonic distribution factor

$$k_{q(2m-1)} = \frac{\sin[q(2m+1)\alpha_1/2]}{q\sin[(2m+1)\alpha_1/2]} = 0.218$$

From Eq. (2.21)

$$W_B = 3 \times 39.3^2 \times 3.53 \times 0.12 \left[\frac{\left(\frac{1}{5} \times 0.218\right)^2 + \left(\frac{1}{7} \times -0.177\right)}{0.96^2}\right] = 5.41 \text{ W}$$

B5. Stator slot eddy-current losses

Neglected.

B6. Loss due to end leakage flux [Eq. (2.22)]

$$W_E = 0.3 \times 3 \times 39.3^2 \left[\frac{0.4 \times 60 \times 3 \times 81^2 \times 9.5}{3^2 \times 10^7} \log \left(1 + \frac{1.06^2}{4 \times 1.585 \times 1.355} \right) \right]$$

$$= 3.5 \text{ W}$$

B7. and B8. Rotor slot and overhang losses

Neglected.

B9. Loss due to skew leakage flux [Eq. (2.23)]

$$\bar{I}' = \bar{I}_1 - \bar{I}_{01} = 33.89 \angle -12.40° \text{ A}$$

Then, from Eq. (2.23),

$$W_k = \frac{\pi^2}{12} \left(\frac{1 \times 33.89}{9 \times 12.4} \right)^2 (54.74 + 118.14 + 57.87) = 17.5 \text{ W}$$

B10. Stator teeth harmonic core loss

Neglected.

Total stray losses

$$W_{t(stray)} = W_{s0} + W_{t0k} + W_p + W_{SL1} + W_{SL2} + W_M + W_B + W_E + W_K$$

$$= 144.67 + 4.59 + 20.0 + 30.07 + 39.87 + 51.0 + 5.41 + 3.5 + 17.5$$

$$= 316.61 \text{ W}$$

2.9. Conclusions

Causes of high-frequency losses in induction motors are space harmonics arising from the stator and rotor geometries such as slot and tooth permeances and discontinuous current distributions. These space harmonics not only produce the so-called stray losses but also generate noise and harmonic torques. In this report, these losses have been segregated into different categories, their causes and types - whether eddy-current or I^2R losses - are identified. Brief discussions of the location of these losses and their nature are also given. Without derivations, formulas for calculating the various losses are included and their applications are illustrated by a numerical example. Means of reducing high-frequency stray losses are also suggested.

In terms of their significance, for normal low-slip operation surface core losses (item A1 in Table 2.1) are the most significant. For the numerical example considered, this loss is over 45 per cent of the total stray loss due to harmonic fluxes resulting from permeance variations. However, a major portion of this loss occurs in the rotor surface due to the stator slot openings. The corresponding stator surface loss due to the rotor slot openings is negligible for semi-closed rotor slotting. This loss is dependent on the stator slot frequency and also on the core material.

Stator and rotor core surface losses caused by the gap leakage harmonic fluxes (item B1 in Table 2.1) constitute about 22 per cent of the total stray losses. These are stray-load losses and are similar to the no-load surface losses except that the former are significant in the stator surface also.

The next significant loss is the tooth-pulsation cage circulating loss (item B3 in Table 2.1) constituting about 16 per cent of the total stray loss. This is a stray-load loss in the rotor cage and is especially significant at high slips.

Tooth-pulsation cage circulating current losses (item A3 in Table 2.1) on no-load are about 6 per cent of the stray losses. These losses are similar to those of item B3.

Other losses are less than 5 per cent of the total stray losses.

In terms of their effectiveness in reducing high-frequency stray losses, use of slot wedges has been found to be most effective. Use of (permissible) large airgaps and appropriate stator/rotor slot ratio also tend to reduce the stray losses.

Reference [28] gives 13 rules which make it possible to reduce the stray full-load losses to 1% of the power input.

The rules refer to the number of stator and rotor slots, slot skewing, coil pitch, parallel winding paths, slot opening, transverse rotor resistance, influence of working and ageing. These rules are as follows:

1. $S > R$
2. Number of stator slots as high as possible.
3. Non-skewed stator and rotor slots, especially if $S < R$.
4. Two-layer chorded stator winding with a chord 5/6.
5. With a delta connection: $|S - R| \neq 2p, 4p, 8p$ [p = pole pairs].
6. With parallel paths: a connection making the secondary armature reaction impossible.

7. Ratio of slot opening w to segment height *h*: rotor: w/h ≤ 1; stator w/h ≤ 3.
8. Re-turn rotor surface to prevent sheets to be short-circuited, stator bore better not re-turned.
9. Use of sharp press-tools if sheets are not annealed.
10. Use of annealed sheets, particularly for small motors.
11. Small stator and rotor slot openings.
12. With skewed machines transverse resistance either very small or very large.
13. Storage of the motors because, due to ageing, the stray losses are reduced after six months to 0.6 of their original value.

3.10 Acknowledgements. The assistance of C. Chen of the University of Kentucky, Lexington, in preparation of this report is gratefully acknowledged.

3.11. Bibliography

1. Agarwal, P.D., and Alger, P.L., 'Saturation factors for leakage reactance of induction motors', AIEE Transactions, Vol. 80, 1961, pp. 1037.

2. Alger, P. L., 'Calculation of armature reactance of synchronous machines', AIEE Transactions, Vol. 47, 1928, pp. 493-513.

3. Alger, P.L., The Nature of Polyphase Induction Machine, Wiley, 1951.

4. Alger, P.L., 'Induced high-frequency currents in squirrel-cage windings', AIEE Transactions, Vol. 77 (III), 1957, pp. 724-729.

5. Alger, P.L., Angst , G. and Davies, E.J., 'Stray load losses in polyphase induction machines', AIEE Transactions, Vol. 79 (III), 1959, pp. 349-357.

6. Anazawa, Y., Kaga, A., Akagami,H., Watabe, S. and Makimo,M., 'Prevention of harmonic torques in squirrel-cage induction motors by means of soft ferrite magnetic wedges', IEEE Transactions, Vol. MAG-18, No. 5, Nov. 1982, pp. 1550-1052.

7. Barton, T.H., and Ahmad, V., 'The measurement of induction motor stray loss and its effect on performance', Proc. IEE, Vol. 105 C, 1957, pp. 69.

8. Bird, B.M., 'Measurement of stray load losses in squirrel-cage induction motors', Proc. IEE, Vol. III, 1964, pp. 1697-1705.

9. Bondi, H., and Mukherji, K.C., 'An analysis of tooth-ripple phenomena in smooth laminated pole-shoes', Proc. IEE, Vol. 104 C, 1957, p. 349-356.

10. Carter, G.W., The Electromagnetic Field in Its Engineering Aspects, Longman, 1954.

11. Chalmers, B.J. and Williamson, A.C., 'Stray losses in squirrel-cage induction motors', Proc. IEE, Vol. 110, 1963, pp. 1773.

12. Chalmers. B.J., and Richardson, J., 'Investigation of high-frequency no-lead losses in induction motors with open stator slots', Proc. IEE, Vol. 113, 1966, pp. 1597-1605.

13. Chalmers, B.J. and Richardson, J., 'Performance of some magnetic slot wedges in an open-slot induction motor', Proc. IEE, Vol. 114, 1967, p. 258-260.

14. Chalmers, B.J., and Sarkar, B.R., 'High-frequency effects in induction motors', Proc. IEE, Vol. 114, 1967, pp. 1518-1519.

15. Chalmers. B.J., and Sarkar, B.R., 'Induction motor losses due too nonsinusoidal supply', Proc. IEE, Vol. 115, 1968, pp. 1777-1782.

16. Chalmers, B.J., and Narain, C.K., 'High-frequency no-load losses of cage induction motors', IEEE Transactions, Vol. PAS-89, 1970, pp. 1043-1048.

17. Christofides, N., 'Origins of load losses in induction motors with cast aluminum rotors', Proc. IEE, Vol. 112, 1965, pp. 2317-2332.

18. Christofides, N., and Adkins, B., 'Determination of load losses and torques in squirrel-cage induction motors', Proc. IEE, Vol. 113, pp. 1995-2005.

19. deJong, H.C.J., and Taegen, F., 'Additional losses in cage induction machines', Proc. ICEM, 1986.

20. Diamant, P., 'The high efficiency induction machine of the 1980's Part I', IEEE Transactions, Vol. PAS-100, 1981, pp. 4965-4968.

21. Dryfus L., 'Theorie der zusatzlichen Eisenverluste in Drehstromasychronmotoren', Arch Elektrotech, Vol. 20, 1928, pp. 37-87, 188-210, 273-298.

22. Freeman, E.M., 'The calculation of harmonic, due to slotting,in the flux-density waveform of a dynamo-electric machine', Proc. IEE, Vol. 109 C, 1962, pp. 581-588.

23. Fuchs, E.F., Chang, L.H., and Appelbaum, J., 'Magnetizing current iron losses and forces of three-phase induction machines at sinusoidal and nonsinusoidal terminal voltages', IEEE Transactions, Vol. PAS-103, 1984, pp. 3303-3312.

24. Fuchs, E.F., Kovacs, K.P. and Roesler, D.J., 'Reduction of lifetime of induction motors due to harmonics of the terminal voltage', Proc. ICEM, 1986.

25. Gibbs, W.J., 'Tooth-ripple losses in unwound pole-shoes', J.IEE, Vol. 94, Pt. II, 1947, pp. 2-12.

26. Greig, J., and Sathirakul, K., 'Pole-face losses in alternators', Proc. IEE, Vol. 108 C, 1961, pp. 130-138.

27. Greig, J. et.al., 'Tooth-ripple losses in electrical machines', Proc. IEE, Vol. 118, 1971, pp. 1269-1274.

28. Heller, B., Hemata, V., Harmonic Field Effects in Induction Machines, Elsevier, 1977.

29. Hentschel, F. and Shehata, M.A., 'Comparative study of the losses in inverter-fed standard squirrel-cage induction motors', Proc. ICEM, 1986, pp. 320-323.

30. Jain, G.C., 'The effect of voltage waveshape on the performance of a three-phase induction motor', IEEE Transactions, Vol. PAS-83, 1964, pp. 561-566.

31. Jimoh, A.A., Findlay, S.R.D., and Poloujadoff, M., 'Stray losses in induction machine, Part II', IEEE Transactions, Vol. PAS-104 (6) 1985, pp. 1500-1505; 1506-1512.

32. Jordan, H., and Taegen, F., 'Uber den Einfluss der Isoslation des Lauferkafigs auf die Drehmomente von Drehstrom-asychronomotoren', AEG Mitt., Vol. 52, 1962, pp. 42-43.

33. Jordan, H., and Taegen F., 'Zur Berechnung der Zahnpulsationverluste von Asynchronmotoren', Elektrotech.Z., Vol. 86, pp. 805-809.

34. Kaga, A., Anazawa, Y., Akagami, H., Watabe, S., and Makimo, M., 'A research of efficiency improvement by means of wedging with soft ferris in small induction motors', IEEE Transactions, Vol. MAG-18, No. 5, Nov. 1982, p. 1547-1549.

35 Kato, K., Kohno, H. Urabe, K., and Takahashi, T., 'Analytical and experimental study for reducing high frequency pulsation losses created by the existence of armature slots using magnetic slot wedges', Elect. Eng. in Japan, Vol. 102, No. 5, 1982, pp. 103-111.

36. Klingshirn, E.A., and Jordan, H.E., 'Polyphase induction motor performance and losses on nonsinusoidal voltage sources', IEEE Transactions, Vol. PAS-87, 1968, pp. 624-631.

37. Kuhlmann, J.H., Design of Electrical Apparatus (3rd ed.), Wiley, 1950.

38. Lee, C.H., 'Saturation harmonics of polyphase induction motors', AIEE Transactions, Vol. 80, 1961, pp. 597-603.

39. Liwschitz, M.M., 'Differential leakage with respect to the fundamental wave and to the harmonics', AIEE Transactions, Vol. 63, 1944, pp. 1139-1149.

40. Loser., F., and Sattler, P.K., 'Additional losses of induction motors', Proc. ICEM, 1986, pp. 324-327.

41. Narbutovskih, P.M., 'Power losses in induction machines', Elect. Eng., Nov. 1934, pp. 1466-1471.

42. Narbutovskih, P.M:, 'Tooth-frequency eddy-current loss', AIEE Transactions, Vol. 56, 1937, pp. 253-256.

43. Oberretl, K., 'Magnetic fields, eddy currents, and losses, taking the variable permeability into account', IEEE Transactions, Vol.PAS-88, 1969, pp. 1646-1657.

44. Odok, A., 'Stray load losses and stray torques in induction machines', AIEE Transactions, Vol. 77, 1958, pp. 43-53.

45. Piepenbreier, B., and Taegen, F., 'Surface losses in cage induction motors', BICEM Proc., 1987, pp. 326-329.

46. Rao, V.S., and Butler, O.I., 'Stray losses of polyphase cage-induction motors with particular reference to the condition of imperfect rotor-bar-iron insulation', Proc. IEE, Vol. 116, 1969, pp. 737-751.

47. Rawcliffe, G.H. and Memon, A.M., 'A simple new test fro harmonic-frequency losses in a.c. machines', Proc. IEE, Vol. 99 (II), 1952, pp. 145.

48. Richter, R. Elektrische Machinen, Vol. I, Springer, 1954.

49. Schwarz, K.K., 'Survey of basic stray losses in squirrel-cage induction motors', Proc. IEE, Vol. III, 1964, pp. 1565-1574.

50. Spooner, E., 'Stray loss in solid-rotor induction machines', Proc. IEE, Vol. 129, Pt. B, 1982, pp. 181-189.

51. Spooner, T. and Kinnard, I.F., 'Surface iron losses with reference to laminated materials', AIEE Transactions, Vol. 43, 1924, pp. 162.

52. Spooner, T., 'Squirrel-cage induction motor core losses', AIEE Transactions, Vol. 44, 1925, pp. 155-160.

53. Spooner, T. and Kincaid, C. W., 'No-load induction motor core losses', AIEE Transactions, vol. 48, 1929, pp. 645-654.

54. Stoll, R.L. and Hammond, P., 'Calculation of the magnetic field of rotating machines, Part 4', Proc. IEE, Vol. 112, 1965, pp. 2083-2094.

55. Taylor, H.W., 'Eddy-current losses in stator winding', Proc. IEE, Vol. 58, 1920, pp. 279-300.

56. Wahsh, S., 'Additional losses in three-phase cage induction machines with PWM inverter', Proc. ICEM, 1988, pp. 621-625.

57. Walker, J.H., 'A theory of induction motor surface losses', Jour. IEE, Vol. 95 (II), 1948, pp. 597.

2.12 Appendix A

Analytical Determination of Surface Losses

A1. Introduction

Much of the published work on the determination of surface losses, as given in this report, is based on empirical or graphical methods [5,7]. Reference [28] gives an analytical method, but does not account for lamination thickness and does not determine the harmonic field. Reference [46], although accounting for the effect of lamination thickness, also does not give the determination of harmonic fields. Clearly, graphical methods [17] are tedious and inaccurate and the empirical method [5] is limited to a specific lamination and frequency. In the following, we present a general method of finding the surface losses analytically. The method is based on the assumption that the stator slots are open and the harmonic field has the distribution as shown in Fig. 2.5. These assumptions have been used by Alger [5], and the proposed method accounts for skin effect and is valid for any lamination thickness and any operating frequency. For rotor tooth "overhang", a factor is introduced in the expression for the surface flux at the rotor tooth.

A2. Airgap flux distribution

Qualitatively, we assume that the harmonic flux density distribution due to slotting is sinusoidal [5] with a double amplitude β, the maximum flux density of the permeance ripple being $\beta/(2-\beta)$ times the fundamental flux density at any point. The flux pulsation, β, as a function of slot opening/airgap, w/g, is shown in Fig. 2.5. The maximum flux density for each harmonic is given by

$$B_k = \frac{\pi}{4}\left(\frac{\beta}{2-\beta}\right)B_g \qquad \text{(A1)}$$

where B_g is the average flux density in the airgap. The flux density distribution may then be written as

$$b_{1k} = B_{1k} \cos kx \tag{A2}$$

where B_{1k} is the same as given by (A1).

A3. Surface flux at the rotor tooth

In order to find the surface flux over a rotor tooth, we divide the tooth surface into N regions, and obtain the flux density in each region. By integrating the harmonic flux density in each of these N regions and subtracting from it the Nth part of the tooth body flux (which causes the tooth pulsation loss) an approximate value of the surface flux in each region is obtained [46]. The accuracy of calculations will depend on the number of regions N.

Referring the flux density given by Eq. (A2) to the rotor coordinates we have

$$b_{1K} = B_{1K} \cos(kx - \omega t) \tag{A3}$$

Now, the flux in the body of one rotor tooth, i.e., the tooth pulsation flux, is obtained by integrating Eq. (A3) over a tooth width at the rotor surface w_{rt0}.. Thus, expressing the result in the form given in [46] we obtain

$$\phi_{rtk} = B_{1k} l\, w_{rt0} \frac{\sin(k\pi k_2/R')}{k\pi k_2/R'} \cos \omega_m t \tag{A4}$$

where

l = rotor stack length, m

R' = number of rotor slots per pole

$$k_2 = \frac{\text{tooth width at the rotor surface}}{\text{rotor tooth pitch}} = \frac{w_{rt0}}{t_{r0}}$$

Notice that K_2 accounts for the rotor tooth overhand effect.

Let us divide the tooth surface into two regions (N = 2). Then, the integration of Eq. (A3) over a region given, approximately, half the tooth body flux of Eq. (A4) and a surface flux which enters only in one half of the tooth but leaves via the other half. Integrating (A3) over 0 to $\frac{1}{2} w_{rt0}$, the flux in each region is

$$\phi_{rk} = \frac{1}{2} B_{1k} l \, w_{rt0} \frac{\sin(k\pi k_2/2R')}{k\pi k_2/2R'} \cos\left(\frac{k\pi k_2}{2R'} + \omega_m t\right) \tag{A5}$$

Then, the surface flux in each of the two regions is approximately given by

$$\phi_{rsk} = \phi_{rk} - \frac{1}{2}\phi_{rtk} \tag{A6}$$

where ϕ_{rtk} and ϕ_{rk} are respectively given in Eqs. (A4) and (A5).

The average value of $(\phi_{rsk}/w_{rt0})^2$ is:

$$\left(\frac{\phi_{rsk}}{w_{rt0}}\right)^2_{ave} = \frac{1}{8}\left(\frac{\pi^2}{16}\right)\left(\frac{\beta}{2-\beta}\right)^2 B_g^2 l^2 C_{1r} \tag{A7}$$

where

$$C_{1r} = \left[\frac{\sin(k\pi k_2/2R')}{k\pi k_2/2R'}\right]^2 + \left[\frac{\sin(k\pi k_2/R')}{k\pi k_2/R'}\right]^2$$

$$- \left[\frac{\sin(k\pi k_2/2R')}{k\pi k_2/2R'} \cdot \frac{\sin(k\pi k_2/R')}{(k\pi k_2/R')} \cos\frac{k\pi k_2}{2R'}\right] \qquad \text{(A8)}$$

A4. No-load rotor surface loss

The no-load surface loss per unit rotor surface is given by [46]:

$$W_s = \frac{\phi^2\lambda^3\rho}{\mu^2}\left[\frac{\sinh(2\lambda d) - \sin(2\lambda d)}{\cosh(2\lambda d) - \cos(2\lambda d)}\right] W/m^2 \qquad \text{(A9)}$$

This method accounts for the skin effect by the factor within braces where

$\phi = \frac{\phi_{rsk}}{w_{rt0}}$ = flux per unit tooth width, W^b/m^2

$\lambda^2 = \mu\omega_k/2\rho$, m^{-2}

$\mu = \mu_r\mu_0$ = permeability, H/m

ρ = resistivity, Ω-m

$\omega_k = 2\pi f_k$ = angular frequency of kth harmonic

d = lamination thickness, m.

Finally the total no-load surface loss becomes, from Eqs. (A8) and (A9):

$$W_{s0} = 2\pi D \frac{1}{\lambda}\frac{1}{8}\frac{\pi^2}{16}\left(\frac{\beta}{2-\beta}\right)^2 B_g^2 l^2 \frac{\lambda^3 \rho}{\mu^2} C_{1r}\left[\frac{\sinh(2\lambda d)-\sin(2\lambda d)}{\cosh(2\lambda d)-\cos(2\lambda d)}\right] \text{ W} \qquad \text{(A10)}$$

In (A10) the factor 2 accounts for the losses due to two equal harmonics of the order $(2s\pm1)$ and $\pi D/\lambda$ is the surface area across the direction of the

A5. Rotor surface loss on load

Proceeding as in reference [5] the rotor surface loss on load is obtained by multiplying Eq. (A10) by a factor

$$K_{FL} = \left(\frac{I}{S' I_0}\right)^2 \frac{1}{\left(\frac{\beta}{2-\beta}\right)^2} \qquad \text{(A11)}$$

to obtain

$$W_{SL2} = 2\pi D l^2 \frac{1}{8}\frac{\pi^2}{16} B_g^2 \frac{\lambda^2 \rho}{\mu^2} C_{1r}\left[\frac{\sinh(2\lambda d)-\sin(2\lambda d)}{\cosh(2\lambda d)-\cos(2\lambda d)}\right]\left(\frac{I}{S' I_0}\right)^2 \qquad \text{(A12)}$$

where

S' = number of stator slots per pole

I = rms stator load current, A

I_0 = rms stator no-load current, A.

A6. Stator surface loss on load:

By analogy with Eq. (A12), the stator surface loss on load is given by:

$$W_{SL1} = 2\pi D l^2 \frac{1}{8}\frac{\pi^2}{16} B_g^2 \frac{\lambda_r^2 \rho}{\mu^2} C_{1s} \left[\frac{\sinh(2\lambda_r d)-\sin(2\lambda_r d)}{\cosh(2\lambda_r d)-\cos(2\lambda_r d)}\right]\left(\frac{I}{R'I_0}\right)^2 W \qquad \text{(A13)}$$

where

R' = number of rotor slots per pole

$\lambda_r = 2\pi(2R'f_1)\mu/2\rho$

$$C_{1s} = \left(\frac{\sin(k\pi K_1/2S')}{k\pi K_1/2S'}\right)^2 + \left(\frac{\sin(k\pi K_1/S')}{k\pi K_1/S'}\right)^2 - \frac{\sin(k\pi K_1/2S)}{k\pi K_1/2S'} \bullet \frac{\sin(k\pi K_1/S')}{k\pi K_1/S'}$$

$$\bullet \cos(k\pi K_1/2S) \qquad \text{(A14)}$$

$$K_1 = \frac{\text{effective tooth width in airgap for stator}}{\text{stator tooth in pitch at airgap}} = \frac{W_{st0}}{t_{s0}}; \quad \text{for stator slot, } K_1 \approx 1.$$

A7. Stator surface loss on no-load:

Due to closed or semi-closed rotor slot, the no-load stator surface losses are negligible.

A8. Sample calculations

The data for the motor are adopted from Kuhlmann [37].

$k = 2S' \pm 1 = 17, 19$

$f_k = 2Sf_1 = 1080$ Hz

$\omega_k = 2\pi f_k = 6785.8$ rad/s

$$\frac{w}{g} = 13.6$$

From Fig. 3.5, the flux pulsation β can be found by using $\frac{w}{g} = 13.6$

$$\beta = 0.85$$

$$B_k = \frac{\pi}{4}\left(\frac{\beta}{2-\beta}\right)B_g = 24555.6 \text{ lines/in}^2 = 0.3806 \text{ tesla}$$

$$K_2 = \frac{w_{rt0}}{t_{r0}} = 0.871$$

$$\mu = 800\,\mu_0 = 1.005 \times 10^{-3} \text{ H/m}$$

$$\rho = 5 \times 10^{-7}\ \Omega\text{M for 1\% Si steel}$$

$$\lambda^2 = \frac{\omega_k \mu}{2\rho} = 6821824.4$$

$$\lambda = 2611.8$$

$$d = 0.019'' = 4.826 \times 10^{-4} \text{ m}$$

$$2\lambda d = 2.521$$

$$C_{1r} = 0.1175$$

$$\frac{\sinh(2\lambda d)-\sin(2\lambda d)}{\cosh(2\lambda d)-\cos(2\lambda d)} = 0.801$$

$$\frac{\lambda^2 \rho}{\mu^2} = 3.37 \times 10^6$$

$$W_{S0} = 2\pi D l^2 \frac{1}{8} \frac{\pi^2}{16} \left(\frac{\beta}{2-\beta}\right)^2 Bg^2 \frac{\lambda^2 \rho}{\mu^2} C_{1r} \left[\frac{\sinh(2\lambda d)-\sin(2\lambda d)}{\cosh(2\lambda d)-\cos(2\lambda d)}\right]$$

= 90.3 W (144 W by using the method of reference [5].

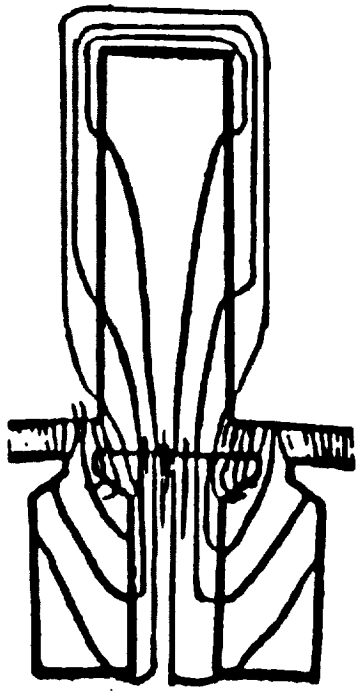

Fig. 2.1. Variation of flux density over tooth top.

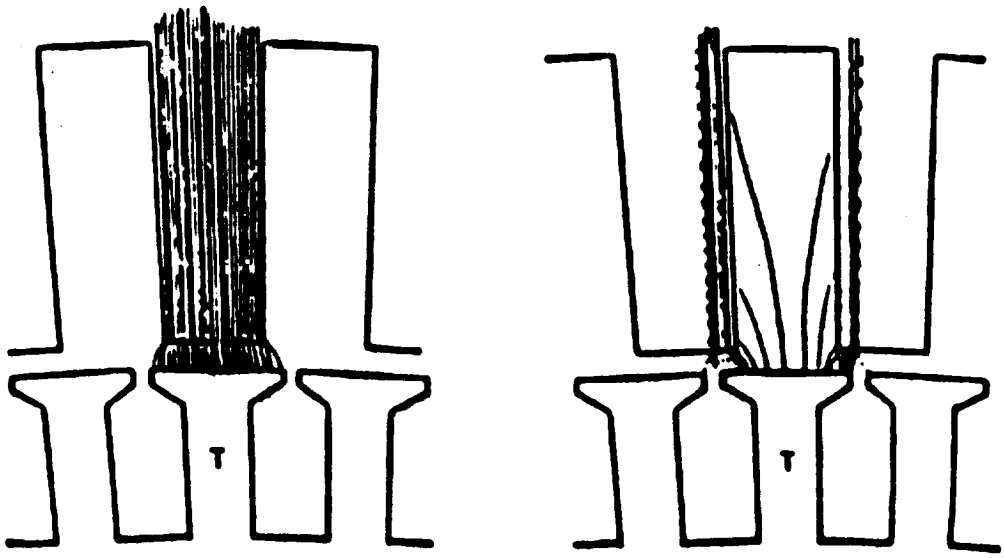

Fig. 2.2. Two relative positions of a rotor tooth T, with respect to stator teeth, showing permeance variations.

(From Reference 42)

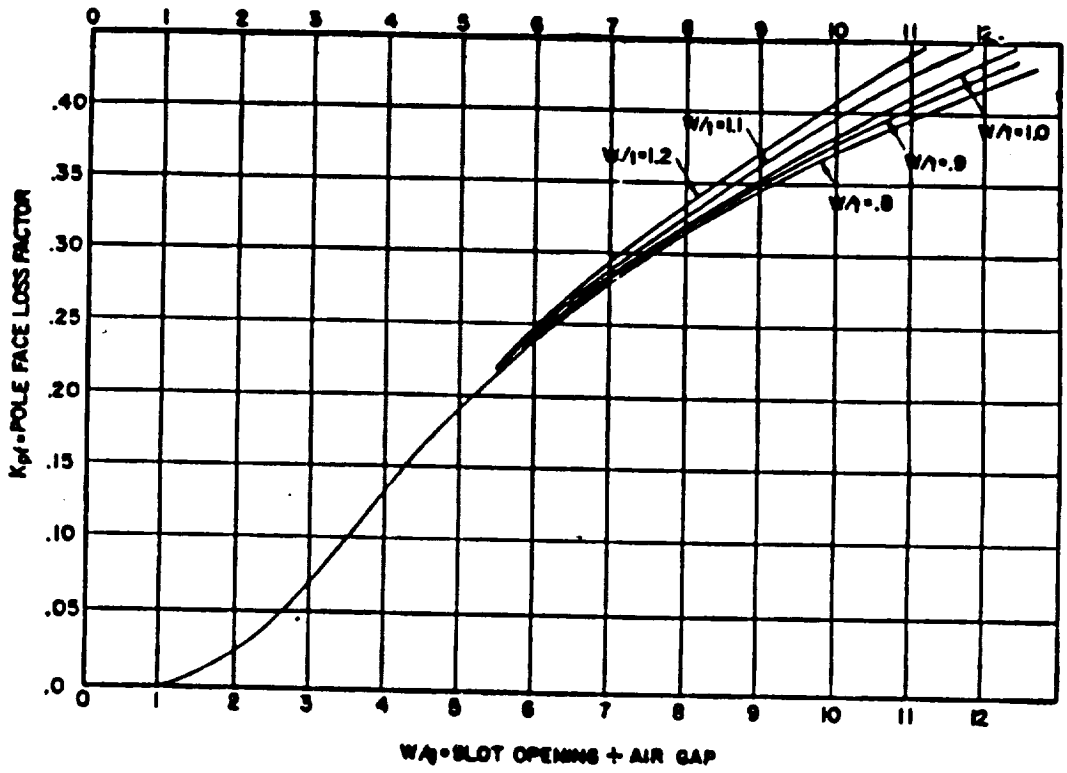

Fig. 2.3. Pole-face loss factor for open slots.

(From Reference 5)

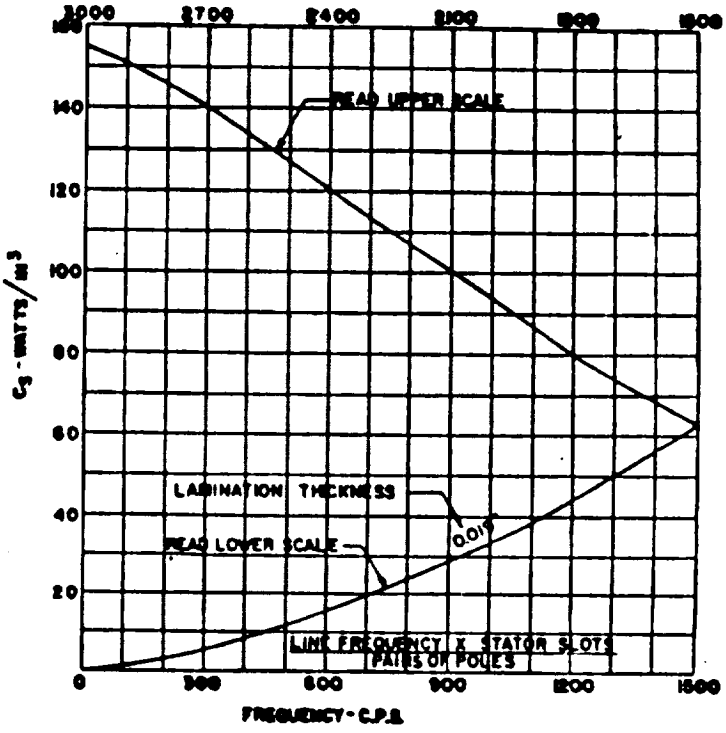

Fig. 2.4. High-frequency steel loss factor, 2.5% silicon steel, at $\mu_r = 800$ (assumed constant).

(From Reference 5)

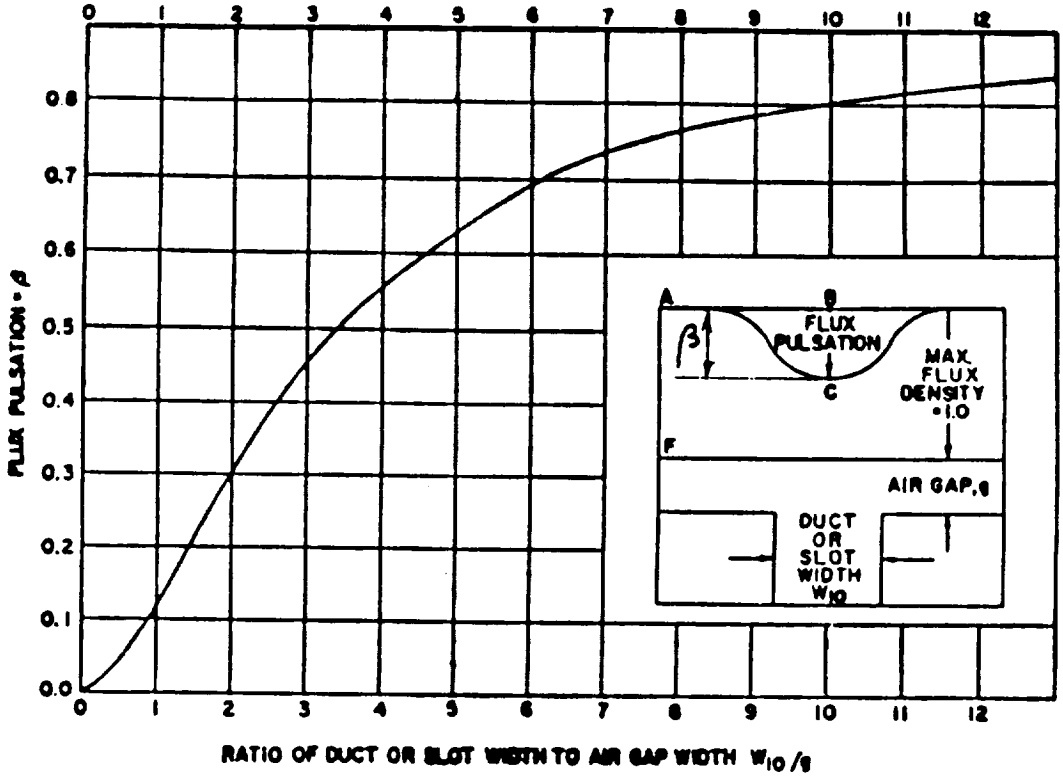

Fig.2.5. Flux pulsation due to slot opening.

(From Reference 5)

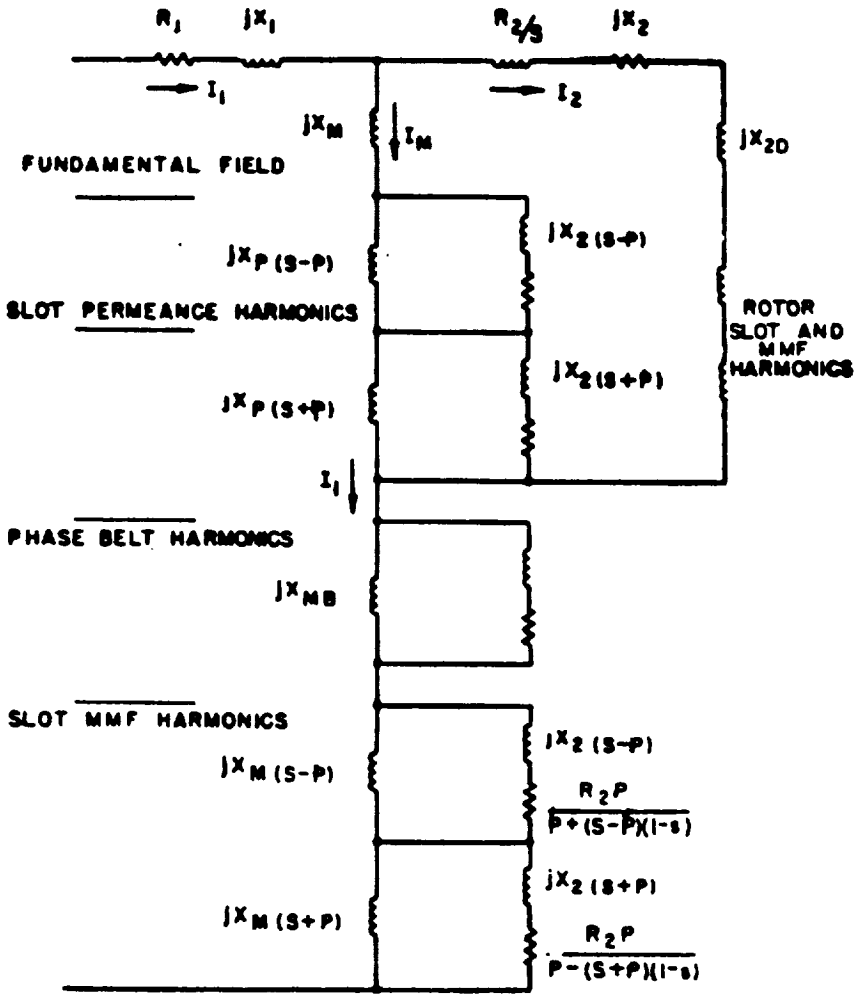

Fig. 2.6. Equivalent circuit representing harmonic airgap fields.

(From Reference 3)

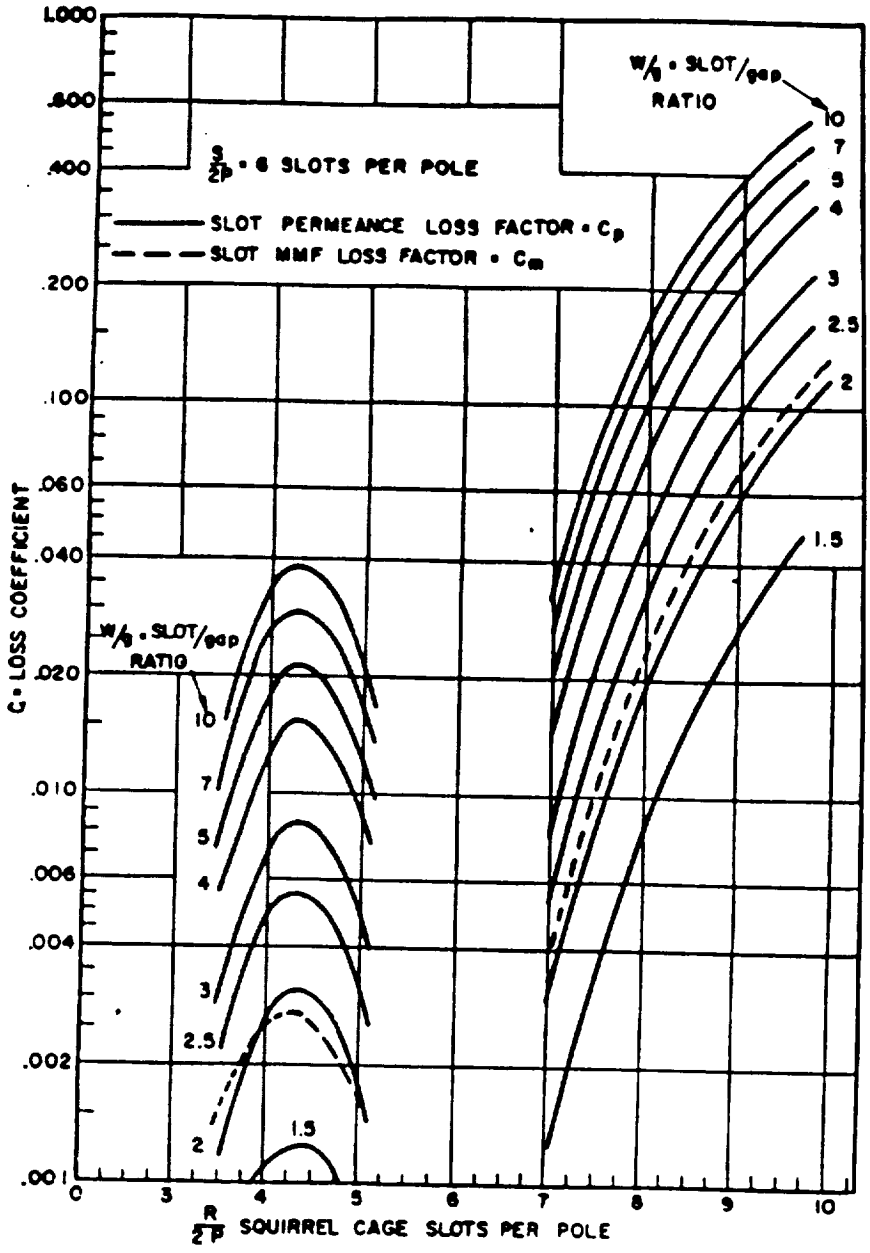

Fig. 2.7. Induced circulating current loss factor for six stator slots per pole.

(From Reference 3)

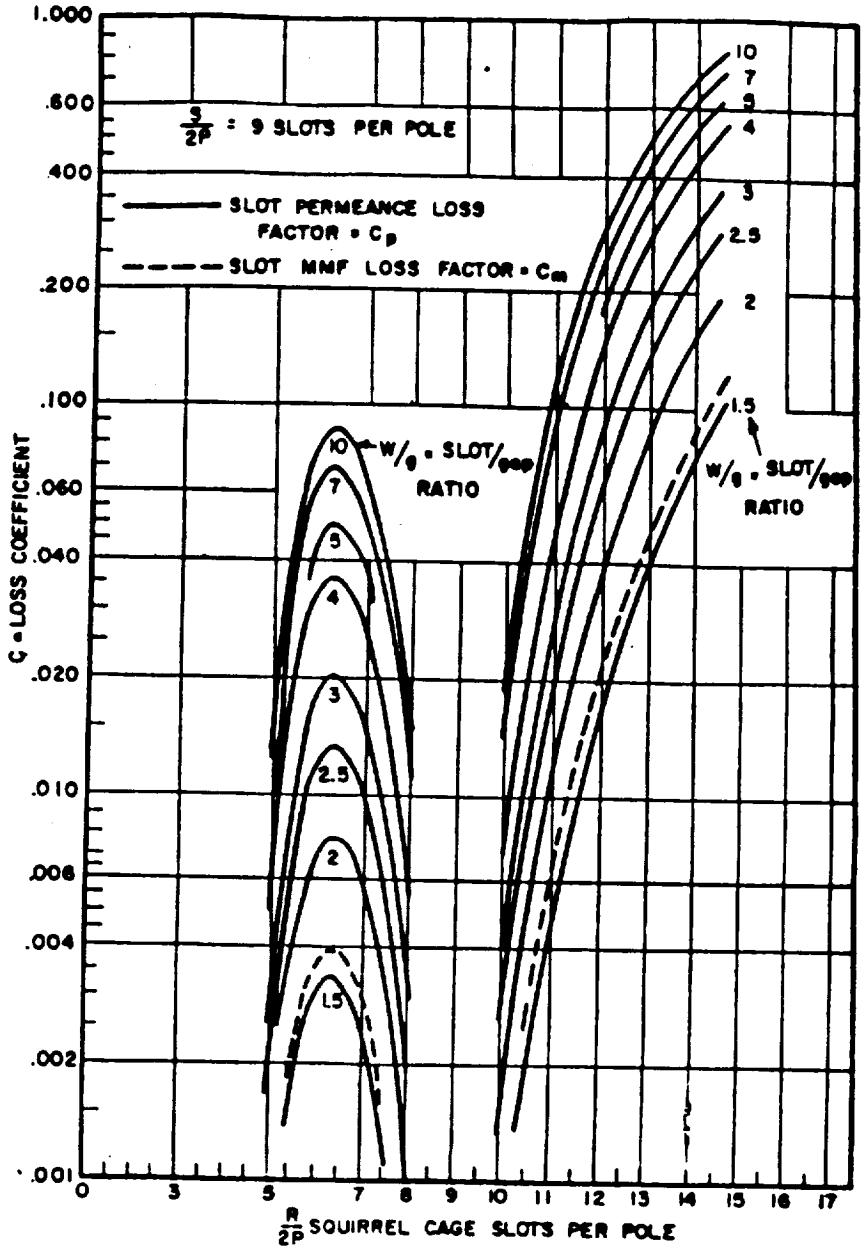

Fig. 2.8. Induced circulating current loss factor for nine stator slots per pole.

(From Reference 3)

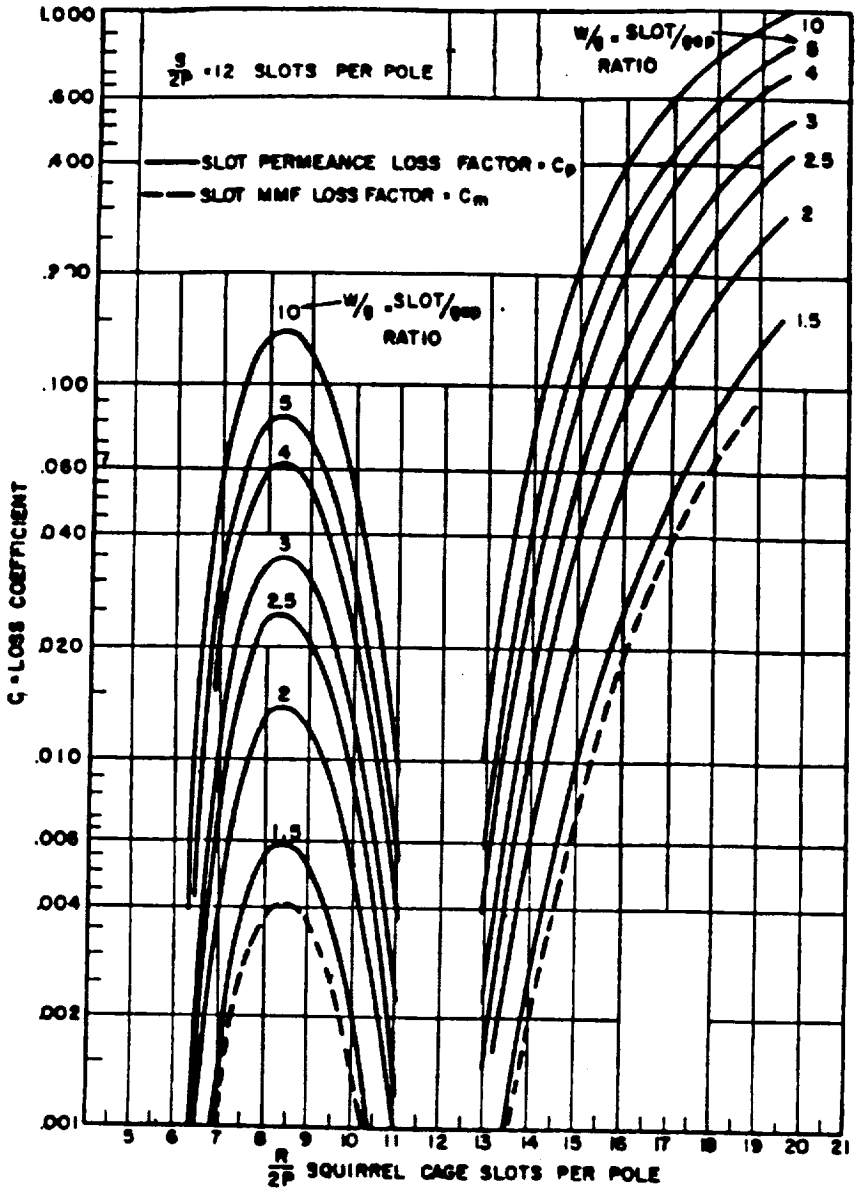

Fig. 2.9. Induced circulating current loss factor for 12 stator slots per pole.

(From Reference 3)

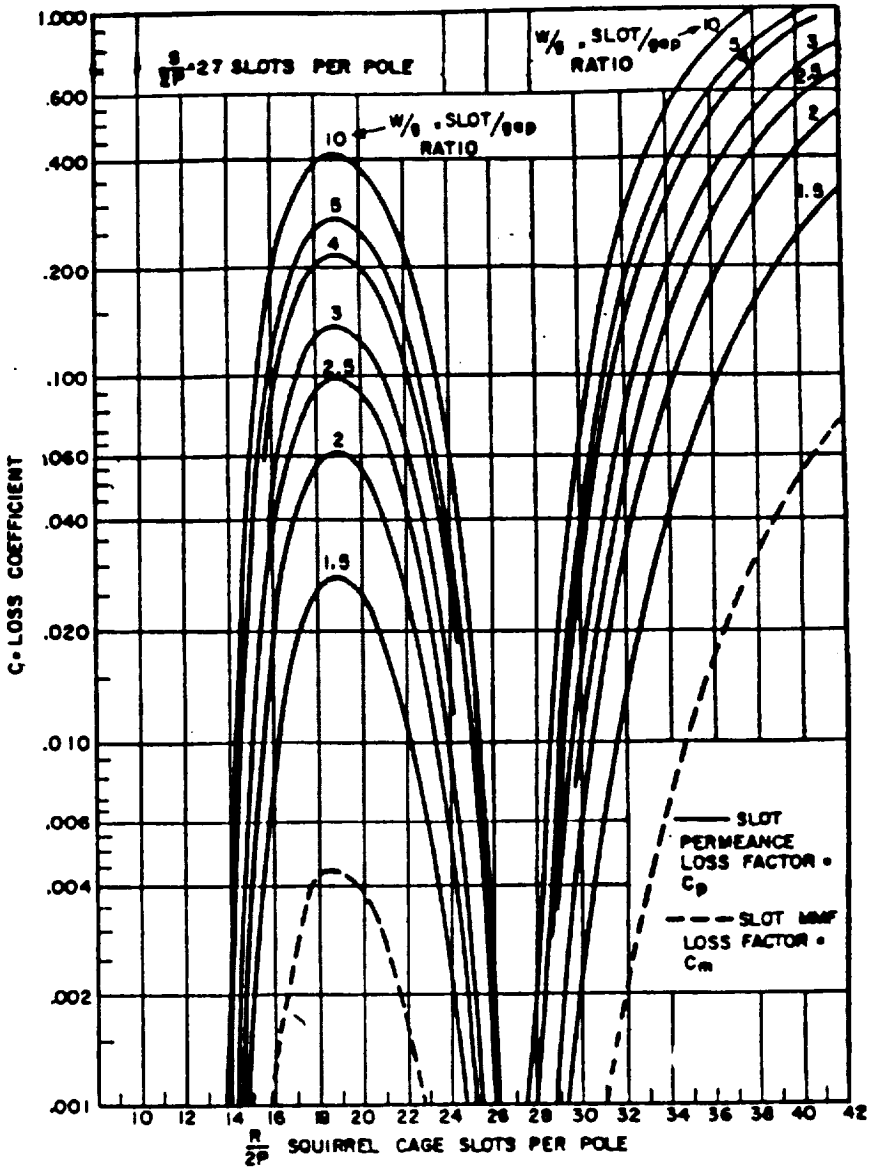

Fig. 2.10. Induced circulating current loss factor for 27 stator slots per pole.

(From Reference 3)

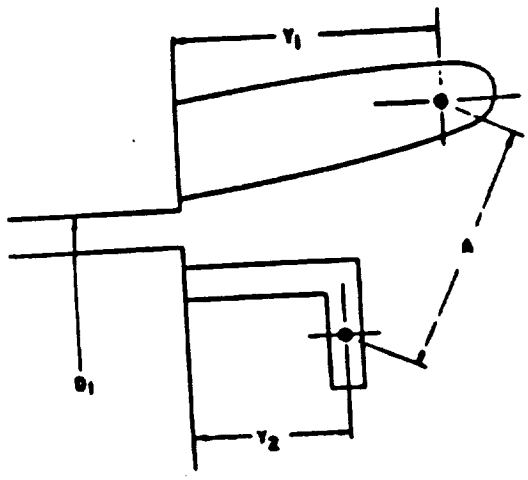

Fig. 2.11. End structure of an induction motor; all distances are in inch.

(From Reference 3)

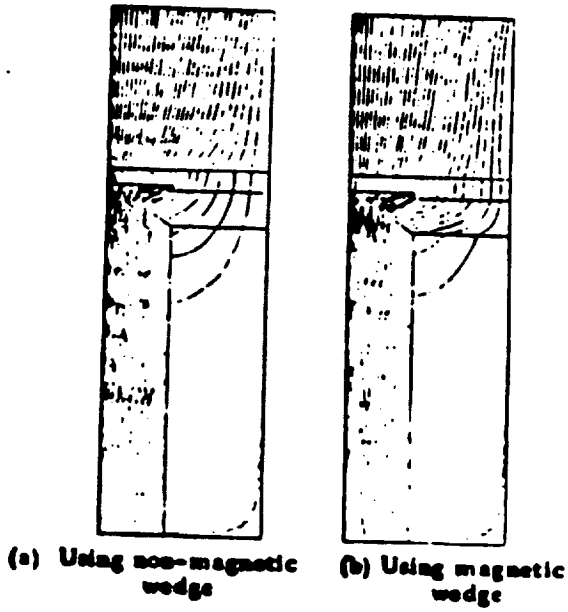

Fig. 2.12. Flux plot (a) without a magnetic wedge and (b) with magnetic wedge.

(From Reference 35)

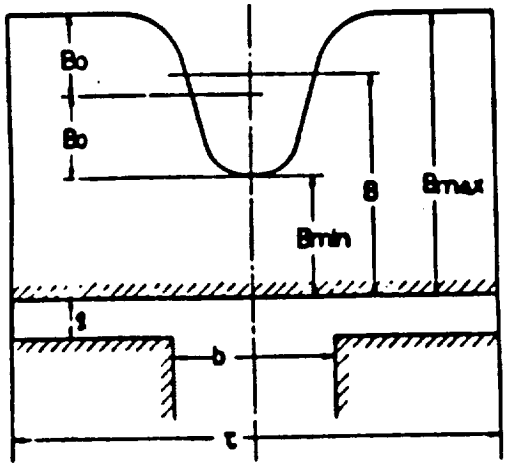

Fig. 2.13. Normal component of flux density on the pole surface.

(From Reference 35)

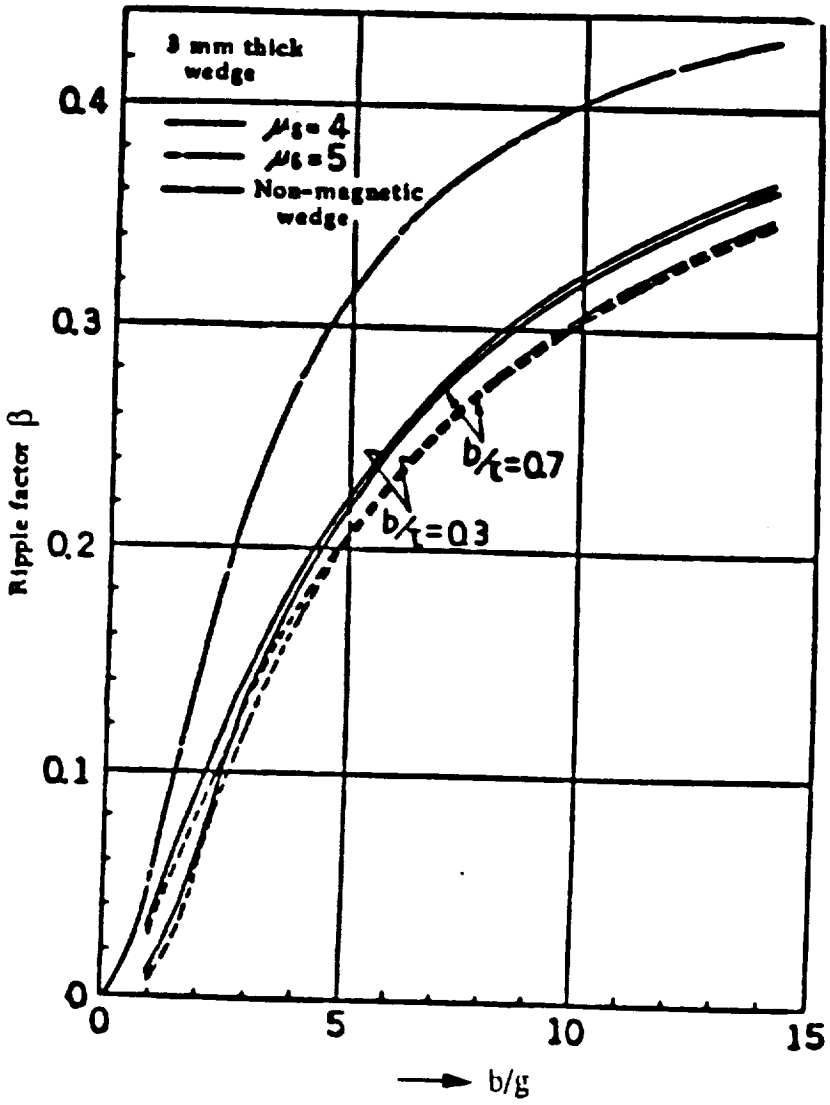

Fig. 2.14. β vs b/g plot.

(From Reference 35)

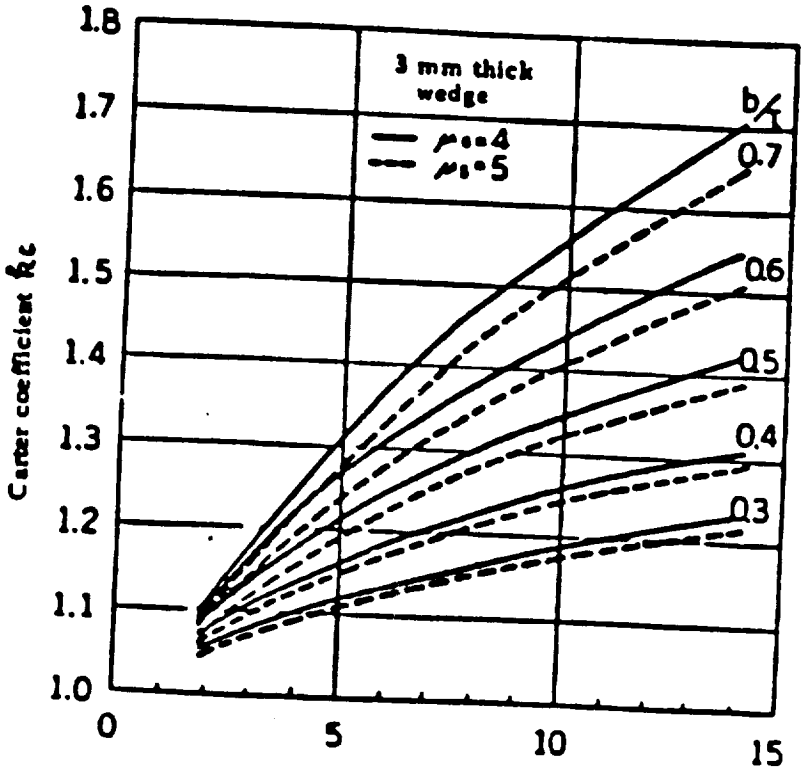

Fig. 2.15. Carter's coefficient when the magnetic wedge is used.

(From Reference 35)

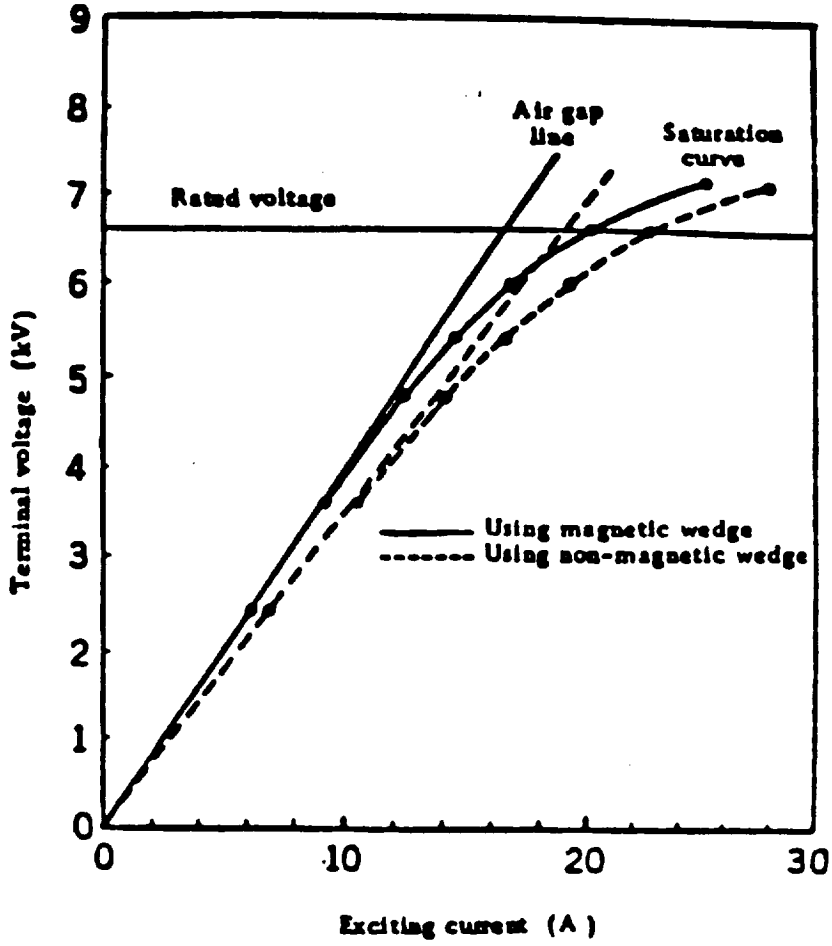

Fig. 2.16. No-load characteristics of a 525 kW induction motor.

(From Reference 35)

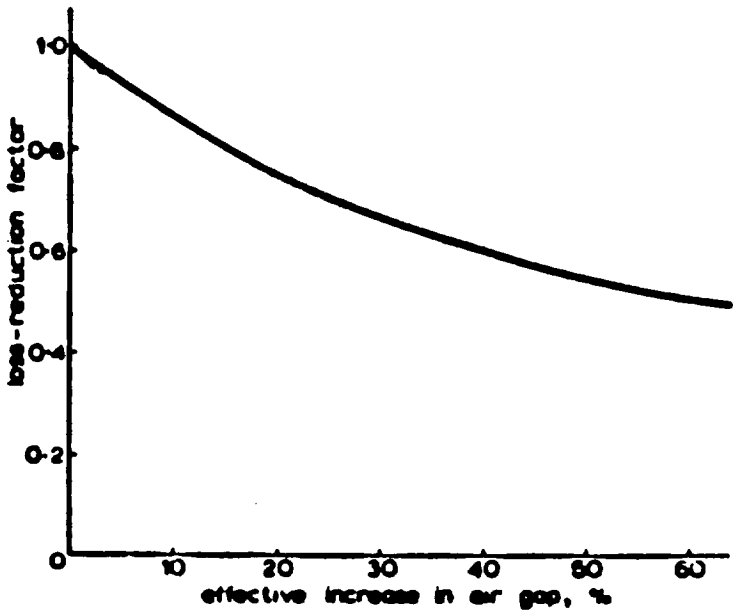

Fig. 2.17. Variation of loss-reduction factor with airgap.

(From Reference 17)

HIGH FREQUENCY LOSSES IN INDUCTION MOTORS

Section 3

High Frequency Time Harmonic Losses in Induction Motors

Syed A. Nasar

Zhenxing Fu

Donald W. Novotny

July 1989

Section 3
High Frequency Time Harmonic Losses in Induction Motors

3.1. Introduction

In the first part of this report we have considered the high-frequency stray losses arising from space harmonics. Because the induction motor is supplied at 400 Hz via an electronic converter with a high frequency (20 kHz) carrier it is importtant that we consider the losses stemming from the carrier frequency. We term these losses as those due to high-frequency time harmonics. The major components of time-harmonic losses at high frequencies are:

(i) I^2R (copper) losses in stator and rotor windings;

(ii) Core losses in stator and rotor cores at the high carrier frequency; and

(iii) Stray losses, which are essentially surface losses in the rotor and stator.

In evaluating these losses, two phenomena--skin effect and the screening effect of the reaction field produced by the induced eddy currents--must be taken into account. We do so by introducing appropriate factors later in the text. The physical significance of skin depth becomes evident if the depth of the material located in the field is several times larger than the skin depth. In this case the electromagnetic wave penetrating into the considered region vanishes at a relatively small depth.

3.2. Resistance and reactance correction factors

Because of a pronounced conductor skin effect, the resistance and reactance of slot-embedded stator and rotor conductors depend on frequency. The modified resistance and reactance, accounting for their skin-effect dependence, are respectively given by

$$R(\omega) = k_{rr}R_0 \tag{3.1}$$

and

$$X(\omega) = k_{xn}X_l(\omega) + X_{end} \tag{3.2}$$

where $X_l(\omega)$ is that portion of leakage reactance which depends on skin effect; X_{end} is assumed to be independent of skin effect. The correction factors k_{rn} and k_{xn} account for the deviation of values of resistance and reactance from their low-frequency values. These correction factors are obtained by solving the field equations for the model shown in Fig. 3.1a and for the nth conductor are given by

$$k_{rn} = \varphi(\xi) + n(n-1)\psi(\xi) \tag{3.1}$$

$$k_{xn} = \frac{3}{2\xi^2}\left[\eta(\xi) + n(n-1)\lambda(\xi)\right] \tag{3.2}$$

where

$$\varphi(\xi) = \xi\,\frac{\sinh 2\xi + \sin 2\xi}{\cosh 2\xi - \cos 2\xi} \tag{3.3}$$

$$\psi(\xi) = 2\xi\,\frac{\sinh 2\xi - \sin 2\xi}{\cosh 2\xi + \cos 2\xi} \tag{3.4}$$

$$\eta(\xi) = \xi\,\frac{\sinh 2\xi - \sin 2\xi}{\cosh 2\xi - \cos 2\xi} \tag{3.5}$$

$$\lambda(\xi) = 2\xi\,\frac{\sinh \xi + \sin \xi}{\cosh \xi + \cos \xi} \tag{3.6}$$

and $\xi = h/\delta$, δ being the skin-depth.

The average values of the correction factors, as obtained from

$$k_r = \frac{1}{M}\sum_{n=1}^{M} k_{rn} \tag{3.7}$$

are given by

$$k_r = \varphi(\xi) + \frac{M^2-1}{3}\psi(\xi) \tag{3.8}$$

and

$$k_x = \frac{3}{2\xi^2 M^2}\left[\eta(\xi) + \frac{M^2-1}{3}\lambda(\xi)\right] \tag{3.9}$$

The correction factor for the rotor with only one conductor in a slot, for M=1 in Eq. (3.8), may be approximated by

$$k_r = \varphi(\xi) \cong 1 + \frac{4}{30}\xi^4 \qquad 0 < \xi < 1 \tag{3.10}$$

$$\cong \xi \qquad \xi > 1 \tag{3.11}$$

As defined earlier, $\xi = h/\delta$, which may also be written as

$$\xi = \left(\frac{\pi\mu_0}{\rho}\frac{c}{b}\right)^{0.5} h f_v^{0.5} \tag{3.12}$$

3.2.1. Corrected rotor resistance

For aluminum rotor bars, $\rho = 425 \times 10^{-10}$ Ωm at 150° C, and we may take $c \cong b$, so that Eq. (3.12) becomes

$$\xi = 9.638\, h f_v^{0.5} \tag{3.13}$$

where f_v is the time-harmonic frequency. Consequently, for the rotor

$$\frac{R_{v(bar)}}{R_{dc(bar)}} = k_r \cong \begin{cases} 1 + 1150\, h^4 f_v^2 & 0 < \xi < 1 \text{ or } f_v < 0.0108 h^{-2} \\ 9.638\, h f_v^{0.5} & \xi > 1 \text{ or } f_v > 0.0108 h^{-2} \end{cases} \tag{3.14}$$

Often, h is expressed in cm, in which case Eq. (3.14) may be written as

$$k_r \cong \begin{cases} 1 + 0.115\, h_{(cm)}^4 f_v^2 \times 10^{-4} & f_v < 108 h_{(cm)}^{-2} \\ 0.0964\, h_{(cm)} f_v^{0.5} & f_v > 108 h_{(cm)}^{-2} \end{cases} \tag{3.15}$$

The corrected rotor resistance is given by

$$\frac{R_{rv}}{R_{r(dc)}} = \begin{cases} 1 + C'_1\, h_{(cm)}^4 f_v^2 & f_v < 108 h_{(cm)}^{-2} \\ C''_1\, h_{(cm)} f_n^{0.5} & f_v > 108 h_{(cm)}^{-2} \end{cases} \tag{3.16}$$

where $C'_1 = 0.115 \times 10^{-4}$ and $C''_1 = 0.0964$. In Eq. (3.16) we have assumed that the end-ring resistance is affected by the skin effect in the same way as the bar resistance.

Major factors influencing R_{rv} are:

(i) rotor bar height or relative height ($\xi = h/\delta$), which determines the nature of the frequency-dependence of the corrected rotor resistance.

(ii) skin effect in the end-ring resistance.

(iii) bar and slot shapes, affecting the value of C''_1 (ranging from 0.025 to 0.15).

3.2.2. Corrected stator resistance

It is generally assumed [3,10] that the results obtained for the model of Fig. 3.1a are approximately valid for circular conductors. To obtain values ofr M, c and h it is necessary to select a reasonable value for the number of conductors per layer and then to convert the round wires in each layer to an equivalent rectangular layer. Using the approach suggested by Niemela, et al., the last conversion can be accomplished in three steps.

step (i) - Express the dimensions of the layer of round wires as shown in Fig. 3.1b(i)

step (ii) - Replace the round wires by conductors of rectangular cross-section, having the same area as that of the round wire. Thus with $h_{cu} = b_{cu}$ in Fig. 3.1b(ii)

$$h_{cu} = \frac{\sqrt{\pi}}{2} d_{cu} \tag{3.17}$$

Step (iii) - Butt the wires together as shown in Fig. 3.1b(iii) for which

$$c = N_1 h_{cu} \tag{3.18}$$

where N_1 = number of round conductors per layer.

For the stator, the correction factors given by Eq. (3.8) may be approximated by

$$k_r \equiv \begin{cases} 1 + \frac{4}{30}\xi^4 + \frac{M^2-1}{3}\left(\frac{1}{3}\xi^4\right) & 0 < \xi < 1 \\ \xi + \frac{M^2-1}{3}(2\xi) & \xi > 1 \end{cases} \tag{3.19}$$

These equations may also be written (for copper conductors in stator slots, $\rho = 205 \times 10^{-10}\ \Omega m$) as

$$k_r \equiv \begin{cases} 1 + C'_2 h_{(cm)}^4 f_v^2 & f_v < 51 h_{(cm)}^{-2} \\ C''_2 h_{(cm)} f_v^{0.5} & f_v > 51 h_{(cm)}^{-2} \end{cases} \tag{3.20a}$$

where

$$\xi = 0.1388 h_{(cm)} f_v^{0.5},$$

$$C'_2 = \left(\frac{4}{30} + \frac{M^2-1}{9}\right) 3.8 \times 10^{-4},$$

and

$$C''_2 = \left[1 + \frac{2}{3}M^2 - 1\right] 0.14,$$

Recall that k_r is the ratio of the stator resistance at a frequency f_v to its dc resistance. Thus,

$$R_{sv} = k_r R_{s(dc)} \tag{3.20b}$$

Plots of correction coefficients and dc resistance $R_{s,dc}(\sim 1/h)$ of stator conductors as functions of relative height ($\xi = h/\delta$) are shown in Fig. 3.2. In this figure, k_r/ξ is for the total effective resistance -- resistance of the conductor in the slot plus the resistance of the end connection. The difference between the dashed-line curves and the solid-line curves arises due to the way in which the resistance of the end connection is taken into account. Solid-line curves correspond to the assumption that the resistance of the end connection has the same correction coefficient as does that in the slot. The dashed-line curves correspond to the assumption that the resistance of the end connection has no skin effect. From these curves it is evident that the losses are minimum for a certain conductor height, known as the critical height of the conductor.

Mathematically, the critical height is obtained from

$$\frac{dR_{s,v}}{d\xi} = 0$$

For a given frequency, δ is fixed; and ξ varies with h. Now,

$$R_{s,v} = k_r \frac{l}{\sigma c h} = \frac{k_r}{\xi} \frac{l}{\sigma c \delta}$$

Thus, $\frac{dR_{s,v}}{d\xi} = 0$ implies that

$$\frac{d}{d\xi}\left[\left(\frac{k_r}{\xi}\right)\frac{l}{\sigma c \delta}\right] = 0$$

or

$$\frac{d}{d\xi}\left(\frac{k_r}{\xi}\right)=\frac{d}{d\xi}\left[\frac{\varphi(\xi)+\frac{1}{3}\left(M^2-1\right)\psi(\xi)}{\xi}\right]=0$$

For M=1,

$$\xi_{critical}=\frac{\pi}{2}=1.57 \qquad (3.20c)$$

For $M \geq 2$

$$\xi_{critical}=\left(\frac{3}{M^2-0.2}\right)^{1/4} \qquad (3.20d)$$

Equations (3.20a) and (3.20b) show the nonuniform increase in the stator resistance. At low frequencies, the resistance increases as f_v^2, whereas at high harmonic frequencies the resistance is proportional to $f_v^{0.5}$. The stator end connection resistance is assumed to vary in a manner similar to the resistance of the conductors in the slot.

We now consider the variation of k_r with M. Combining Eqs. (3.18a) and (3.20a) yields

$$k_r=\left(0.14\ k_{fill}\frac{bH}{c}\right)\frac{1}{M}\left[1+\frac{2}{3}\left(M^2-1\right)\right]f_v^{0.5} \qquad (3.20e)$$

Note that for large M's, (3.20e) becomes

$$k_r=\alpha M f_v^{0.5} \qquad (3.20f)$$

where α is a proportionality constant.

Now, if H = constant, for large M, k_r is directly proportional to M and R_{sv} increases with k_r, since R_{dc} = constant. Next, if M = constant, as H increases, R_{dc}(~ 1/H) decreases and k_r(~ H) increases. Thus the corrected resistance $R_{sv} = \sim k_r R_{dc}$ remains approximately unchanged with an increase in H.

The factors influencing R_{sv} are:

(i) number of layers of conductors, M; k_r is sensitive to M.

(ii) height of conductor layers, h, which determine the nature of the frequency-dependence of the corrected stator resistance.

(iii) skin-effect, affecting the end-connection resistance.

(iv) conductor shape, material, and temperature.

3.2.3. Corrected rotor leakage reactance

For the rotor we have M=1 and k_x of Eq. (3.9) may be approximated by

$$k_x \cong \begin{cases} 1 & 0 < \xi < 1 \\ \dfrac{3}{2\xi} & \xi > 1 \end{cases} \qquad (3.21)$$

Substituting $\xi = 0.1\, h_{(cm)} f_v^{0.5}$ in Eq. (3.21) yields

$$k_x \cong \begin{cases} 1 & f_v < 108 h_{(cm)}^{-2} \\ C''_3 h_{(cm)}^{-1} f_v^{-0.5} & f_v > 108 h_{(cm)}^{-2} \end{cases} \qquad (3.22a)$$

where $C''_3 = 15$.

The rotor end-ring leakage reactance is practically independent of skin effect, as indicated by Eq. (3.2). Therefore, the corrected rotor leakage reactance becomes

$$X_{2v} = k_x \frac{f_v}{f_1} X'_2(f_1) + \frac{f_v}{f_1} X_{2end}(f_1) \qquad (3.22b)$$

where $X'_2(f_1) = (X_2 - X_{2end})$ at the fundamental frequency f_1.

Figure 3.3 shows a substantial increase in the effective reactance of the conductor as the slot opening or the ratio l/a is reduced (where l and a are slot dimensions shown in Fig. 3.3(a)). Notice that the variation of reactance with l/a is greater for higher values of h/δ.

3.2.4. Corrected stator leakage reactance

Since we have M layers of conductors in stator slots, k_x of Eq. (3.9) may be approximated by

$$k_x \cong \begin{cases} 1 & 0 < \xi > 1 \\ \\ \dfrac{1}{M^2}\left(\dfrac{1}{2} + M^2\right)\dfrac{1}{\xi} & \xi > 1 \end{cases} \qquad (3.23)$$

which may also be written as (for copper windings)

$$k_x \cong k_x \cong \begin{cases} 1 & f_v < 51 h_{(cm)}^{-2} \\ \\ C''_4 h_{(cm)}^{-1} f_v^{-0.5} & f_v > 51 h_{(cm)}^{-2} \end{cases} \qquad (3.24a)$$

where

$$C''_4 = \frac{7.14}{M^2}(M^2 + 0.5)$$

Again the stator end-connection leakage reactance is independent of skin effect. The corrected stator leakage reactance becomes:

$$X_{1v} = k_x \frac{f_v}{f_1} X'_1(f_1) + \frac{f_v}{f_1} X_{1end}(f_1) \qquad (3.24b)$$

where $X'_1(f_1) = (X_1 - X_{1end})$ at the fundamental frequency f_1.

Figure 3.4 shows the ratio of the measured leakage inductance to the normal leakage inductance at fundamental frequency [3]. Notice that the leakage inductance does not drop as fast as indicated by skin effect. This is due to the fact that the end leakage inductance is relatively independent of the skin effect in the slots.

3.3. I^2R loss calculations

Knowing the corrected resistances and leakage reactances, the I^2R losses in the rotor and stator may be determined from the approximate equivalent circuit which consists of the resistances and leakage reactances in series. The equivalent circuit shown in Fig. 3.5 is developed from that of a conventional induction motor by setting

$$s_v = \frac{vf_1 - (1-s)f_1}{vf_1} \cong 1 \quad \text{for } v >> 1$$

The magnetizing reactance being relatively large is not included in the circuit of Fig. 3.5.

From the circuit the harmonic current is given by

$$I_v^2 = \frac{V_v^2}{(R_{sv} + R_{rv})^2 + (X_{1v} + X_{2v})^2} = \frac{V_v^2}{Z_v^2} \tag{3.25}$$

where V_v = RMS input harmonic voltage at f_v

$$R_{sv} = (k_r)_s R_{s(dc)}$$

$$R_{rv} = (k_r)_r R_{r(dc)}$$

$$X_{1v} = (k_x)_s \frac{f_v}{f_1} X_1(f_1) + X_{1end}$$

$$X_{2v} = (k_x)_r \frac{f_v}{f_1} X_2(f_1) + X_{2end}$$

and

f_1 = input fundamental frequency (60 Hz).

Using the frequency constraints on the correction factors for high frequencies, we obtain

$$Z_v = (R_{sv} + R_{rv}) + j(X_{1v} + X_{2v})$$

$$= \left(C''_2 h R_{s(dc)} + C''_1 H R_{r(dc)}\right)_{(cm)} f_v^{0.5}$$

$$+ j\left\{\left[\frac{C''_4}{f_1 h} X'_1(f_1) + \frac{C''_3}{f_1 H} X'_2(f_1)\right]_{(cm)} f_v^{0.5} + [X_{1end}(f_1) + X_{2end}(f_1)]\frac{f_v}{f_1}\right\} \tag{3.26}$$

Then, the losses are given by:

$$\text{stator copper loss - } (W_{cu})_{sv} = 3I_v^2 R_{sv} \tag{3.27a}$$

$$\text{rotor copper loss - } (W_{cu})_{rv} = 3I_v^2 R_{rv} \tag{3.27b}$$

The ratio of copper loss at a high harmonic frequency to that at fundamental frequency is:

for stator $f_v > 51\ h^{-2}_{(cm)}$:

$$\frac{(W_{cu})_{sv}}{(W_{cu})_{s1}} = C''_2 h_{(cm)} f_v^{0.5} \left(\frac{I_v}{I_1}\right)^2 \tag{3.27c}$$

for rotor $f_v > 108 h^{-2}_{(cm)}$:

$$\frac{(W_{cu})_{rv}}{(W_{cu})_{r1}} = C''_1 H_{(cm)} f_v^{0.5} \left(\frac{I_v}{I'_2}\right)^2 \tag{3.27d}$$

where I_1 and I'_2 are, respectively, the stator and rotor currents on load at fundamental frequency.

3.4. High-frequency core losses

High-frequency stator mmf produces a rotating magnetic field, with the synchronous speed $\omega_{sv} = 2\pi f_v$, in the airgap. This high-frequency field penetrates the stator and rotor teeth surfaces to a skin depth giving rise to traditional core losses at the (fundamental) carrier frequency, f_v. Because the field does not significantly penetrate the

tooth body, there will be no respective loss. The induced eddy currents produce a reaction field, which will further reduce the resultant flux density. According to Richter [8] the respective stator and rotor core losses are given by

$$(W_{fe})_{sv} = \left[\sigma_e\left(\frac{f_v}{100}\right)^2 k_{sk}^2 k_{er} + \sigma_h\left(\frac{f_v}{100}\right)k_{sk}^2\right]\left(\frac{B_{mv}}{100}\right)^2 \text{ W/kg} \tag{3.28a}$$

$$(W_{fe})_{rv} = \left[\sigma'_e\left(\frac{f_v}{100}\right)^2 k_{sk}^2 k_{er} + \sigma'_h\left(\frac{f_v}{100}\right)k_{sk}^2\right]\left(\frac{B_{mv}}{100}\right)^2 \text{ W/kg} \tag{3.28b}$$

where f_v = harmonic frequency

B_{mv} = maximum harmonic airgap flux density, gauss

$$k_{sk} = \frac{\sqrt{2}}{\xi}\sqrt{\frac{\cosh\xi-\cos\xi}{\cosh\xi+\cos\xi}} = \text{skin-effect factor} \tag{3.29a}$$

$$k_{cr} = \frac{3}{\xi}\left(\frac{\sinh\xi-\sin\xi}{\cosh\xi-\cos\xi}\right) = \text{reaction-field factor} \tag{3.29b}$$

$\xi = 2d\lambda$

$\lambda = \sqrt{\mu\omega_v/2\rho} = \frac{1}{\delta}$

$2d$ = lamination thickness

δ = skin depth, m

μ = $\mu_r\mu_0$ = core permeability, H/m

ρ = resistivity of laminations, Ω-mm^2/m ~ 0.15 Ω-mm^2/m

Plots of Eqs. (3.29a) and (3.29b) with ξ ($\sim \sqrt{f}$) are shown in Fig.3.6.

To determine B_{mv}, we observe that the harmonic field due to high carrier frequency does not contribute to the magnetizing field (Fig. 3.5).

The harmonic flux per pole is given by

$$\phi_v = B_{mv} \frac{\pi D}{p} l \tag{3.30a}$$

The corresponding harmonic voltage becomes

$$E_v = 4.44\, f_v\, N_{eff} \phi_v = N_{eff} B_{mv} \frac{\pi D l}{p} \tag{3.30b}$$

where N_{eff} = effective number of stator turns/phase and $N_{eff} = \sqrt{k_x}\, N$, (k_x being the correction factor for leakage reactance and N is actual number of turns/phase).

The effective number of turns N_{eff} in Eq. (3.30b) is a consequence of skin effect which tends to reduce the number of turns and the corresponding reactance. For instance, without skin effect, the leakage flux linkage is given by

$$\lambda_l = \frac{X_{l\,v}}{\omega_v} I_{1v}$$

With skin effect, the leakage flux linkage becomes

$$\lambda_{l\,v} = \frac{k_x X_{l\,v}}{\omega_v} I_{1v}$$

Assuming the leakage permeance Λ_l to be the same in both cases, the above flux linkages may be written as

$$\lambda_l = \frac{N^2 \Lambda_l}{\omega_v} I_{1v}$$

and

$$\lambda_{lv} = k_x N^2 \frac{\Lambda_l}{\omega_v} I_{1v}$$

$$= N_{eff}^2 \frac{\Lambda_l}{\omega_v} I_{1v}$$

Consequently, $N_{eff} = \sqrt{k_x}\, N$.

Referring to the equivalent circuit shown in Fig. 3.5, we obtain:

$$B_{mv} = \frac{|V_v - (R_{sv} + jX_{1v})I_v|}{4.44\, f_v\, N_{eff} \left(\frac{\pi D}{p} l\right)} T \qquad (3.30c)$$

Notice that the core losses at high carrier frequency are very small for the following reasons:

(i) From an equivalent circuit viewpoint, since $s_v \cong 1$, the magnetizing impedance, being very large compared to $(R_{rv} + X_{2v})$, may be neglected. Consequently, $I^2_{mv} R_{cv} \cong 0$.

(ii) From a physical point of view, since the high frequency field does not penetrate the tooth body, the corresponding loss is negligible. Sample calculations validate this fact.

3.5. Stray losses

As mentioned earlier, high frequency harmonic fields penetrate the iron core through a skin depth. Therefore, at high carrier frequency there are no tooth pulsation losses and cage-circulating current I^2R losses will be negligible. The remaining stray loss components are the surface losses of the following origins:

(i) slot leakage flux

(ii) zig-zag leakage flux

(iii) end-connection leakage flux

3.5.1. Surface loss due to slot-leakage flux

The slot leakage flux penetrates the slot walls (and bottom) through a skin depth. This flux induces eddy currents producing surface eddy-current losses, at the fundamental of the carrier frequency. This portion of stray losses is generally negligible in the motor at the fundamental input frequency (~ 60 Hz).

Figure 3.7 shows the stator-slot leakage flux paths and the corresponding flux density distribution along the slot depth, where δ is the skin depth for the conductors and δ_c is the skin depth for the core lamination. The average stator-slot leakage flux per slot at the slot walls per unit slot depth is given by:

$$\phi_{1v} = \frac{1}{N_1}\left(\frac{X_{1vslot}}{2\pi f_v} I_v \frac{1}{S_1}\right)\frac{1}{(H_1/\xi)} \text{ Wb/m} \tag{3.31}$$

where

N_1 = number of stator turns per phase

S_1 = number of stator slots per phase

H_1/ξ = approximate sum of skin depths for M layers of conductors.

From Appendix A of Part of 2 of this report, the surface loss per unit surface area is given by

$$W'_s = \frac{\phi^2 \lambda^3 \rho}{\mu^2} \left(\frac{\sinh 2\lambda d - \sin 2\lambda d}{\cosh 2\lambda d - \cos 2\lambda d} \right) k_{er} \ W/m^2 \tag{3.32}$$

where

ϕ = flux per meter, Wb/m

ρ = core resistivity (= 5×10^{-7} Ωm for 1% Si steel)

μ = $\mu_r \mu_0$ = core permeability, H/m

$2d$ = lamination thickness, m

λ = $\sqrt{\mu \omega_v / 2\rho} = 1/\delta_c$, m^{-1}

δ_c = skin depth of lamination (Fig.3.7), m

ω_v = $2\pi f_v$

k_{er} = reaction-field factor defined by Eq. (3.29b)

ξ = $2d\lambda$.

The total surface loss due to stator slot leakage is

$$W_{1SL} = [S(2H_1+b)\delta_c]\frac{\phi_{1v}^2\rho}{\mu^2}\left(\frac{\sinh 2\lambda d-\sin 2\lambda d}{\cosh 2\lambda d-\cos 2\lambda d}\right)k_{er} \quad W \tag{3.33}$$

where S = total number of stator slots and $(2H+b)\delta_c$ = surface area of slot lamination across which leakage flux flows (Fig. 3.7).

Figure 3.8 shows the rotor-slot leakage fluxes and flux density distribution, where δ is the skin depth of the conductor and δ_c the skin depth of the core. The average rotor-slot leakage flux per slot at the slot walls per unit slot depth is:

$$\phi_{2v} = \frac{1}{N_2}\left(\frac{X_{2vslot}}{2\pi f_v} I_v \frac{1}{R_1}\right)\frac{1}{(H_2/\xi)} \text{ Wb/m} \tag{3.34}$$

where

N_2 = rotor number of turns per phase

R_1 = number of rotor slots per phase

δ = (H_2/ξ) = approximate skin depth of the rotor bar.

As in Eq. (3.32) the total surface loss due to rotor-slot leakage is

$$W_{2SL} = [R(2H_2+b)\delta_c]\frac{\phi_{2v}^2\lambda^3\rho}{\mu^2}\left(\frac{\sinh 2\lambda d-\sin 2\lambda d}{\cosh 2\lambda d-\cos 2\lambda d}\right)k_{er} \quad W \tag{3.35}$$

where R = total number of rotor slots and $(2H+b)\delta_c$ = surface area across which leakage flux flows, and the corresponding loss occurs.

3.5.2. Surface loss due to zigzag leakage flux

Dips in the carrier frequency stator flux distribution around the airgap due to slot openings cause slot frequency ($2S'f_v$, S' = stator slots per pole) pulsations in the radial flux density around the airgap. These pulsations cause surface losses. To calculate these losses, we use the method of Appendix A of Part 2 of this report. As found in Part 2, these surface losses are primarily due to the stator slot openings. Referring to Fig. 2.5 and Appendix A of Part 2, the maximum pulsation flux density is

$$B_{vk} = \frac{\pi}{4}\left(\frac{\beta}{2-\beta}\right) B_{vg} \tag{3.36}$$

where B_{vg} is the average flux density in the airgap at f_v.

Here we have used B_{vk} because B_{vk} gives rise to surface loss due to zigzag leakage, whereas B_{vg} produces the tooth surface losses, which have already been considered as core losses.

Using the approach given in Part 2 of this report, the surface pulsation flux due to zigzag leakage is, approximately, given by

$$\phi_{vrsk} = \frac{1}{2} B_{vk} l\, w_{rt0}\left[\frac{\sin(k\pi k_2/2R')}{k\pi k_2/2R'}\cos\left(\frac{k\pi k_2}{2R'} + \omega_m t\right) - \frac{\sin(k\pi k_2/R')}{k\pi k_2/R'}\cos\omega_m t\right] \tag{3.37}$$

where

l = axial core length, m

w_{rt0} = rotor tooth width at the airgap, m

R' = number of rotor slots per pole

k = $2S' \pm 1$

S' = number of stator slots per pole

$$k_2 = \frac{w_{rt0}}{t_{r0}}$$

t_{r0} = rotor tooth pitch.

Then

$$\left(\frac{\phi_{vrsk}}{w_{rt0}}\right)^2_{ave} = \frac{1}{8}\frac{\pi^2}{16}\left(\frac{\beta}{2-\beta}\right)^2 B_{vg}^2 l^2 C_{v1r} \tag{3.38}$$

where

$$C_{v1r} = \left(\frac{\sin k\pi k_2/2R'}{k\pi k_2/2R'}\right)^2 + \left(\frac{\sin k\pi k_2/R'}{k\pi k_2/R'}\right)^2$$

$$- \frac{\sin\left(k\pi k_2/2R'\right)}{k\pi k_2/2R'} \cdot \frac{\sin\left(k\pi k_2/R'\right)}{k\pi k_2/R'} \cos\frac{k\pi k_2}{2R'} \tag{3.39}$$

The total rotor surface losses due to zigzag leakage flux is

$$W_{s0v} = 2(\pi D\delta)\frac{1}{8}\frac{\pi^2}{16}\left(\frac{\beta}{2-\beta}\right)^2 B_{vg}^2 l^2 \frac{\lambda^3 \rho}{\mu^2} C_{v1r} k_{er}\left(\frac{\sinh 2\lambda d - \sin 2\lambda d}{\cosh 2\lambda d - \cos 2\lambda d}\right)$$

where the factor 2 accounts for the harmonic fields ($2S' \pm 1$) and D is the diameter at the bore.

3.5.3. Surface loss due to end-connection leakage flux

The end-connection leakage fluxes of the stator and rotor will partly link with the core and structural parts, penetrate the core in the axial direction through a skin depth induce eddy currents in the core and cause additional main frequency (f_v) eddy current

losses. Referring to Fig. 2.11 of Part 2 of this report, the end-connection leakage fluxes produce a total loss given by

$$W_{E,v} = 0.3\ m I_v^2 \left[\frac{1.6 f_v m N^2 D}{p^2 10^7} \log\left(1 + \frac{A^2}{4 Y_1 Y_2}\right) \right] k_{sk}^2 k_{re}\ W \tag{3.41}$$

where:

$k_{sk} = \frac{\sqrt{2}}{\xi} \sqrt{\frac{\cosh\xi - \cos\xi}{\cosh\xi + \cos\xi}}$ = skin effect coefficient

$k_{re} = \frac{3}{\xi} \frac{\sinh\xi - \cos\xi}{\cosh\xi + \cos\xi}$ = correction factor for the reaction effect of eddy-current

I_v = rms current per phase at f_v

m = number of phases

N = effective winding turns per phase

D = bore diameter

p = number of poles

A = slant distance between the assumed center of the stator and rotor peripheral currents

Y_1, Y_2 = axial distance between stator and rotor end-current centers to the end of the laminated core.

3.6. Sample calculations

From the given data by Kuhlmann [37]:

3.6.1. I^2R copper losses for stator and rotor (at 20 kHz)

For rotor:

$\xi = 18.38 > 1$ from Eq. (3.13)

$k_r = 18.38$ from Eq. (3.15)

$R_{rv} = 2.2\ \Omega$ from Eq. (3.16)

$k_x = 0.0816$ from Eq. (3.21)

$X_{2v} = 47.9\ \Omega$ from Eq. (3.2)

For stator:

$\xi = 3.38 > 1$ from Eq. (3.13)

$k_r = 79.4$ from Eq. (3.19)

$R_{sv} = 11.9\ \Omega$ from Eq. (3.16)

$k_x = 0.3$ from Eq. (3.24)

$X_{1v} = 63.3\ \Omega$ from Eq. (3.2)

Thus:

$I_v = 1.133$ A from Eq. (3.25)

$$(W_{cu})_{sv} = 3I_v^2 R_{sv} = 45.83\ \text{W}$$

$$(W_{cu})_{rv} = 3I_v^2 R_{rv} = 8.5\ \text{W}$$

Total copper losses:

$$(W_{cu})_v = (W_{cu})_{sv} + (W_{cu})_{rv} = 45.83 + 8.5 = 54.33 \text{ W}.$$

3.6.2. Core losses: Refer to Section 3.4).

α $= 205.2 \text{ cm}^{-1}$

ξ $= 9.903$

k_{er} $= 0.30303$

k^2_{sk} $= 0.02039$

N_{eff} $= 44$ turns

$B_{m,v}$ $= 20.5$ Gauss

For the stator:

$$(W_{fe})_{sv} = 0.59 \times 10^{-2} \text{ W/kg}$$

For the rotor:

$$(W_{fe})_{rv} = 1.28 \times 10^{-2} \text{ W/kg}$$

For core losses:

$$(W_{fe})_v = (W_{fe})_{sv} G_s + (W_{fe})_{rv} G_r = 0.12 \text{ watts}$$

where

G_s = corresponding stator tooth weight

G_r = corresponding rotor tooth weight

3.6.3. Additional stray losses:

Surface loss due to stator slot leakage:

$$\phi_{1v} = \frac{0.1643}{14940} \text{ Wb}$$

$W_{1SL} = 6.8$ watts

Surface losses due to rotor slot leakage:

$$\phi_{2v} = \frac{0.2734}{1230} \text{ Wb}$$

$W_{2SL} = 7.43$ watts

Surface loss due to zigzag leakage flux:

$\beta = 0.85$

$B_{vk} = 11.9 \times 10^{-4}$ Tesla

$C_{v,1r} = 0.1175$

$\xi = 9.903$

$W_{s0,v} = 0.026$ watts

Surface loss due to end-connection leakage flux:

$W_{E,v} = 0.0155$ watts

Total surface losses:

$$W_{stray,v} = W_{1SL} + W_{2SL} + W_{s0,v} + W_{E,v} = 6.8 + 7.43 + 0.026 + 0.0155 = 14.3 \text{ watts}$$

3.6.4. Total additional losses due to 20 kHz carrier frequency:

$$W_v = (W_{cu})_{sv} + (W_{cu})_{rv} + (W_{Fe})_{sv} + (W_{Fe})_{rv} + W_{1SL} + W_{2SL} + W_{s0,v} + W_{E,v}$$

$$= 45.83 + 8.5 + 0.12 + 6.8 + 7.43 + 0.026 + 0.0155$$

$$= 68.75 \text{ watts.}$$

$$\left(\frac{(W_{cu})_v}{W_v}\right) = \frac{(W_{cu})_{sv} + (W_{cu})_{rv}}{W_v} = 79.25\% \cong 79\%$$

$$\left(\frac{(W_{fe})_v}{W_v}\right) = \frac{(W_{fe})_{sv} + (W_{fe})_{rv}}{W_v} = 0.175\% \cong 0.2\%$$

$$\left(\frac{W_{stray,v}}{W_v}\right) = \frac{W_{1SL} + W_{2SL} + W_{s0,v} + W_{E,v}}{W_v} = 20.8\%$$

3.7 References

(1) Andresen, E. Ch., Schindler, A., "Additional induction motor losses due to transistor inverter supply,"

(2) Chalmers, B. J., Sarkar, B. R., "Induction-motor losses due to nonsinusoidal supply waveforms," Proc. IEE, Vol. 115, No. 12, Dec. 1968, pp. 1777-1782.

(3) DeBuck, F. G. G., "Losses and Parasitic torques in electric motors, subjected to PWM-waveforms," IEEE-IAS Annual Meeting '77, pp. 922-929.

(4) Fuchs, E., Chang, L. H. and Appelbaum, J., "IEEE Trans.-PAS, Vol. PAS-103, No. 11, Nov. 1984, pp. 3303-3312, "Magnetizing current, iron losses and forces of ".

(5) Hentschel, F. Shehata, M. A., "Comparative study of the losses in inverter-fed standard squirrel-cage induction motors," pp. 320-323.

(6) Largiader, H., "Design aspects of induction motors for traction applications with supply through static frequency changers," Brown Boveri Review, 57 (1970) 4, pp. 152-167.

(7) Mitschenko, W., Sergel, I., Echtler, K., "Betrieb eines Asynchronomotors mit optimaler spannungsund Frequenzregelung bei konstanter verlustsume," Bull. ASE/UCS, 65, (1974) 3, pp. 162-171.

(8) Stoll, R. L., "The analysis of eddy-currents," Oxford University Press, 1974.

(9) Richter, R., "Elektrische Maschinen," Vol. 1, Julius Springer Verlag, Berlin, 1924.

(10) de Buck, F. G. G. and etc., "A simple but reliable loss model for inverter-supplied induction motors," IEEE Trans. on Industry Applications, vol. IA-20, No. 1, Jan/Feb. 1986, pp. 190-202.

(11) Swann, S. A. and Falmon, J. W., "Effective resistance and reactance of a rectangular conductor placed in a semiclosed slot," Proc. IEE, vol. 100, 1963, pp. 1656-1662.

(12) Lammeraner, Jeff and Stafl, Milos, "Eddy currents," Iliffe Books Ltd., 1966.

(13) Kimoh, A. A., Findlay, S. R. D. and Poloujadoff, M., "Stray losses in induction machine, Part II," IEEE Trans., Vol. PAS-104(6), 1985, pp. 1500-1572.

(14) Alger, P. L. and etc., "Stray load losses in polyphase induction machines," AIEE Trans., Vol. 79 (III), 1959, pp. 349-357.

(15) Niemela, V. A., Skutt, G. R., Urling, A. M., Chang, Y. N., Wilson, T. G., Owen, H. A. and Wong, R. C., "Calculating the short circuit impedances of a multiwinding transformer from its geometry," PESC Record, 1989, pp 607-617.

3.8. Appendix

A comparison between two- and one-dimensional solutions to the diffusion equation

S. A. Nasar

Two-dimensional results given by L. V. Bewley: Two-Dimensional Fields in Electrical Engineering, Dover 1960

Copper loss in the nth conductor per unit conductor length is

$$W_p = \frac{\rho I^2}{2hc}\left\{\left[n^2 + (n-1)^2\right]X - 2n(n-1)Y\right\} \tag{3.8.1}$$

where

$$X = kh\left(\frac{\sinh 2kh + \sin 2kh}{\cosh 2kh - \cos 2kh}\right) \tag{3.8.2}$$

and

$$Y = 2kh\left(\frac{\cos kh \sinh kh + \cosh kh \sin kh}{\cosh 2kh - \cos 2kh}\right) \tag{3.8.3}$$

From (our) one-dimensional analysis:

$$W_p = \frac{1}{2} I^2 R'_0 \xi \left[\frac{\sinh 2\xi + \sin 2\xi}{\cosh 2\xi - \cos 2\xi} + 2n(n-1)\frac{\sinh \xi - \sin \xi}{\cosh \xi + \cos \xi}\right] \tag{3.8.4}$$

where $\xi = kh$

and $R'_0 = \frac{1}{\sigma hc}$ = resistance per unit conductor length.

Now, the last term in (4) may be written as:

$$2n(n-1)\frac{\sinh \xi - \sin \xi}{\cosh \xi + \cos \xi} \cdot \frac{\cosh \xi - \cos \xi}{\cosh \xi - \cos \xi}$$

$$= 2n(n-1)\frac{\sinh \xi \cosh \xi - \sin \xi \cosh \xi - \sinh \xi \cos \xi + \cos \xi \sin \xi}{\cosh^2 \xi - \cos^2 \xi}$$

$$= 2n(n-1)\frac{\frac{1}{2}(\sinh 2\xi + \sin 2\xi) - \cosh \xi \sin \xi - \sinh \xi \cos \xi}{\frac{1}{2}(\cosh 2\xi - \cos 2\xi)} \tag{3.8.5}$$

Combining (3.8.4) and (3.8.5) yields:

$$W_p = \frac{1}{2} I^2 R'_0 \xi \left\{[2n(n-1)+1]\frac{\sin 2\xi + \sin 2\xi}{\cosh 2\xi - \cos 2\xi}\right.$$

$$\left. -2n(n-1)\frac{\cosh \xi \sin \xi + \sinh \xi \cos \xi}{\frac{1}{2}(\cosh 2\xi - \cos 2\xi)}\right\}$$

$$= \frac{1}{2} I^2 R'_0 \left\{ [n^2 + (n-1)^2]\xi \frac{\sinh 2\xi + \sin 2\xi}{\cosh 2\xi - \cos 2\xi} \right.$$

$$\left. - 2n(n-1)2\xi \frac{\cosh \xi \sin \xi + \sinh \xi \cos \xi}{\cosh 2\xi - \cos 2\xi} \right\}$$

$$= \frac{I^2}{2\sigma he} \left\{ [n^2 + (n-1)^2]x - 2n(n-1)Y \right\} \qquad (3.8.6)$$

Comparing (3.8.1) and (3.8.6) indicates that the two results are identical.

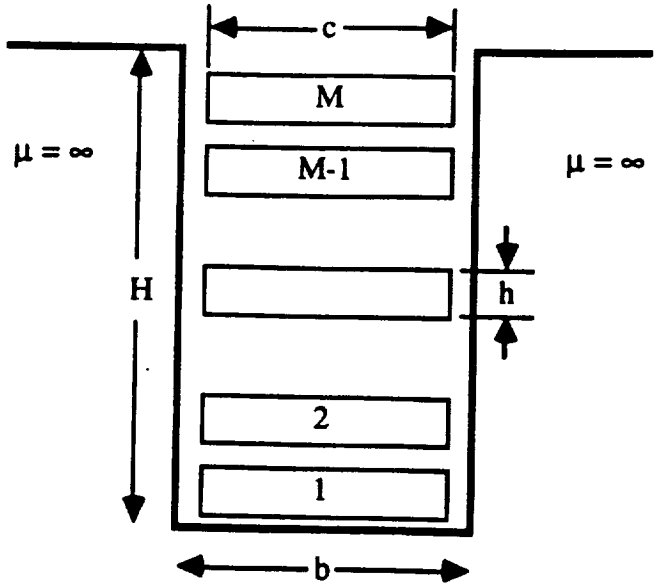

Fig. 3.1a Open slot with M conductors.

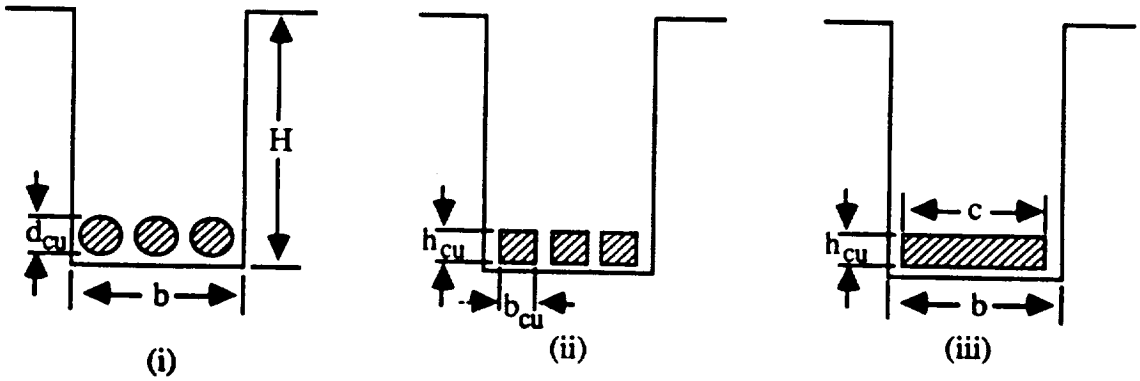

Fig. 3.1b Steps in Transforming a Layer of Round Wires into a Rectangular Layer

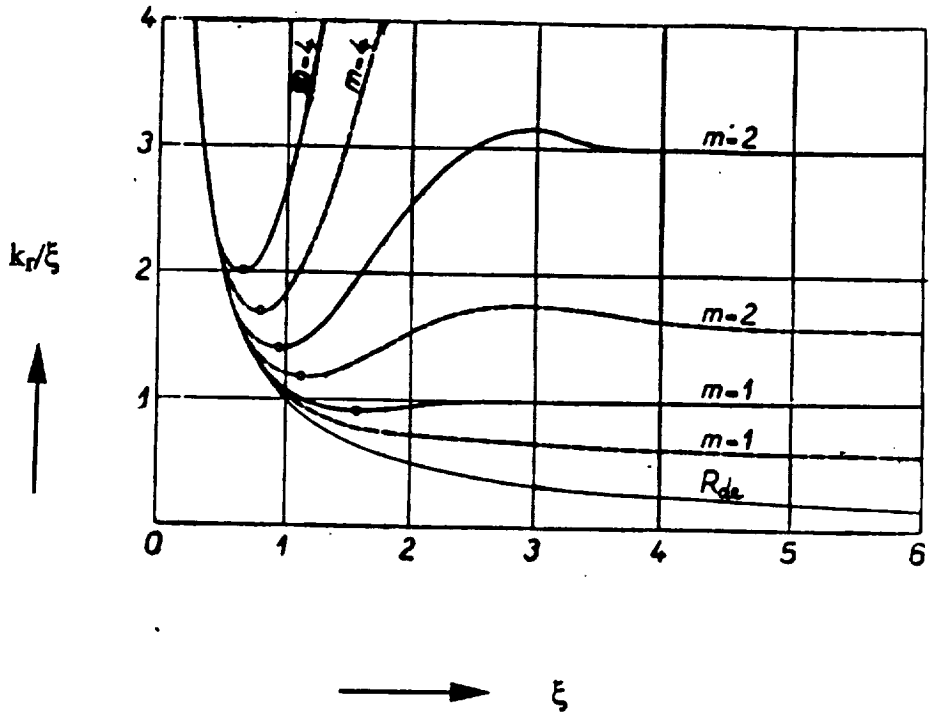

Fig. 3.2. k_r/ξ and R_{dc} vrs $\xi = h/\delta$. $\xi = 0$ to $6 \sim f_v = 0$ to 84 kHz.
[$\xi = h/\delta$, h = conductor thickness, δ= skin depth.]
(From Ref. 7)

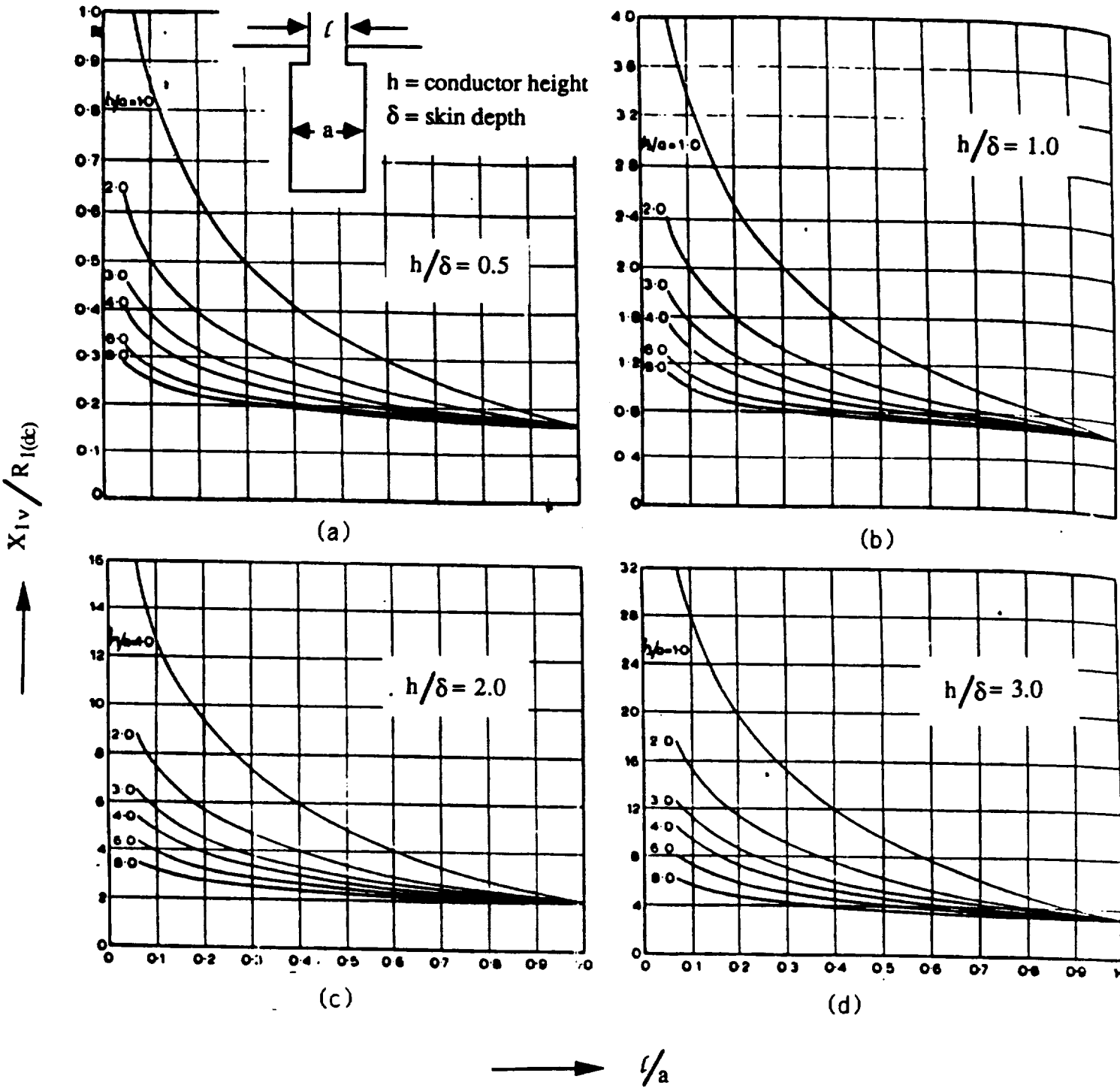

Fig. 3.3. Variation of effective reactance with slot opening.
(from Ref. 11).

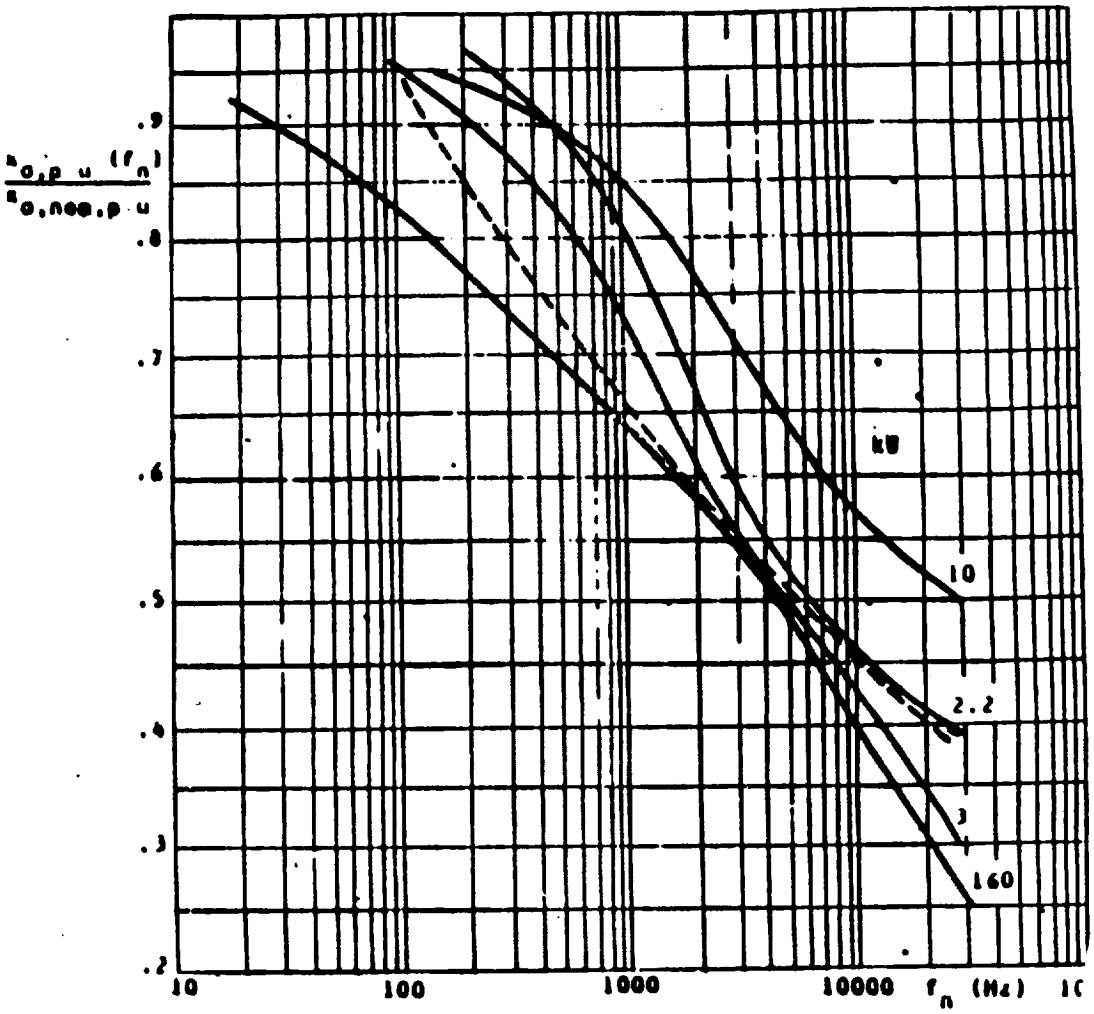

Fig. 3.4. Leakage $x_{\sigma,pu}(f_n)/x_{\sigma,nom,pu}$ as function of frequency f_n, as measured on nomially saturated 2.2-, 3-, 10-, and 160-kW motors.
_____Measured inductance; -----Averaged inductance.
(From Ref. 3).

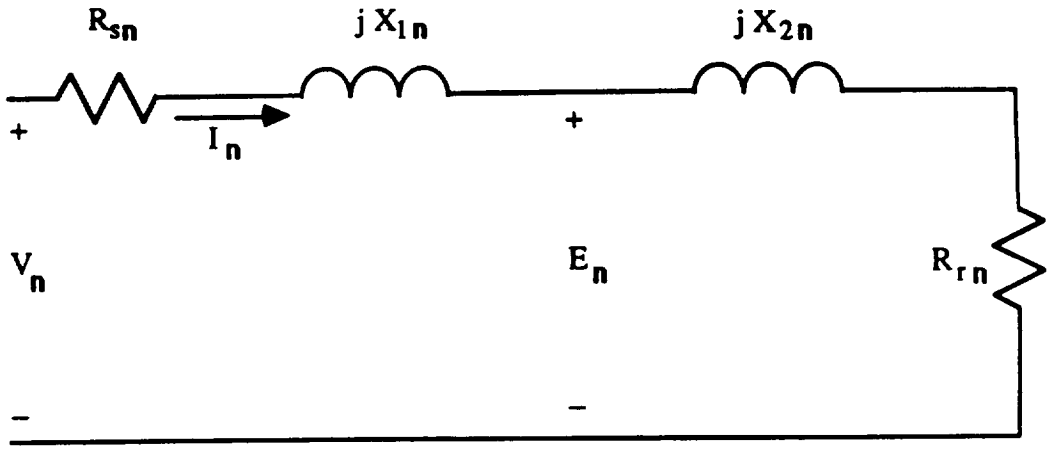

Fig. 3.5. Equivalent circuit at high frequency.

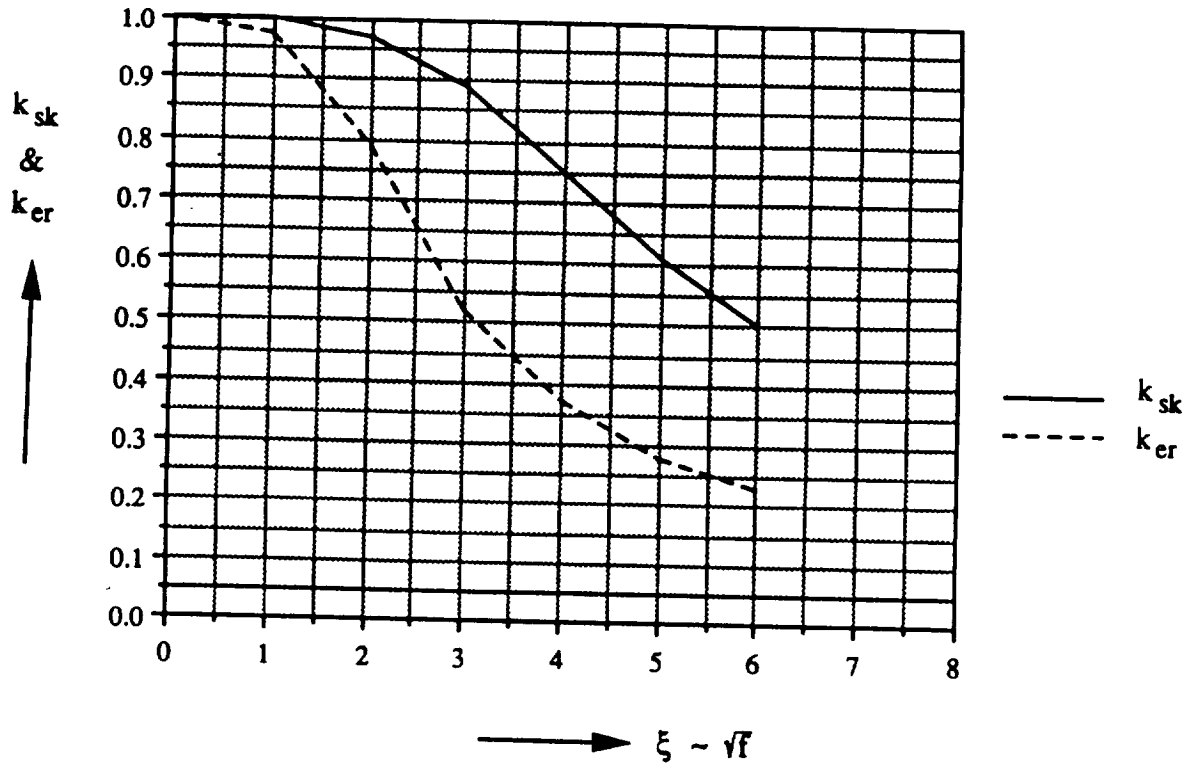

Fig.3.6. Variation of k_{sk} and k_{er} with ξ or $\sqrt{f}$.

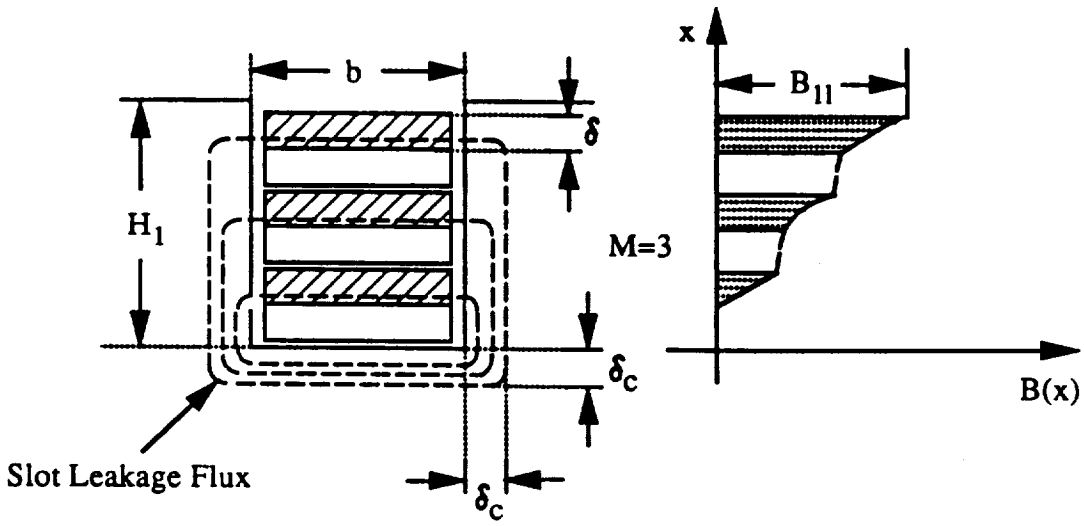

Fig. 3.7. Stator-slot leakage flux and flux density distribution

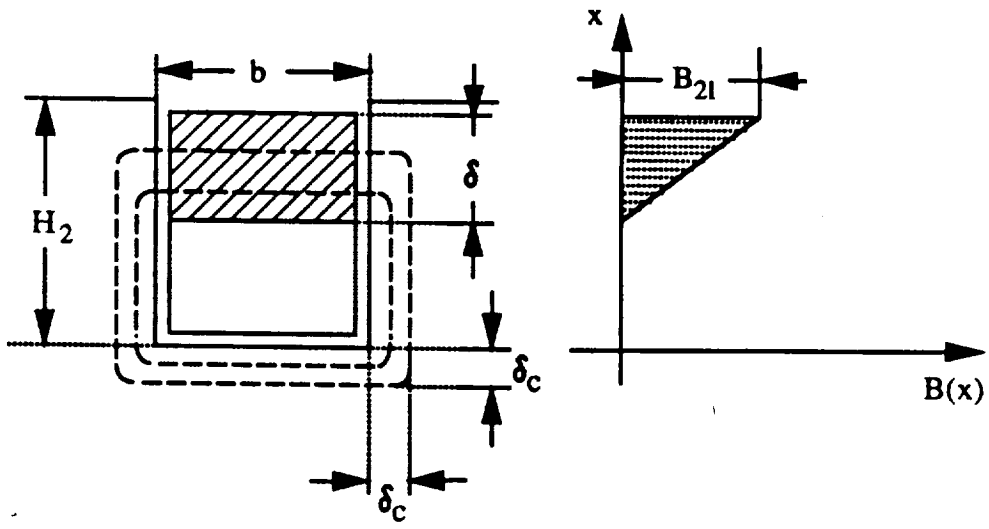

Fig. 3.8. Rotor-slot leakage flux paths and flux density distribution

Appendix C

Frequency Dependence of Time Harmonic Losses in Induction Machine

Presented at

1990 International Conference on Electric Machine

Baston Massachusetts

June 1990

Frequency Dependence of Time Harmonic Losses in Induction Machines

Donald W. Novotny
University of Wisconsin
Madison, Wisconsin

Syed A. Nasar
University of Kentucky
Lexington, Kentucky

Borislav Jeftenic
University of Belgrade
Belgrade, Yugoslavia

Douglas Maly
University of Wisconsin
Madison, Wisconsin

Abstract

The influence of time harmonic frequency on the losses in power converter driven induction machines is examined with special emphasis on switching frequencies in the 15-25 kHz range. A qualitative theoretical analysis is presented which indicates that conductor losses fall approximately inversely with frequency for these high frequencies but that the leakage flux core losses tend to increase approximately as the square root of the frequency. There is, therefore, a switching frequency which yields minimum loss and beyond this point the core losses cause a slow increase in total losses. Preliminary experimental results tend to confirm these conclusions but additional experimental work is needed for validation and to supply useful quantitative results.

1 Introduction

An important issue in modern power electronic motor drives is the effect increasing the time harmonic frequency has on time harmonic motor losses. There are many motor related reasons concerning control characteristics and motor acoustic noise which argue for switching frequencies in the range of 10-20 kHz in the power converter. Minimizing the size of reactive elements in the power converter also implies increased switching frequencies, possibly well beyond the 20 kHz level required to eliminate acoustic noise. Opposing these arguments is the possibility of high motor losses caused by the high time harmonic frequency impressed on the motor.

The primary goal of this paper is to examine the influence of time harmonic frequency on these losses. In particular, the analysis is focused on converters which place a substantial portion of the harmonic energy at relatively high frequencies; in the range of 15 - 25 kHz or higher. The conductor I^2R losses and the core losses are examined qualitatively and a preliminary series of tests are carried out to investigate the validity of the qualitative predictions. The results appear to indicate that in general the time harmonic losses for a fixed value of time harmonic voltage will decrease as the frequency increases. However, at sufficiently high frequencies a minimum loss point is predicted to be reached and beyond this frequency the losses increase slowly but steadily (varying approximately as $f^{1/2}$).

2 Loss Analysis

2.1 Conductor Losses

At harmonic frequencies skin and proximity effects become significant factors in determining conductor losses. For slot imbedded conductors, the variation of the conductor resistance and inductance with frequency follows the general pattern illustrated in Fig. 1 [1, 2]. The initial change in R and L as frequency increases is rapid, being approximately dependent on f^2. This region occurs where the skin depth and conductor size are of the same order of magnitude. As the frequency continues to increase, the rate of change decreases and the variation ultimately becomes proportional to $f^{1/2}$ as the skin depth becomes small compared to conductor size. While these results apply in general, the portion of the conductors in the slots are affected to a much greater degree since the slot (leakage) fluxes are much larger than the fluxes surrounding conductors in air, such as the end turn conductors. Proximity effects are thus much larger for the slot imbedded conductors.

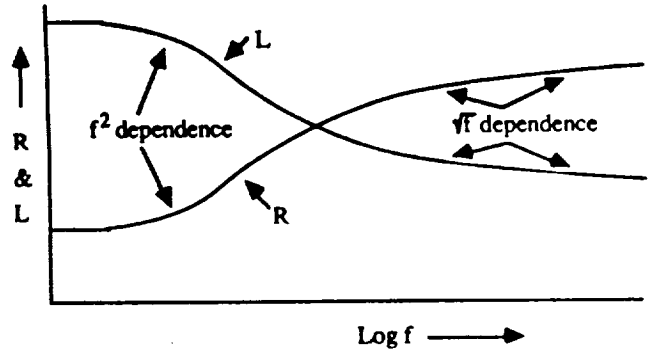

Fig.1 Skin Effect R and L Variation for Conductors in Slots

Assuming the harmonic frequency is much larger than the fundamental frequency, the harmonic slip will be close to unity and the reactive terms (leakage and magnetizing reactances) will be much larger than the resistive terms in the harmonic equivalent circuit. The harmonic magnetizing current is therefore negligible and the harmonic motor current is determined almost entirely by the applied harmonic voltage and the harmonic leakage reactance. The conductor losses are then given to a good approximation by [2]

$$P_{rv} \approx I_v^2(R_s + R_r) \approx \left(\frac{V_v}{2\pi f_v L_\sigma}\right)^2 (R_s + R_r) \qquad (1)$$

where

f_v = time harmonic frequency
I_v = harmonic current
V_v = harmonic voltage
L_σ = total leakage inductance
R_s = stator resistance
R_r = rotor resistance

It is clear that for a fixed value of I_v skin and proximity effects will increase the conductor losses. However, for a fixed value of V_v the inverse square frequency dependence of the current tends to compensate for the resistive increases

resulting from skin effect. While it is true that the leakage inductance L_σ is reduced by skin effect, this reduction is much less than might be expected since only the slot portion of the inductance is significantly affected. The variation of the leakage inductance (and winding resistances) is strongly dependent on motor details such as size, pole number, slot shape, slot depth and the ratio of stack length to diameter. Measurements on actual machines indicate that L_σ is reduced to 0.5 to 0.3 of the rated frequency value at $f_v = 20$ kHz [2]. A useful first approximation is to take

$$L_\sigma \sim K_L f_v^{-0.16} \tag{2}$$

as a generic frequency dependence of L_σ [2].

Since the single conductor cage winding typically exhibits skin effect even at the fundamental frequency, for harmonic frequencies the variation is well into the frequency range where R_r follows an $f_v^{0.5}$ frequency dependence (the end ring also exhibits an increasing resistance because of the way the bar currents enter the ring). The rotor conductor losses thus are expected to vary approximately as

$$P_{rrv} \sim \left(\frac{V_v}{2\pi f_v K_L f_v^{-0.16}}\right)^2 K_r f_v^{0.5} \sim \frac{V_v^2}{f_v^{1.2}} \tag{3}$$

and thus drop somewhat faster than inverse to the harmonic frequency. This strong dependence clearly indicates that the rotor conductor losses drop significantly as the harmonic frequency increases.

The stator winding behavior is, however, quite different. Typically the wire size is such that very little skin effect occurs at fundamental frequency. At harmonic frequencies near the fundamental, the increase in resistance can be in the f_v^2 region with the result that (using the approximation in Eq. 2) the stator losses initially behave as

$$P_{rsv} \sim V_v^2 f_v^{0.3} \tag{4}$$

and therefore can exhibit a moderate increase as f_v increases. This creates a very different conductor loss distribution between rotor and stator and can lead to increased stator winding temperature. The loss distribution within the stator slot is also non-uniform with the uppermost conductors having the highest loss [3]. As the harmonic frequency continues to increase, the rate of rise of the stator resistance decreases and eventually approaches that of the rotor as expressed in Eq. (3). It is, therefore, true that for sufficiently high harmonic frequencies the total stator conductor loss decreases with approximately an $f_v^{-\alpha}$ dependence where α is approximately 1.2, the same as the rotor loss in Eq. (3). There is, therefore, a significant reduction in total conductor I^2R loss as the frequency of the time harmonic voltage excitation increases especially for frequencies where the skin depth is small compared to the conductor size in both rotor and stator.

2.2 Core Losses

The core losses associated with high frequency time harmonics are influenced by a number of factors which combine to make predictions very difficult. These factors include the following four principal effects:

1) because the motor slip is very nearly unity for the higher time harmonics, the only significant flux in the machine is leakage flux.

2) for frequencies where the skin depth in the core material (δ_{fe}) is small compared to the lamination thickness, the flux only penetrates the core to approximately a skin depth.

3) the redistribution of the conductor currents caused by skin effect alters the leakage paths.

4) the eddy currents in the core material can set up a significant reaction field which opposes the inducing field.

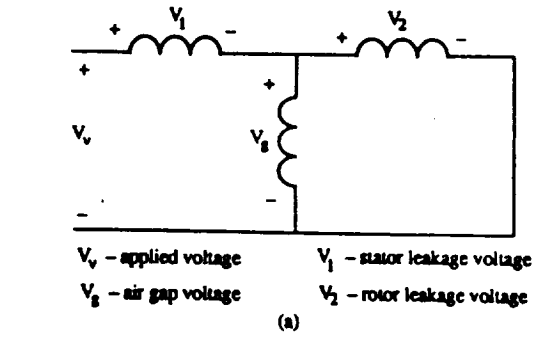

(a)

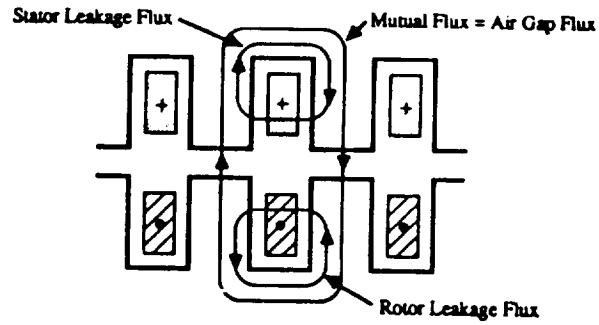

(b)

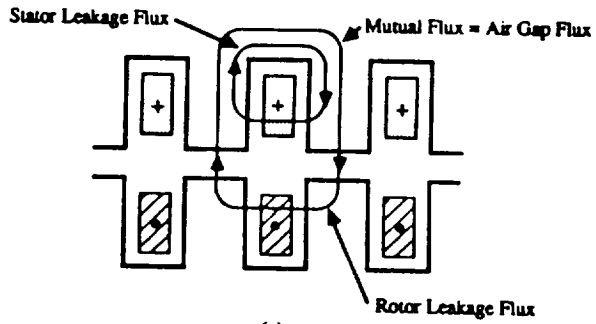

(c)

Fig. 2 Equivalent Circuit and Flux Paths for Time Harmonics (slip = 1.0)

The leakage flux distribution associated with the high slip operating condition common to all high frequency time harmonics is illustrated in Fig. 2. As indicated by the equivalent circuit shown in the figure, the air gap flux and the rotor leakage flux are very nearly equal under this condition with the result that there is virtually no rotor core flux (Fig. 2c). The core losses therefore tend to be concentrated in the stator teeth and portions of the stator core near the stator slot bottoms. There is also some loss in the rotor teeth caused by the rotor leakage flux. Note that the usual concept of rotor leakage flux encircling the rotor conductor (Fig. 2b) is inappropriate for core loss considerations since the loss is proportional to B^2. The

usual concept of leakage, which is based on superposition, is quite acceptable for calculation of leakage inductance but must be abandoned when core losses are of interest.

The basic variation of the core losses with frequency can be explored using the usual core loss model described by

$$P_c = P_h + P_e = \left[k_h B^n f + k_e B^2 f^2\right] \text{Vol} \qquad (5)$$

where

P_c = total core loss
P_h = hysteresis loss
P_e = eddy current loss
B = flux density
f = frequency
Vol = volume of core carrying flux
k_h, k_e = material dependent constants
n = hysteresis exponent, typically n ≈ 1 to 1.5

Although this model only applies to the simple case where:

i) there is negligible reaction field - i.e. B is the pre-existing field and does not change as a result of eddy currents,
ii) the flux is uniform - i.e. no lamination skin effect,

it serves as a useful representation if the primary effects of the reaction field are included separately [4].

In the time harmonic situation the total leakage flux is directly determined by the time harmonic applied voltage V_v

$$\phi_v = k_v \frac{V_v}{f_v} \qquad (6)$$

and, conceptually, the time harmonic flux density is then given by

$$B_v = \frac{\phi_v}{A_l} = k_v \frac{V_v}{f_v A_l} \qquad (7)$$

where A_l is the effective area of the leakage flux path. While A_l is clearly different for different portions of the leakage path, it will generally be sufficient for an overall analysis to consider an average area for the entire path.

Reaction field effects - As noted above, the eddy current reaction field has two basic effects; reducing the internal B field and redistributing the field (skin effect) [4]. For the leakage fields under consideration, the reduction of the field will not take place since the total leakage flux is a fixed value determined by Eq. (6). Thus, any tendency to reduce the flux will simply result in additional motor current to maintain the flux at the required level. One effect of the eddy current reaction field is, therefore, to reduce the leakage inductance [5]. This reduction is in addition to the reduction caused by conductor skin effect.

The second effect of redistributing the leakage flux will tend to confine the leakage fields to local regions near the slot and air gap surfaces. To a first approximation, the field will only penetrate the lamination to one skin depth δ_{fe}

$$\delta_{fe} = \sqrt{\frac{\rho_{fe}}{\pi \mu_{fe} f_v}} \qquad \delta_{cu} = \sqrt{\frac{\rho_{cu}}{\pi \mu_{cu} f_v}} \qquad (8)$$

where

ρ_{fe} = resistivity of iron ρ_{cu} = resistivity of copper
μ_{fe} = permeability of iron μ_{cu} = permeability of copper

and to a first approximation the B field can be assumed to be uniform over this distance and zero beyond. This concept can be used to estimate the effective area A_l as a function of frequency.

Frequency dependance of core losses - To examine the frequency dependence of the time harmonic core loss, three limiting cases are considered.

Case 1 - $\delta_{cu} >> t$, t = conductor thickness, $\delta_{fe} >> d$, d = lamination thickness. This case corresponds to low time harmonic frequencies with, for example, a wound rotor motor. The core losses would be given by Eq. (5) with B evaluated from Eq. (7) with A_l = constant (i.e. no change in flux paths). The result is

$$P_c = \left(K_{h1} V_v^n f^{1-n} + K_{e1} V_v^2\right) \text{Vol} \qquad (9)$$

where K_{h1} and K_{e1} are constants.

For a constant time harmonic excitation voltage V_v, the loss depends on n, the hysteresis loss exponent. Since n is usually greater than one, the loss will decline with frequency. Usually the hysteresis loss is small compared to the eddy current loss at higher frequencies and, hence, to a first approximation the total core losses would be nearly independent of the time harmonic frequency.

Case 2 - $\delta_{cu} < t$, $\delta_{fe} >> d$. The major influence of conductor skin effect on core loss is in the rotor of cage machines. As the rotor current is forced to the top of the rotor bar by conductor skin effect, the rotor leakage flux is also forced upward toward the rotor surface (tooth tops). This has the effect of reducing the area through which the rotor leakage flux must pass, thus tending to increase B. It also reduces the volume of core material which is carrying flux, but these two effects do not completely cancel. A third effect is the change in ratio between the stator and rotor leakage inductances and hence in the flux ratio. As the rotor leakage inductance decreases, more of the total leakage flux is forced to exist in the stator leakage paths, thus increasing the stator leakage flux.

While the actual change in losses is very much motor design dependent, it seems clear that forcing more of the total leakage flux into stator paths will increase the losses because of the B^2 dependence of the eddy current losses. It is also true that this effect is already significant in most machines under 60 Hz, line start conditions. At the extreme, the rotor leakage flux will be confined almost entirely to the rotor tooth tops very much like the so called zig-zag leakage flux. For most machines, it is likely that even low frequency time harmonics (i.e. 5th and 7th of fundamental) will result in all rotor flux confined to such a surface layer with additional increases of frequency having rather small impacts on the distribution of flux (as a result of rotor bar skin effect). With the assumption of fixed flux paths, the eddy current losses are independent of frequency since the frequency increase is exactly compensated by the decrease in flux density. The hysteresis losses will decrease and eventually become negligible.

In general, over the range of frequencies included in cases 1 and 2, one would expect a decrease in core loss at fairly low time harmonic frequencies and a leveling out at high frequencies. Depending on the relative importance of hysteresis losses and the flux redistribution discussed above, the net reduction in total loss at the lower time harmonic frequencies will vary from machine to machine.

Case 3 - $\delta_{cu} < t$, $\delta_{fe} < d$. When the time harmonic frequency is large enough so the skin depth in the iron (δ_{fe}) is small compared to the lamination thickness, the leakage flux can be viewed approximately as confined to a skin depth layer at the iron surface. The situation is now somewhat as depicted in Fig. 3. The region of highest core loss is at the bottom of the

stator slots where the total leakage flux must be accommodated. The flux level along the stator slot walls drops off as the stator tooth top is approached and the flux in the air gap and rotor surface is the rotor leakage flux.

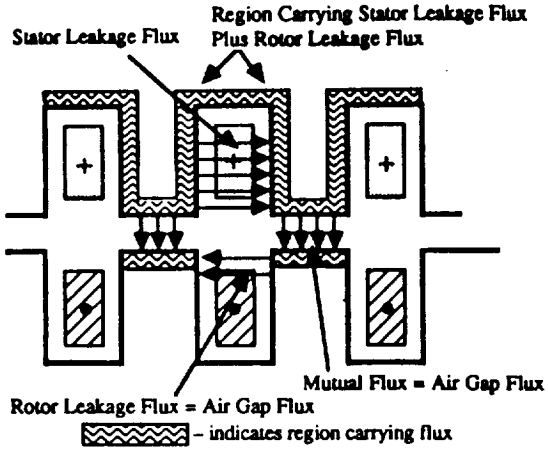

Fig. 3 Flux Paths for High Frequency Time Harmonic Showing Effect of Skin Effect in Laminations

The loss for this condition can be approximated by neglecting the hysteresis loss and assuming the area available for the leakage flux is limited to one skin depth. The flux density will then be given by Eq. (7) with $A_l = l\,\delta_{fe}$

$$B_v = k_v \frac{V_v}{f_v l \delta_{fe}} = \frac{k_v V_v}{l\sqrt{\frac{\rho_{fe} f_v}{\pi \mu_{fe}}}} = K f_v^{-1/2} V_v \qquad (10)$$

and the core loss becomes (since Vol ~ δ_{fe})

$$P_{cv} \approx k_e B_v^2 f_v^2 \,\mathrm{Vol} \approx K_1 V_v^2 f_v^{1/2} \qquad (11)$$

Thus, for a fixed value of time harmonic excitation voltage, the eddy current losses tend to increase as $f_v^{0.5}$, a slow but steady growth. This slow growth can be expected to persist until some other effect (capacitive currents) becomes significant.

It is also interesting to express the loss in terms of the physical parameters of the core, the resistivity and permeability. In terms of the k_e and δ_{fe} the loss is

$$P_{cv} = K_2 \frac{k_e V_v^2}{\delta_{fe}} \qquad (12)$$

and since

$$k_e = \frac{K_e}{\rho_{fe}} \qquad (13)$$

$$P_{cv} = K_3 \frac{V_v^2 f_v^{1/2} \mu_{fe}^{1/2}}{\rho_{fe}^{3/2}} \qquad (14)$$

Total time harmonic losses - The discussion and analysis indicates that for a fixed time harmonic excitation voltage the conductor losses tend to decrease rapidly (as $f_v^{-1.2}$) and the core losses increase slowly (as $f_v^{0.5}$) as the frequency increases and becomes large compared to the fundamental frequency. This implies there is some time harmonic frequency where the total losses are a minimum as illustrated in Fig. 4. The location of this minimum is design dependent, the low frequency ratio of leakage flux core and copper losses being an important parameter.

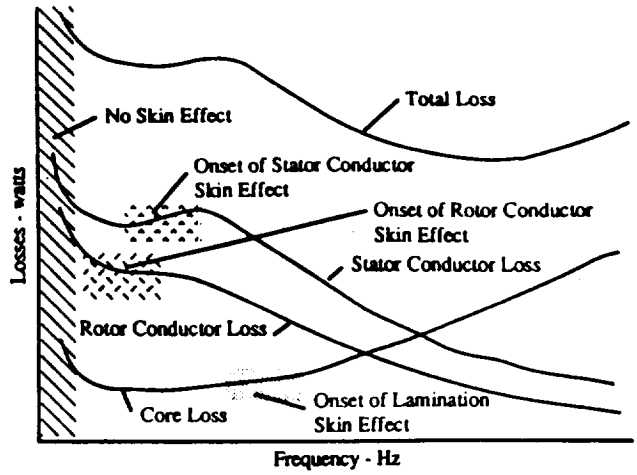

Fig. 4 Variation of Time Harmonic Induction Motor Losses with Frequency for Constant Time Harmonic Voltage

3 Experimental Verification

3.1 Description of Experiments

Preliminary experimental investigation of the qualitative theoretical analysis was attempted by means of experiments on three different induction motors of essentially the same power rating (approximately 1 hp). For the purposes of these tests the most important differences between the tested motors are:

- Motor 1 is a cage-rotor machine with open rotor slots.
- Motor 2 is a cage-rotor machine with closed rotor slots.
- Motor 3 is a wound-rotor machine with open rotor slots.

Also, motor 1 is a single phase motor and 2 and 3 are three phase motors. The motor nameplate data are supplied at the end of the paper.

In the experiments one of the machine phases was supplied by a high-frequency (60-25,000 Hz) sinusoidal power source. The other two stator phases (one phase for motor 1) were fed from a dc power supply and the rotor was blocked. The dc current value was determined according to nominal saturation of the machine. Unfortunately, because of practical limitations, the output voltage of the high-frequency power amplifier was limited to 5 volts at the higher frequencies. During the experiments the voltage was held constant at this value for all frequencies. This low voltage is a significant limitation on the applicability of the test results and will be remedied in future testing.

All measurements of the alternating current supply were by means of a digital storage oscilloscope. According to well-established theory for single phase supplied polyphase induction motors, the phases are uncoupled at locked rotor and polyphase performance can be inferred from single phase measurements. This assertion was experimentally verified at rated frequency. For the one test on the wound rotor motor with the secondary open, the test is similar to operation at zero slip and the input power is essentially all core loss. It can be shown for this situation that the single phase input power is approximately one-half of the corresponding three phase power. This was also experimentally verified at rated frequency.

3.2 Leakage Inductance Measurements

The leakage inductance vs frequency characteristics for the tested motors are presented in Figs. 5,6 and 7. The influence of the flux level as established by the direct current is small in the case of first motor with open slots (Fig. 5), and large in the case of motor 2 with closed slots (Fig. 6). The relative change of inductance with respect to frequency is also largest in the case of motor 2 (Fig. 6). This is most likely a consequence of the closed slots and the resulting enhanced skin effect in the rotor bars. The opposite effect (a small relative change in inductance) exists in the case of the wound-rotor motor (Fig. 7), as a result of the open slots and the reduced skin effect influence in the multi-turn, small diameter rotor conductors.

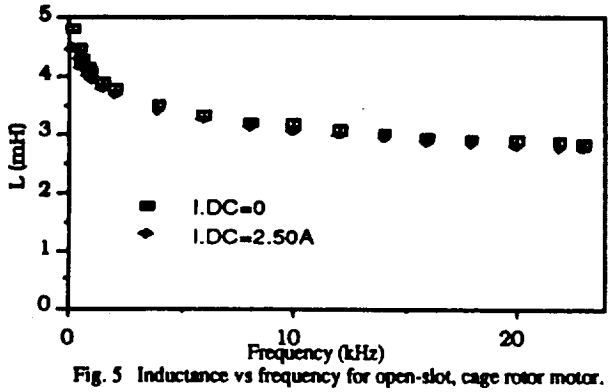

Fig. 5 Inductance vs frequency for open-slot, cage rotor motor.

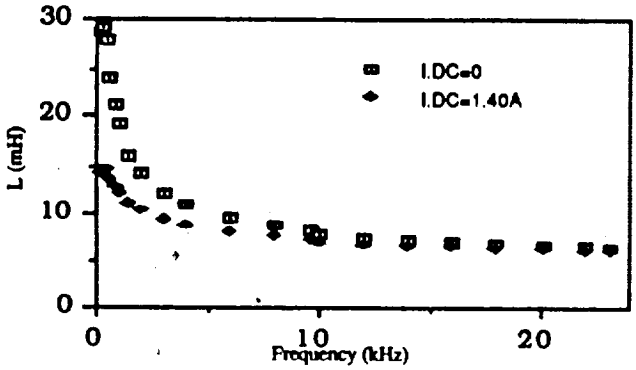

Fig. 6 Inductance vs frequency for closed-slot, cage rotor motor.

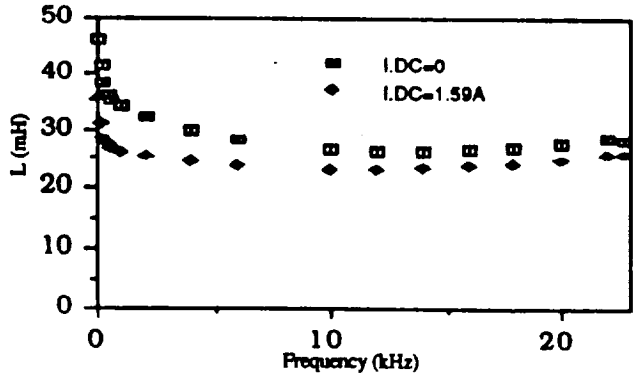

Fig. 7 Inductance vs frequency for wound-rotor motor, rotor shorted.

For the three motors the ratio of leakage inductance at 20 kHz compared to nominal frequency ranges from about 0.5 (Fig. 6) to about 0.7 (Fig. 7). This is somewhat less variation than suggested by Eq. 2 but not unreasonably so considering that only three small motors were examined and that one was a wound rotor machine in which the change is expected to be small. The only anomaly in the data is the small increase of inductance at high frequency in Fig. 7. No satisfactory explanation of this result has been developed. Except for this issue the experimental results are as expected based on the qualitative analysis presented in Section 2.

3.3 Power Loss Measurements

The characteristic power losses vs frequency for the tested motors are shown in Fig. 8, 9 and 10. In all of these figures the influence of the flux level as established by the direct current is relatively small. Unlike the theoretical analysis there is not any increase of the power losses at high frequency. This is apparently a consequence of the fact that although in these tests the measured power represents the sum of conductor and core losses, the conductor losses are still dominant at the test frequencies. In Fig. 10 the curve becomes very flat at the high end but does not show an increase.

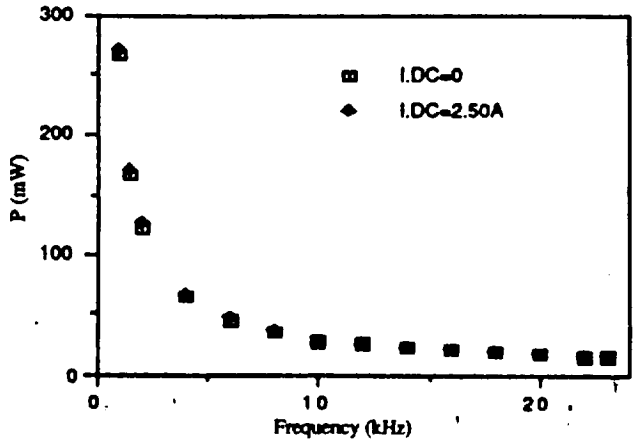

Fig. 8 Power loss vs frequency for open-slot, cage rotor motor.

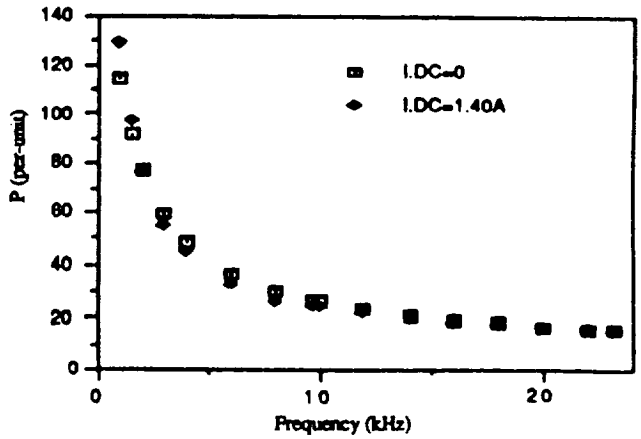

Fig. 9 Power loss vs frequency for closed-slot, cage rotor motor.

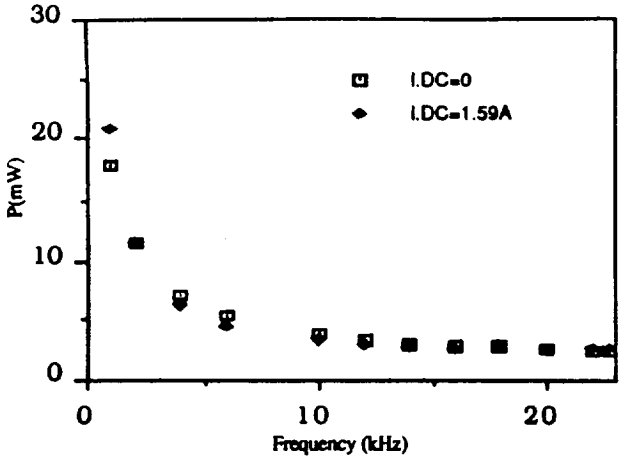

Fig. 10 Power loss vs frequency for wound-rotor motor, shorted-rotor test.

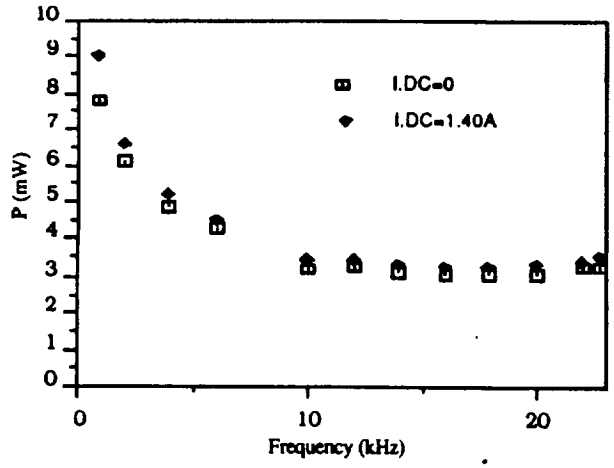

Fig. 11 Power loss vs frequency for wound-rotor motor, open rotor test.

In the case of the wound-rotor motor we could make the same test but with an open-circuited rotor. The measured power in this test is the sum of the stator conductor losses and main flux core losses. The results of this test are presented in Fig. 11 and the small increase of power losses at high frequency is easy to note. Although the core losses in this case are not in any sense the same as under a shorted-rotor condition, the test does indicate that core losses do increase at high frequency despite the very much reduced flux associated with constant voltage operation.

4 Summary and Conclusions

The qualitative analysis of time harmonic losses presented in this paper indicates that conductor losses tend to decrease slightly faster than inversely with frequency at fixed voltage for sufficiently high harmonic frequencies. This is fundamentally a result of the harmonic currents being reactance limited and the fact that the harmonic leakage inductance decrease resulting from skin and proximity effects is relatively small (only the slot portion being significantly affected).

Conversely, the approximate analysis indicates that harmonic (leakage flux) core losses at constant voltage tend to initially decrease and then slowly increase at higher frequencies as a result of skin effect in the core laminations. A time harmonic frequency where the total losses reach a minimum is therefore indicated.

A preliminary series of measurements, although severely restricted by equipment limitations and range of machine size, was qualitatively supportive of the theoretical results. The significance of flux level, slot type and other design details was clearly demonstrated. The experimental data also indicates that, for the small motors tested, the minimum loss frequency is probably significantly higher than the 20 kHz maximum frequency of the tests.

Acknowledgement

Support for this work from the NASA Lewis Research Center, Cleveland, Ohio and the Wisconsin Electric Machines and Power Electronics Consortium (WEMPEC) is gratefully acknowledged.

References

[1] Stoll, R. L., "The Analysis of Eddy-Currents," Oxford University Press, 1974.

[2] de Buck, F. G. G. Gistelinck, P., de Backer, D., "A simple but reliable loss model for inverter-supplied induction motors," **IEEE Trans. on Industry Applications**, vol. IA-20, No. 1, Jan./Feb. 1986, pp. 190-202.

[3] de Buck, F. G. G., "Losses and Parasitic torques in electric motors subjected to PWM-waveforms," **IEEE-IAS Annual Meeting '77**, pp. 922-929.

[4] Stoll, D.F.H., Hammond, P.,"Calculation of the magnetic field of rotating machines," **Proc. IEE**, Vol. 112, No. 11, Nov. 1965, pp. 2083-2094.

[5] Christofides, N., "Origins of load losses in induction motors with cast aluminium rotors," **Proc. IEE**. Vol. 112, No. 12, Dec. 1965, pp. 2317-2332.

Appendix-Test Motor Nameplate Data

Motor 1- 1 hp, 1725 rpm, 6.4 A, 230 V, 60 Hz (Single-phase).
Motor 2 - 1 hp, 5094 rpm, 2.57 A, 230 V, 86 Hz.
Motor 3 - 1/3 hp, 1725 rpm, 1.4 A, 220 V, 60 Hz (Wound-rotor).